European Coordination for Accelerator Research and Development

PUBLICATION

Measurement-based characterization of multipixel avalanche photodiodes for scintillating detectors; EuCARD Editorial Series on Accelerator Science and Technology, (j-P.Koutchouk, R.S.Romaniuk, Editors), Vol.14

Dziewiecki, M (Warsaw University of Technology Poland)

23 February 2013

The research leading to these results has received funding from the European Commission under the FP7 Research Infrastructures project EuCARD, grant agreement no. 227579.

This work is part of EuCARD Work Package **2: DCO: Dissemination, Communication & Outreach**.

WARSAW UNIVERSITY OF TECHNOLOGY

Faculty of Electronics and Information Technology

Ph.D. Thesis

Michał Dziewiecki, M.Sc.

Measurement-based Characterization of Multipixel Avalanche Photodiodes for Scintillating Detectors

Supervisor
Janusz Marzec, D.Sc.

Warsaw, 2012

Abstract

Multipixel avalanche photodiodes (MAPD) are recently gaining popularity in high energy physics experiments as an attractive replacement for photomultiplier tubes, which have been extensively used for many years as a part of various scintillating detectors.

Their low price, small dimensions and another features facilitating their use (like mechanical shock resistance, magnetic field immunity or moderate supply voltage) make the MAPDs a good choice for commercial use as well, what is reflected in growing number of producers as well as MAPD models available on the market.

This dissertation presents Author's experience with MAPD measurements and modelling, gained during his work on the T2K (*Tokai-to-Kamioka*) long-baseline neutrino experiment, carried out by an international collaboration in Japan.

First, operation principle of the MAPD, definitions of various parameters and measurement methods are discussed. Then, a device for large-scale MAPD measurements and related data processing methods are described. Finally, the Author presents an attempt of analysis and interpretation of the results.

This book ia a direct translation of a PhD thesis written in Polish. In comparison to the original, however, a chapter describing the current state of the neutrino science is missing. The Author decided not to place it here as it's only a study of the literature. Moreover, some minor mistakes were corrected in the english issue.

Contents

Chapter 1

Introduction

Scintillating detectors are a well known tool for high energy photon and elementary particles detection. They are widely used in science (experimental particle physics) as well as medicine (computed tomography, scintigraphy, PET), industry and border protection. Its popularity comes from many advantages, such as a large scope of sizes, a wide range of particles and radiation energy being detected, a rather high radiation resistance, the ability to work at room temperature, and finally, reasonable requirements for operating conditions (they usually do not need cooling systems, no working gas is used).

Each scintillating detector consists of at least two basic components: a scintillator and a light detector. Depending on their intended use, individual detectors differ by the material used for the scintillator and its mechanical form (crystal scintillators, liquid, plastic, in a form of blocks, plates or fibers – for detection of different kinds of particles of various energies, with various sensitivity, spatial resolution and pulse decay time), and the light detector used.

The choice of the photodetector for a particular application depends mainly on the number of photons emitted by the scintillator. In high-energy physics experiments, where registration of individual particles is required, a light beam produced is generally very weak. In these applications, photomultiplier tubes (PMTs) are the most widely used photodetectors. Their advantages (first of all low noise and high output signal, achieved by means of internal electron gain) far outweighed the disadvantages, which are typical for all electron tubes (high price, quite large dimensions, mechanical weakness, sensitivity to magnetic field), partly due to the lack of a real competition from the semiconductor devices. An established position of the photomultipliers does not mean, however, that its successor among semiconductors is not looked for. Such a device should preserve as many advantages of the photomultiplier as possible and furthermore be free of the PMT's drawbacks and be able to work where PMTs cannot be used (e.g. in a presence of a strong magnetic field or within a limited space).

The first device that could compete (to some extent) with the photomultiplier was the avalanche photodiode (APD) – a semiconductor device, which – like the photomultiplier – uses electron gain effect to increase output signal. Unfortunately, the similarity between these two instruments is mainly qualitative – the avalanche photodiode is far away from its tube competitor in achieved gain, dynamic range and noise level as well as achievable photosensitive surface. As a result, APDs are rather inpopular in scintillating detectors (nevertheless, they are used from time to time).

The so-called hybrid photodetector (*HPD*), which is a combination of a photomultiplier with a solid state avalanche diode, seemed to be a new hope for a moment – but in fact it didn't succeed, mainly due to the inheritance of specific drawbacks from the two parent units, with the absence of any clear advantage over the photomultiplier.

During recent years, a new, interesting solution appeared on the market. It's the MAPD – Multipixel Avalanche Photodiode. It's based on on the principle of avalanche photodiodes on the one hand, on the other hand, however, constitutes a new quality in terms of performance.

One of the first devices running the MAPD detectors on a large scale is the so-called near detector of the T2K experiment, which investigates the properties of neutrinos.

As a part of the construction work of the detector, a team from the Department of Nuclear and Medical Electronics of the Warsaw University of Technology, Institute of Radioelectronics, the mother institution of the Author, was asked to investigate about 1,200 MAPDs, namely the product of Hamamatsu, called MPPC. This work needed a number of issues to be resolved:

- development of methods for MAPD measurement and specific instruments, ensuring high reproducibility of the results, the ability to precisely control the measurement conditions over a wide range, high throughput, reliability, and allowing a simultaneous measurement of all key parameters of the MAPD;
- development of suitable data processing algorithms, which guarantee high quality of the results and are characterized by moderate computational effort;
- interpretation of results and creation of new models describing the operation of the MAPD, as well as verification of the existing ones.

Chapter 2

Multipixel Avalanche Photodiode

2.1 Avalanche Photodiodes

Avalanche photodiodes (APDs) are fast and very sensitive semiconductor light detectors. They utilize the avalanche phenomenon (similarly to photomultiplier tubes) which allows to amplify the signal present at the output of the device. This feature is achieved thanks to a specific design of the silicon structure.

In comparison to a common PiN photodiode, the doping profile of an avalanche photodiode is more complicated and designed so that there are two layers in the junction area:

- The absorption layer, where free carriers (electron-hole pairs) are generated. The moderate electric field existing in this layer allows to separate carriers and provides their transport with the greatest possible speed (due to the collisions with the atoms of the medium, achievable velocity of electrons in silicon is about 10^7 cm/s at the electric field intensity of 10^4 V/cm).
- The multiplication layer, where the electric field intensity exceeds the value of $1,75 \cdot 10^5$ V/cm. In these conditions, a free carrier can achieve enough energy to generate new electron-hole pairs between successive collisions with the atoms of the crystal network. Thus, an effect of avalanche multiplication takes place[1].

In the semiconductor structure, the avalanche gain can be realized by two types of carriers – electrons and holes. Due to the difference in mobility of the carriers, the probability of the generation of a new pair by an electron and a hole is different. The ratio of hole to electron ionization determines the noise associated with the phenomenon of multiplication

[1] The multiplication layer has the ability of photon absorption, as well.

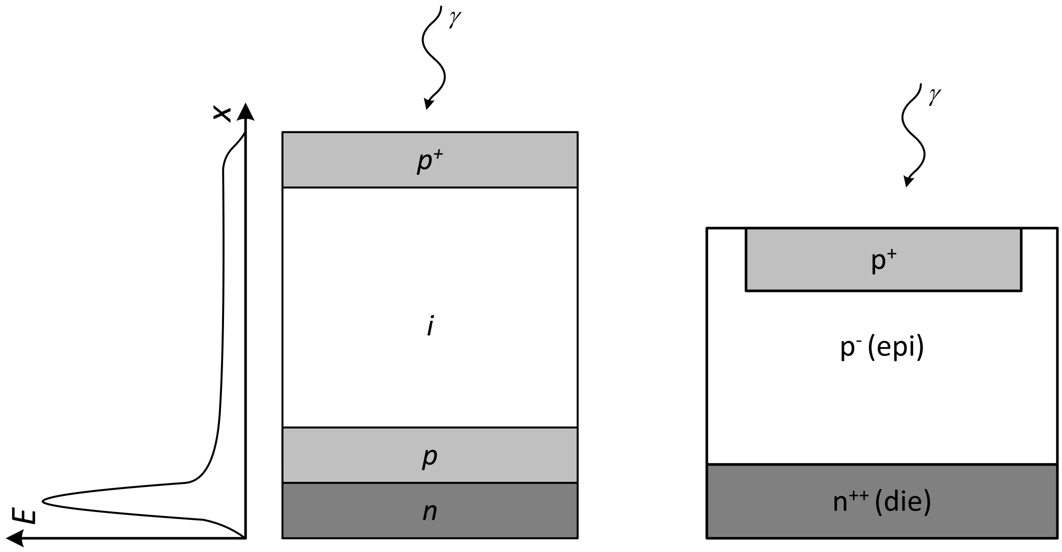

Figure 2.1: Left: a diagram of avalanche photodiode structure with the the electric field intensity profile. Right: The layout of the Multi-Pixel Photon Counter (MPPC) by Hamamatsu – an example of a multipixel avalanche photodiode [29]

and in fact it is desirable that one of these components strongly dominates. In case of silicon photodiodes, this ratio is about 2×10^{-2} for typical *reach-through* structures and about 2×10^{-3} for so-called *Slik* – *Super-Low k* structures [20].

For the silicon diode, the semiconductor layers alignment is such that electrons are transported from the absorption layer to the multiplication layer rather than holes; this is because electrons have greater ionization capability. However, the detailed parameters of the design (thickness of each layer, the direction where the light beam comes from) depend on the application – mainly on the length of the incident light wave[2].

The appearing of a suitably strong electric field in the multiplication layer needs accordingly high junction bias voltage. This voltage is very close to the breakdown voltage (of avalanche-type breakdown) of the diode and typically has a value from a few dozen to more than 1000 V. Depending on the relationship of the bias voltage and the avalanche breakdown voltage (V_{br}), two modes of operation of the avalanche photodiode are possible: proportional and Geiger mode.

[2]There are also solutions built similarly to an avalanche photodiode structure, but not using the photoelectric effect. Such a device is designed to amplify an electron beam coming from outside and is used for example in hybrid photodetectors (HPD), which combine elements of an avalanche diode and a photomultiplier.

Proportional mode operation

In the proportional mode, the junction is always polarized with a voltage slightly lower than its breakdown voltage. Under such conditions, the total photocurrent is almost a linear function of the amount of primary carriers generated in the photoelectric effect – the operation of an APD is very similar to operation of a photomultiplier, with the difference that the reproduction occurs at any depth over the multiplication layer, rather than on discrete dynodes.

In contrast to the photomultiplier tube, the process of charge multiplication in the avalanche diode involves two types of carriers, and both mechanisms operate in a positive feedback loop[3]. In such a simple model, the avalanche gain of the photodiode will be:

$$M = \frac{\alpha}{1 - \alpha \cdot \beta} \ , \tag{2.1}$$

where α and β are the coefficients of electron and hole multiplication, respectively.

The avalanche gain (called also simply 'electron gain') is a very narrow function of voltage, rapidly growing when the bias voltage approaches the breakdown voltage for which the value of $\alpha \cdot \beta$ reaches unity.

The excess noise of the avalanche photodiode. In fact, the operation of the avalanche photodiode in the proportional mode is possible with gain reaching values of 10^2, rarely 10^3. Further increase of the gain is pointless due to rapid growth of the excess noise.

The essence of the excess noise of the avalanche photodiode and photomultiplier is similar – it is the result of the statistical fluctuations in the number of carriers produced during avalanche reproduction. With the PMT, where only electron multiplication takes place (there are no holes in vacuum), the dominant component of the noise is the fluctuation of the number of electrons generated on the first dynode. In this case a simple way to minimize this phenomenon is to increase the gain of the first stage – the relative amplitude of the fluctuations will decrease with the square root of the gain.

In case of the avalanche photodiode, the description of this phenomenon is more complicated due to presence of two types of carriers, accompanied by two different multiplication factors. The power spectral density of the noise is given by:

$$\frac{\mathrm{d}i_n^2}{\mathrm{d}f} = 2eI_g \cdot M^2 \cdot F \ , \tag{2.2}$$

where e is the electron charge, I_g the total generation current (both thermal and photonical), and M is avalanche gain defined by equation 2.1. F defines the excess noise factor,

[3] This is possible because the electron and hole avalanches grow geometrically in opposite directions.

associated with statistical gain fluctuations:

$$F = M \cdot k + (2 - \frac{1}{M}) \cdot (1 - k) \ , \tag{2.3}$$

where k is the ratio of electron and hole multiplication factors per length unit[4] [18]. F is the ratio of the actual power spectral density of the photodiode noise to the noise resulting only from the discrete nature of primary photoelectrons (the shot noise).

It should be noted that the signal-to-noise ratio (SNR) of the avalanche photodiode will be worse than for a common PiN diode due to excess noise described above (typical value of F is about 5). However, this loss can be compensated by the profit of higher signal level and thus lower influence of the noise introduced by co-operating preamplifier.

The noise level of an avalanche photodiode operating in proportional mode (with corresponding preamplifier) allows the detection of light pulses of several photons. This sensitivity is sometimes insufficient for scintillating detectors which have to detect single ionizing particles.

Geiger mode

The Geiger mode operation is characterized by a bias voltage above the breakdown voltage of the junction. This situation occurs when the product of the multiplication coefficients for electrons and holes exceeds unity. Since the geometrical development of the avalanches for both carrier types takes place in opposite directions, the resultant carrier avalanche can develop at steady position, thus finite thickness of the multiplication layer does not prevent the avalanche from unlimited growing.

In Geiger mode, each carrier getting to the multiplication layer becomes a source of an uncontrolled development of the avalanche. This means that each electron (it does not mean whether it is generated by the photoelectric effect or by thermal generation) will cause a large current flow through the diode, and this flow will continue as long as the junction bias voltage is above the breakdown voltage (V_{br}). The recovery of the diode to its basic state requires a quenching system – that is, a device that automatically reduces the voltage across the diode after an avalanche occurs. The simplest solution is a serial resistor of quite high resistance. In this case, only a charge required to discharge the junction capacitance to the V_{br} level will flow as the result of the avalanche (assuming that the charge, which at this time will pass through the resistor, is negligible).

In Geiger mode, the term 'avalanche gain' (or 'electron gain') slightly changes its meaning – it determines the number of charges generated in the multiplication layer as a result

[4]The presented model can be applied for the electrons injected in the multiplication area as primary carriers. In the opposite case, when holes are injected, k shall be substituted by $1/k$.

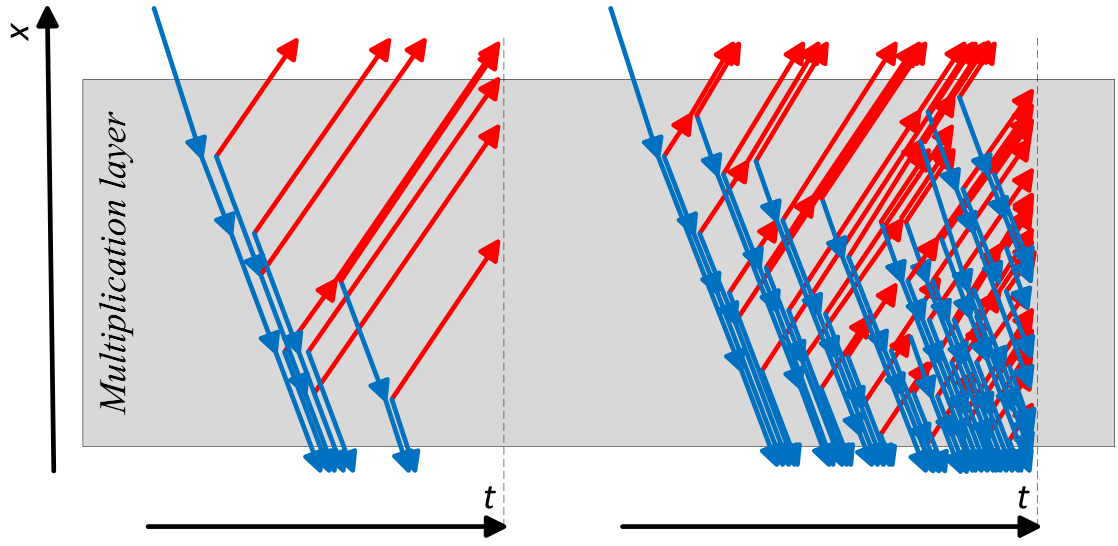

Figure 2.2: Carrier multiplication in proportional (left) and Geiger mode (right). In proportional mode, the hole multiplication occurs relatively rarely, and avalanche declines by itself. In Geiger mode, the number of carriers still grows with time and only a reduction of the the electric field intensity can lead to the suppression of the avalanche. Blue arrows represent electrons, and red – holes

of the creation of a single avalanche (it is not relevant here, if the avalanche was triggered by one or more primary electrons). In the described method of the avalanche quenching, its value should depend exactly on the junction capacitance and the overvoltage – the difference between the bias voltage and breakdown voltage, which is the final junction voltage just after the avalanche occurs:

$$G = \frac{C_j}{e}(V_{op} - V_{br}) \ , \tag{2.4}$$

where C_j denotes the junction capacitance, e the electron charge, V_{op} the bias voltage, and V_{br} – the breakdown voltage of the junction. (We assume that the junction capacitance during the discharge process remains constant[5].) The value of $V_{op} - V_{br}$, the overvoltage, will be since now denoted as ΔV.

In Geiger mode, the APD gain reaches a level of approximately 10^6 (it depends on the junction area, determining its capacity), at least three orders of magnitude greater than with the proportional mode, and comparable with the electron gain of the photomultiplier.

A Geiger-mode avalanche photodiode (GAPD) can be used as a photon counter (acronym SPAD is encountered for *Single Photon Avalanche Diode*). Unfortunately, such a device has a quite significant drawback which is greatly reduced dynamics – on the

[5]This is a legitimate assumption as the relative voltage drop across the junction resulting from the discharge is small and non-linear nature of the junction capacitance is not crucial. Nevertheless, this simple model was turned out to be inaccurate; this issue will be described in next sections of this paper.

one hand by the background of dark counts, and on the other by re-charging time after the avalanche discharge, which is the dead time of the detector. The dead time and the saturation effect associated with it is a significant flaw of GAPD in comparison to photomultipliers. These retain high linearity over a wide range of light level, allowing also to work with fast multi-photon pulses.

2.2 MAPD – an array of avalache photodiodes

The basic disadvantage of the avalanche photodiodes operating in Geiger mode – low upper limit of their dynamic range (the limit of the counting frequency) – has been virtually eliminated in a device called the Multipixel Avalanche Photodiode (MAPD)[6].

The idea of the MAPD

The essence of the MAPD design is to divide the avalanche photodiode structure into a number of cells (pixels) with their own quenching resistors and working independently of each other, but connected to a common output (Figure 2.3)[7]. With a separate serial resistors, a detection of a photon in one pixel does not affect the rest of the structure. The resulting device shows a number of important advantages in comparison to a single GAPD:

- The MAPD has much higher counting rate limit. The dead time associated with the junction re-charge from V_{br} back to V_{op} applies only to this cell, where an avalanche was triggered, while other ones are constantly able to detect another photon.
- A simultaneous detection of multiple photons is possible. It will be shown that the MAPD is a quasi-analog device, where the response amplitude is proportional to the quantity of cells illuminated by a photon.
- The MAPD can have a large area. In case of a single GAPD an increase in the area over a fraction of mm^2 can cause an increase in the dark rate to a level practically

[6]From this point, we will sometimes call this device simply a ‘photodiode’, as long as the context allows it. One should pay attention to some chaos, which – so far – appears in the naming of this device. It happens that the same abbreviation is used for slightly different structures by various institutes or producers, or that the same device is sometimes called differently. The Author decided to use the ‘MAPD’ abbreviation to the whole family of devices operating on the principle being presented.

[7]There are innovative solutions without quenching resistors, and without any dead areas within the structure, enabling pixel density in excess of 100,000 per square millimeter, which is unreachable for other technologies. They are called *Micropixel Avalanche Photodiodes* and are the subject of current research – also carried by the Author – and generally are not to be subject of this book.

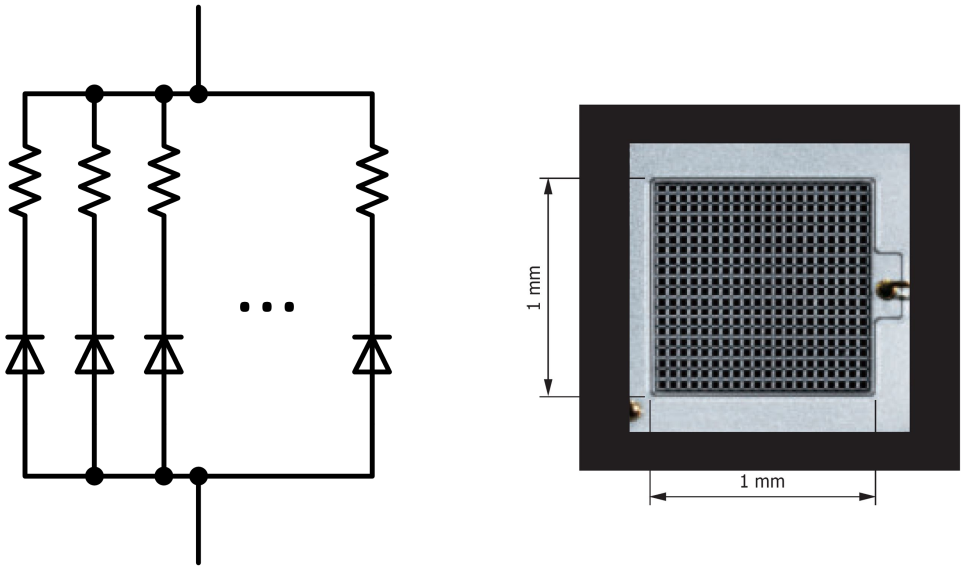

Figure 2.3: MAPD schematic diagram(left) and a photograph of the sillicon structure with visible pixels. A 400-pixel MPPC device by Hamamatsu is shown.

obstructing the detector. In the case of MAPD it matters only that the dark rate does not reach significant values in a single pixel – and the pixel size is always small, regardless of the size of the entire structure.

Technology

The MAPD is a monolithic semiconductor device – the photodiode array is formed on a single silicon die together with quenching resistors. Depending on the desired spectral characteristics it can be made on a p-type substrate (for larger wavelengths) or an n-type one (for small wavelengths), but in modern commercial solutions it seems that the second technology is strongly dominating[8]. For the creation of MAPD, a technology developed in the late 80th and 90th in the CPTA institute in Moscow and called MRS-APD (*Metal-Resistor-Semiconductor*) [13][19] was crucial. It allows to put quenching resistors directly on the surface of the photodiode[9]. In modern designs, the resistors are usually placed at the edges of the pixels, and the top electrode is formed as a grid over the dead areas between pixels, so that it makes possibly smallest obstacle to the incident light.

A single pixel is a square of about 10 to 100 μm wide, and the whole structure, containing from 100 to tens of thousands of pixels[10], covers an area of 1 to tens of mm^2.

[8]Unfortunately, the information about the technology provided by the manufacturers is usually very limited.

[9]Photodiodes made using this technology have already been used in experimental applications [3].

[10]The upper limit of the number of pixels seems to be still growing, the bottom is rather constant – MAPD with too few pixels loses its advantages.

The number of pixels in a specific device depends on its purpose – for low light conditions, 'coarse' solutions are better suited (higher sensitivity and gain), while working on a stronger light needs larger number of pixels (higher saturation level) .

The manufacturers generally do not provide informations about the semiconductor structure, but some of the parameters are to be fairly easy determined. For example, the MPPC photodiodes produced by Hamamatsu, where general doping charastericties is published [29] (Fig. 2.2), the junction thickness can be estimated basing on its capacitance. Assuming relative dielectric constant for silicon $\varepsilon_r = 11.66$ [17], the measured capacitance $C_{pix} = 90$fF and horizontal dimensions of the structure specified by the manufacturer, the junction thickness should be about 1.8 μm.

The same way, one can determine the concentration of dopants in the junction area, using the characteristics of the junction capacitance $C_{pix}(\Delta V)$. The junction thickness W_d is a function of the applied voltage and the doping level, and is given by:

$$W_d = \sqrt{\frac{2\varepsilon_0\varepsilon_r(V_d + V_r)}{e}\left(\frac{1}{N_a} + \frac{1}{N_d}\right)} \,, \tag{2.5}$$

where V_d is the diffusion voltage, V_r the reverse bias voltage[11], e is the electron charge, and N_A and N_d the concentrations of dopants, acceptor and donor, respectively. Assuming that $V_r \gg V_d$ and $N_a \gg N_d$ (this comes from the junction structure – see figure 2.2), we can write:

$$N_D = \frac{2\varepsilon_0\varepsilon_r \cdot V_r}{e \cdot W_d^2} \,. \tag{2.6}$$

According to the measurements [25], full depletion of the junction occurs at a reverse voltage $V_r \cong 20$V. On this basis, the value of N_d in the junction area can be estimated to be $8 \times 10^{15} cm^{-3}$. Of course, this calculation is valid for an individual product – an MPPC photodiode by Hamamatsu.

At the end of this short technology description it should be mentioned that not all pixels of the structure must be always connected to common terminals. There are also multi-channel solutions, in which the pixel array is divided into several subgroups with independent terminals (often separate silicon structures mounted in a common housing are used [23]). These devices can be treated as an equivalent to multianode photomultipliers.

[11] A positive value.

2.3 MAPD characteristics

Operating principle

The process of the detection of a photon in the MAPD can be divided into three phases:

– a photon absorption (and photoelectron drift),

– avalanche carrier multiplication (and discharge of the junction capacitance),

– junction recharge (which means a current flow in an external circuitry).

Photon absorption (photoelectric effect) can occur in any area of the semiconductor, however, the only interesting cases are these where the phenomenon occurs in the depletion layer, where the existence of electric field ensures that the carriers quickly access the multiplication layer (an absorbption of a photon in the multiplication layer itself is also possible). The thickness and depth of the junction will affect the photodiode spectral sensitivity characteristics.

Avalanche multiplication has a form of a self-sustaining avalanche, whose development is limited by the quenching resistor. During the discharge, the only significant source of the charge is the junction capacitance of the pixel. After the discharge, which leads to voltage drop down to V_{br}, the avalanche decays.

Due to the Geiger mode operation, each pixel can respond only to a single photon at a time. Therefore, it is required that the incident light has possibly uniform distribution over the entire active area to fully utilize the dynamic range of the MAPD – in particular, the device will be extremely inefficient with a spot illumination. When an MAPD operates with a fiber input, its size should be selected regarding the fiber diameter (for example, in the ND280 detector of the T2K experiment, the fiber of 1 mm diameter works with square MAPD structure of 1.3×1.3 mm – a small margin was left due to imperfect positioning of the fiber and the conical shape of the the light beam leaving it).

Junction recharge is the last of the key steps in the process of light detection. It causes electrical current to flow outside the pixel. This current is divided into two circuits:

– external measurement circuit (that means – beyond MAPD terminals),

– internal circuit consisting of all pixels in the MAPD structure.

The ratio between the two components is determined by the ratio of internal resistance of the MAPD and resistance of the external circuit (Fig. 2.4).

At this point, the second component of the recharging current should be described. The current flow through all pixels causes partial discharge of the junctions, which is negligible when only single pixel is activated, but may be significant in the case of a strong pulse of light, where a lot of pixels are triggered at the same time. Reducing of the bias voltage of inactive pixels will result in deterioration of the detector linearity. For this reason, it is important to minimize the contribution of this component of the recharge current. In practice this means a need to keep the external circuit impedance as low as possible when working with strong light pulses.

It should also be noted that while the time constant of a single pixel recharge depends in principle only on the pixel capacitance and quenching resistance, a large-scale time constant of the whole device (which is also the time constant of the output pulse tail) will be subject to the resistance of the external circuitry. This is another reason to minimize the external circuit resistance[12].

It should be noted, however, that excessive reduction of the load resistance of the MAPD causes a decrease in the output signal voltage and makes the signal-to-noise ratio worse when working with voltage amplifier. The experience of the Author shows that the optimum load resistance is comparable or slightly larger than the series resistance of the whole MAPD structure.

Basic MAPD parameters

It turns out that quite a complete description of the behavior of the MAPD can be obtained by giving only few basic parameters. Most of them are commonly used in electronics, but sometimes they must be understood in a specific way.

Breakdown voltage (V_{br}) defines the demarcation point between proportional and Geiger-mode operation of the diode – it is the voltage, above which an avalanche of carriers has the ability of self-sustaining. The value of the V_{br} is distinctly dependent on the junction temperature, with a slope of about 50 mV per Celsius degree[13]. Another characteristic

[12]This is true under the assumption that we want to shorten the output pulses as much as possible. It has to be mentioned that MAPDs often work with voltage amplifiers, whose construction is relatively simple and usually give greater design freedom compared to the charge amplifiers, commonly used as preamps with low amplitude pulsed signals. The relatively high output amplitude of the MAPD does not require a charge amplifier to be used.

[13]This particular value was measured by the Author for the Hamamatsu MPPC. Although the intention was to describe the theoretical basics of MAPD first, then the methods of measurement, and finally the results – this structure will be impaired from time to time. In fact, the research of the MPPC was an

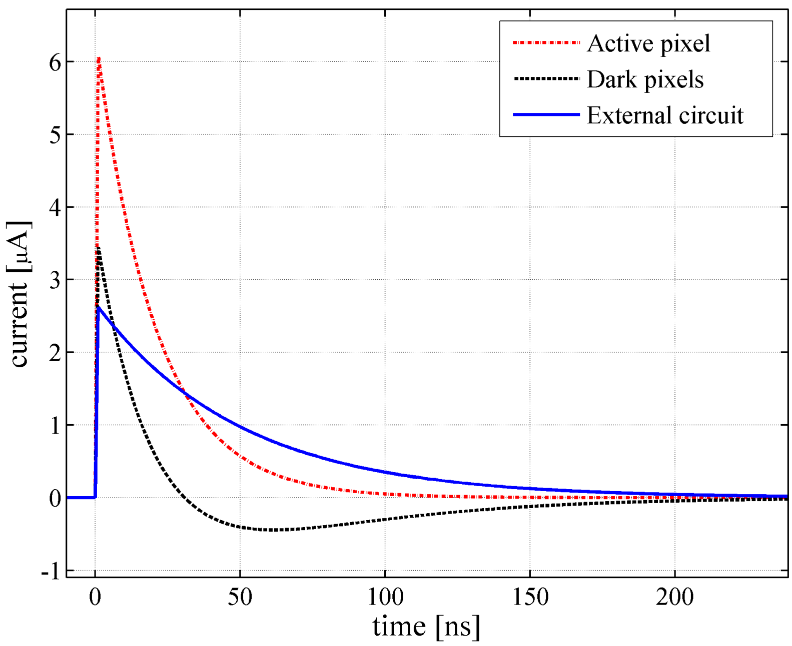

Figure 2.4: MAPD pixel recharge process following the avalanche discharge. It is assumed that a single pixel has following parameters: $R_{pix} = 230$ kΩ, $C_{pix} = 90$ fF, total pixel count $N = 667$, and load resistance $R_{out} = 470$ Ω. $\Delta V = 1,3$ V.

feature of the breakdown voltage is a considerable production dispersion. Due to this fact, an individual measurement of V_{br} is required for each item, and operating voltage must generally be individually selected.

With MAPD, a very frequently used parameter is the overvoltage: $\Delta V = V_{op} - V_{br}$, where V_{op} is the bias voltage of the diode. It turns out that most of the phenomena occurring in the MAPD are dependent rather on ΔV than on the absolute bias voltage.

Photon detection efficiency. The probability of electrical pulse generation in response to a single photon incident on the MAPD structure is described by the Photon Detection Efficiency (PDE). The PDE is the product of probabilities of three events that must occur in order to generate an electrical signal from a photon:

– The photon has to meet the active area of the structure. Individual pixels are separated from each other by a dead area and the ratio of the active pixel area to the total area of the structure is called the Fill Factor (FF). This parameter is strongly dependent on the pixel size and for fine-grained small detectors (small pixels) it may drop to about 20%.

iterative job, and it often happened that the measurement results affected the theoretical assumptions, models, and, of course, made a need for further measurements.

– A photoelectric effect must take place in the junction area. The probability of such an event is called Quantum Efficiency (QE). This parameter is a function of the incident light wavelength and the maximum sensitivity depends on technology used, junction thickness and thickness of the 'dead' silicon above the junction. The value of the quantum efficiency for described detectors reaches a level of about 90%.

– The generated carrier must reach the multiplication layer (rather than recombine during its drift). The probability of avalanche generation is denoted as P_{av}.

Finally:

$$\mathrm{PDE} = \mathrm{FF} \cdot \mathrm{QE} \cdot P_{av} \ . \quad (2.7)$$

The maximum PDE value in typical products depends mainly on the size of a pixel and is included in the range o fless than 20% for fine-grained detectors to 80% for the models with a small number of large pixels.

The value of P_{av}, and therefore the PDE, is strongly dependent on the overvoltage, and increases with the voltage up to saturation when P_{av} approaches to values close to 100%. In a typical range of operating voltages, the PDE dependence on overvoltage can be considered as linear, and the use of a quadratic approximation already gives a very good fit [25]. The PDE value (at constant ΔV) is practically independent of the temperature of the MAPD structure.

Electron gain of the MAPD is defined the same way like for a single avalanche photodiode operating in Geiger mode – as the number of carriers (of one type) in a single avalanche. Alternatively, one could define the gain as a large-scale parameter, similarly to analog detectors – as the ratio of the total number of generated electrons to the number of photoelectrons.

The delicate difference between the two definitions is visible at high detector occupancy – when more than one photon arrives at the same time to a single pixel (the response of the pixel is a single, standard avalanche – some photons remain unregistered) [14]. The details of this phenomenon will be described below.

The gain for $\Delta V > 0$ can be calculated using the same formula as in case of an ordinary GAPD (equation 2.4). For $\Delta V < 0$ $G = 1$ (but it is often assumed that in this range $G = 0$, which in fact is not a significant difference while normal values of G are higher by many orders of magnitude). With the bias voltage just below V_{br}, the diode is operating in the proportional mode, which means that the 'corner' of the gain characteristics is in fact

[14] The practice shows that the use of the first of the two definitions can avoid some of the misunderstandings in the description of the MAPD and thus it will be used later in this book.

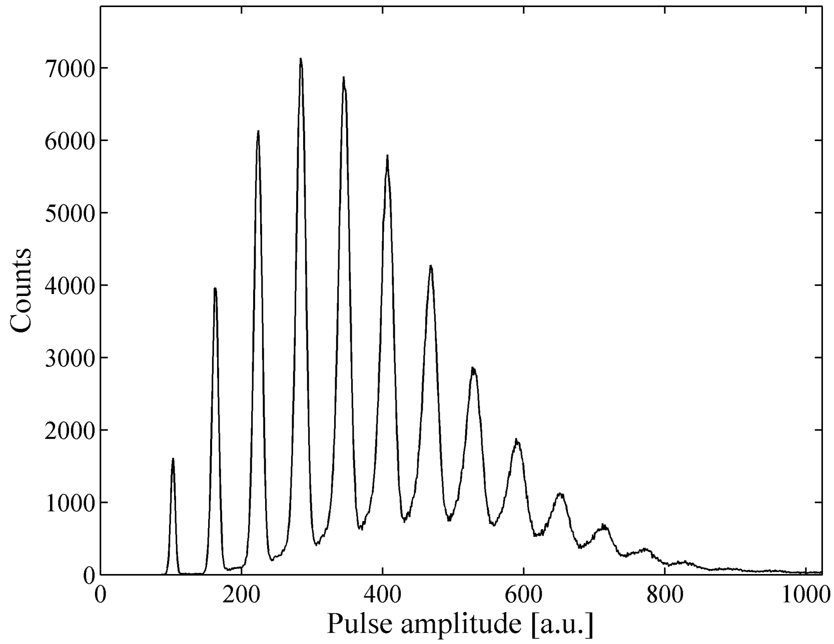

Figure 2.5: A typical histogram of output pulse amplitudes for an MAPD illuminated by weak light pulses. The events associated with activation of different numbers of cells are clearly distinguishable. With stronger light, the discrete nature of the response is lost, mainly due to the summing of gain deviations of individual pixels

somewhat smoothed. Extrapolation of the linear part of the characteristics of $G(V_{op})$ to the intersection with the horizontal axis is a commonly used method of determining the breakdown voltage (V_{br}) of the diode.

The gain values achieved by modern MAPDs are in the range of $10^5 - 10^7$. This value depends primarily on the pixel size.

A characteristic feature of the MAPD in comparison to photomultipliers or proportional-mode APDs are extremely small gain fluctuations (Figure 2.5). In the case of photodiodes operating in the proportional mode, the gain is dependent on the random nature of the processes taking place in an avalanche. In Geiger mode, the gain value depends only on the capacitance of the junction, which is at first stable, and at second – not significantly different among individual pixels. However, significant signal fluctuations come from the correlated noise, as described on page 24.

Recovery time. The time needed to recharge the pixel after an avalanche (recovery time, τ_r) can be treated as a dead time when the pixel is not capable to detect following photons. This effect reduces the amplitude of MAPD under high light intensity. Thus, the effective number of fired pixels will be smaller than the number of photons hitting the MAPD structure at the same time. To illustrate this, the following formula is presented in various publications:

$$N_f = N_{tot} \cdot (1 - e^{-N_\gamma \cdot \mathrm{PDE}/N_{tot}}) \tag{2.8}$$

where N_f denotes a real number of activated pixels, N_{tot} the total number of pixels in the device, N_γ the number of photons coming at the same time and PDE the photon detection efficiency.

In practice, the idea of 'photons coming at the same time' is applicable only when we analyze the response of the device to very short light pulses[15]. We can assume that 'at the same time' means events occuring in less than τ_r, assuming that at this time the pixel is completely dead, and then immediately becomes fully operational. However, charging a capacitor, which we are dealing with, is, of course, not an instant phenomenon, but a process, which takes some time. This means that the pixel is 'completely dead' only during the avalanche, and then its gain begins to gradually grow as the junction voltage increases. If the pixel is triggered during this time, it will generate a response, but with a reduced amplitude.

Following the above assumptions, an effective value of the MAPD gain under heavy continuous load can be calculated from the time distribution between successive interactions of photons $p(t)$ and the relationship between the gain and the charging time $G(t)$:

$$G_{eff} = \int_0^{+\infty} p(t) \cdot G(t) dt \ . \tag{2.9}$$

Assuming that absorptions of particular photons are independent events, the time between these events should have an exponential distribution. The dependence between gain and time closely follows the charging curve of the capacitor by a series resistance:

$$G(t) = G_0 \cdot (1 - e^{-t/\tau_r}) \ . \tag{2.10}$$

As a result,

$$G_{eff} = \int_0^{+\infty} f_{pix} \cdot e^{-f_{pix} \cdot t} \cdot G_0 \cdot \left(1 - e^{-\frac{t}{\tau_r}}\right) dt \ , \tag{2.11}$$

which finally leads to following formula:

$$G_{eff} = G_0 \cdot (1 - \frac{f_{pix}}{f_{pix} + 1/\tau_r}) \ , \tag{2.12}$$

where G_0 is the gain of a fully charged pixel, $f_{pix} = f_\gamma \cdot \frac{\mathrm{PDE}}{N_{tot}}$ is the counting frequency of a single pixel (f_γ – the rate of photons coming), and τ_r is the time constant of pixel recharge, which is a measure of the pixel dead time. A typical value of τ_r is approximately 10 ns

[15] Although, this situation is quite common for scintillating detectors.

(with a pixel capacitance of approximately 0.1 pF and quenching resistance approximately 100 kΩ)[16]. Due to the technology the resistors are made (polysilicon), the resistance varies quite strongly with temperature, which causes some changes of the dead time [10].

Equation 2.12 does not include another phenomenon – a dependence between the PDE (and more precisely the P_{av}) and ΔV. The probability of triggering of a not-fully-charged pixel is smaller than a fully-charged one and as a result the actual signal is slightly lower than provided by the equation. The Author could not find an analytical solution of this case, but very good results can be obtained by introducing an effective time constant – τ_{eff} instead of τ_r. For a linear dependence of PDE(ΔV), $\tau_{eff} \approx 1.4\tau_r$. It should be noted, that in the case of use of τ_{eff} instead of τ_r, the value of G must be meant in accordance with the definition suitable for analog detectors – as a ratio of the total number of generated electrons to the number of primary photoelectrons[17].

Another effects that are not taken into account in this analysis are the phenomena associated with correlated noise, which modify the distribution of time intervals between the appearance of successive photoelectrons. It can be assumed that the actual dynamic range of the diode is lower than the calculated value by a factor at least equal to the CT+AP fraction which is described on page 25.

Figure 2.6 presents the dependence of the detector current on the number of incident photons per time unit.

Finally, it should also be mentioned, that in the case of strong light pulses, the effective value of τ_r may increase for high load resistance, as described on page 17.

Time resolution is one of the strongest points of the MAPD. Due to the small junction width (single μm) and strong electric field, both carrier drift and avalanche development time is very short. Measurements [22] indicate the time resolution of 100 ps FWHM for a complete system with preamp, achieved even with single photons.

[16]The values measured for the MPPC diode (Hamamatsu).

[17]This is because we identify some phenomena – like the reduction of P_{av} – as gain changes. In fact they *are not* changes of electron gain.

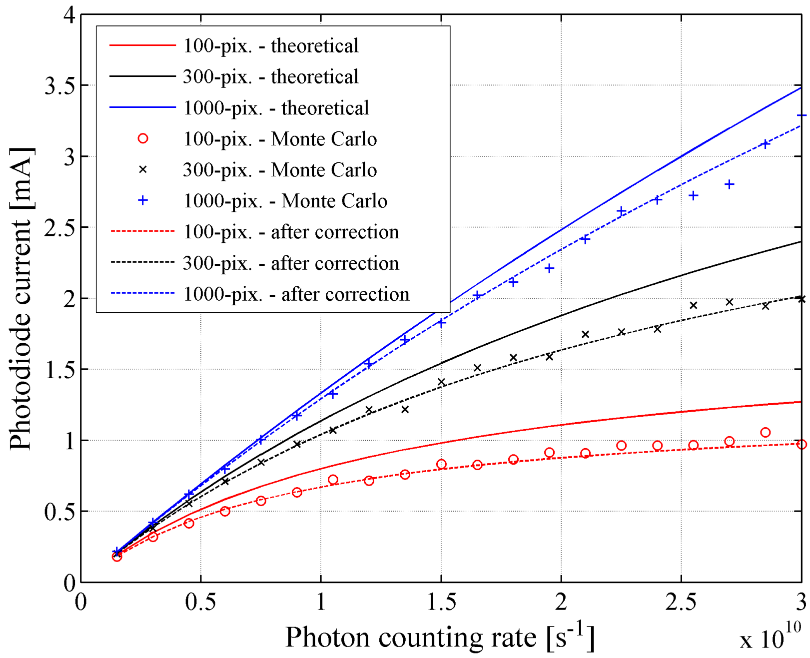

Figure 2.6: Dependence of the detector output current on the incident light for three different detector granularities; the plots show the results obtained analytically from the equation 2.12 (solid line), the data from the Monte-Carlo analysis taking into account the linear relationship of PDE(ΔV) (points) and the analytical results obtained after the introduction of τ_{eff} instead of τ_r (dashed line)

Parasitic effects

The main undesirable effect associated with MAPD operation is the noise. It can be divided into two main components:

- dark pulses, giving uncorrelated noise;
- correlated noise, consisting of two characteristic phenomena: crosstalk and afterpulses.

Dark pulses. Thermal generation of carriers in the depletion layer causes the development of carrier avalanches, identically with the case of a photon detection, and the formation of the so-called dark pulses at the output of the MAPD. So far, the high background of dark pulses (dark counts) is the biggest drawback of the MAPD, when compared to the photomultipliers. The MAPD structure with the active area of the order of one millimeter square gives approximately between 10^5 and 10^6 dark counts per second at room temperature, which is by orders of magnitude higher value than in case of PMTs. The dark rate is approximately a linear function of ΔV (which is directly related to the characteristics of P_{av}) and an exponential function of temperature. Detector cooling can bring a measurable impact on reducing this effect (There are MAPD models with built-in Peltier cooling [5]).

Cross-talk (CT) is one of two mechanisms of correlated noise. It is related to an optical coupling of neighboring pixels. As a result of relaxation in atoms excited during the build-up of the avalanche, one photon will be generated for about 10^5 generated carriers. Then, this photon can be absorbed in neighboring pixels and cause an avalanche. The dependence of CT effect on ΔV can be assumed to be quadratic (linear dependence of number of photons generated from the electron gain and a linear dependence of P_{av} on voltage), which is confirmed by experiments [25]. Common CT values under typical operating conditions are within 5 - 25%[18]. Given number should be understood as the fraction of avalanches caused by crosstalk among the total number of registered avalanches. A characteristic feature of this parameter is that it is not constant for all pixels (CT is smaller for pixels at the edge of the structure, where the probability that the photons escape outside is higher). At constant ΔV, the crosstalk is independent of temperature. This means that, unfortunately, cooling of the device will not allow crosstalk reduction.

Afterpulses (AP) arise as a result of trapping of some carriers generated in an avalanche. Such carrier can be released later (often after a time much longer than τ_r), becoming the source of a new electron avalanche. A close square-type correlation was found between the fraction of afterpulses and ΔV [25][21]. Same as in the case of CT – the fraction of AP is independent of the temperature at a constant ΔV.

The time at which an afterpulse occurs is described by a combination of few exponential distributions with different expected values; they're associated with semi-stable quatum states with different life time. For example, in the case of MPPCs there were three overlapping distributions found, with time constants of 20 to less than 300 ns.

The afterpulse fraction for typical operating voltage ($\Delta V = 1.5V$) is about 10% for the measured MPPC model.

The correlated noise is the main cause of the amplitude fluctuation of the MAPD output signal. Thus, the oft-cited parameter is its total fraction, CT+AP, at the standard operating voltage. Note that this parameter will be further understood as the probability of generating at least one additional avalanche in response to one registered photon.

[18]The MPPC devices used in T2K experiment.

Table 2.1: A basic list of an MAPD and photomultiplier tube parameters

Parameter	PMT H8711 ($V_s = 800$V)	MAPD S10362-11-050C
Active area	4,2 x 4,2 mm^2	1 x 1 mm^2
Electron gain	$3,5 \cdot 10^6$	$7,5 \cdot 10^5$
Detection efficiency	25% (QE, 380 nm)	50% (PDE, 440 nm)
Dark rate (at room temp.)	$1,4 \cdot 10^3$ s^{-1} (79 s^{-1}mm^{-2})	$0,4 \cdot 10^6$ s^{-1} ($0,4 \cdot 10^6$ s^{-1}mm^{-2})
Signal fluctuations (σ_{rel} for 1 p.e.)	0.53 (1. dynode)	0.4 (CT+AP)
Time resolution	330 ps	200 - 300 ps
Linear range (gain change $\leq 5\%$)	$0 - 7,2 \cdot 10^9$ s^{-1}	$0 - 4 \cdot 10^9$ s^{-1}

MAPD parameters and its range of applications

MAPD is intended to be a substitute for the photomultiplier tubes, primarily in various types of scintillation detectors. Therefore, it seems appropriate to compare these two devices. Such a comparison is shown in Table 2.1[19]. The chosen representatives are a 400-pixel MPPC (Hamamatsu) S10362-11-050C and H8711 photomultiplier from the same company [14]. This model is a multi-channel photomultiplier and is often used to acquire the optical signal from fibers, widely used in high-energy physics experiments [33] and seems to be a good subject for comparison with mentioned photodiode.

The numbers in the table should be treated with caution. Both photomultiplier and MPPC included in this comparison are made in several versions (they differ in spectral sensitivity, etc.), whose parameters are slightly different from those shown here for the basic models.

For clarity, the technical parameters, which are normally slightly differently defined for both devices, were brought to a homogeneous form.

It's easily noticeable that the only significant difference between the photomultiplier and MAPD is the dark count rate – if we assume different active areas, the PMT is more than three orders of magnitude less noisy than the MAPD. Other parameters of the two instruments are similar. A significant difference in the dark current can seem devastating for the MAPD. In practice, however, the high background does not need to be a real problem. It's because of at least two reasons:

– Most of the dark pulses are single-photon ones. Pulses of light coming from the scintillator are usually a bit higher, and proper setting of the discrimination level

[19] The data for multi-channel photomultiplier represents a single channel.

Table 2.2: General comparison of selected characteristics of an MAPD and photomultiplier tube

Attribute	**PMT**	**MAPD**
Electron gain	high $10^5 - 10^7$	high $10^5 - 10^7$
Detection efficiency	medium $10 - 40\%$	medium-high $20 - 80\%$
Dark current	low	high
Active area	any up to 0,25 m^2	small-medium 1 - 50 mm^2
Temperature impact	limited (dark current)	essential (V_{br})
Supply voltage	high ($\approx$ 1kV)	moderate ($\approx$ 100V)
Power consumption	considerable (voltage divider)	negligible
Case size	big	small
Mechanical strength	poor	high
Magnetic field immunity	poor	high
Radiation hardness	high	moderate
Light immunity	poor (damage possible)	high
Price	high	moderate

solves the problem quite efficiently.

– Often it is possible to supply the scintillator with two photodetectors (typically – the two ends of an WLS fiber). This allows an elimination of the dark pulses by coincidence circuits.

The comparison of the gain fluctuations of both devices requires a short comment. While this statement is reliable for a large number of photons, at low intensities we have to remember that a completely different kind of phenomena cause these fluctuations. For the photomultiplier, the variation of the number of electrons generated on the first dynode can result in fluctuations of the signal at a level which could be lower than the single-photon pulse. In case of the MAPD, these dispersions have a discrete character and almost always manifest themselves in the form of increasing the amplitude of the signal exactly by one p.e. (excepting a low fraction of early afterpulses getting from incompletely charged pixels).

Table 2.2 shows the descriptive summary of the characteristics of both types of detectors. On its basis one can draw the following conclusions:

1. MAPDs are unsuitable where a large area of the detector is needed. They are rather intended to be used in cooperation with fibers (also WLS fibers and Sci-Fis [33][32]).

2. A number of features such as small size, relatively low operating voltage, immunity to accidental strong light illumination and high mechanical strength, make MAPD detector much more convenient to use than the photomultiplier.

3. The impact of large dark rate should be analyzed each time before starting a design, but it does not have to be a real problem in practice.

4. Although this is not a technical parameter, one can not forget the rather large difference in price, with the benefit to MAPD. Considering continuous development of MAPD technology, it should be assumed that the difference will be yet more distinct over time.

These conclusions concern primarily to the application of MAPD in scintillating detectors, which currently represent the main potential field of its applications.

2.4 MAPD modelling

The creation of an appropriate model is crucial for the analysis and simulation of all instruments. For MAPD, used models can be divided into two groups: electrical and physical models.

Electrical models

The electrical model allows to simulate the shape of the electrical signal resulting from avalanche discharge of the MAPD cells (pixels), without investigating the details of the process of the avalanche development. In contrast to more complex physical models, it can be easily utilized in the *Spice*-type software for electronics simulations, making it especially useful in the design of the front-end electronics; it is also necessary for the calibration of the measuring apparatus for MAPD tests. Electrical model describes the process of the pixel charging, which is crucial for the analysis of the operation at high rates. In the end, together with models that describe the physical phenomena that cause an avalanche, it makes it possible to create a complete Monte-Carlo simulation model [25].

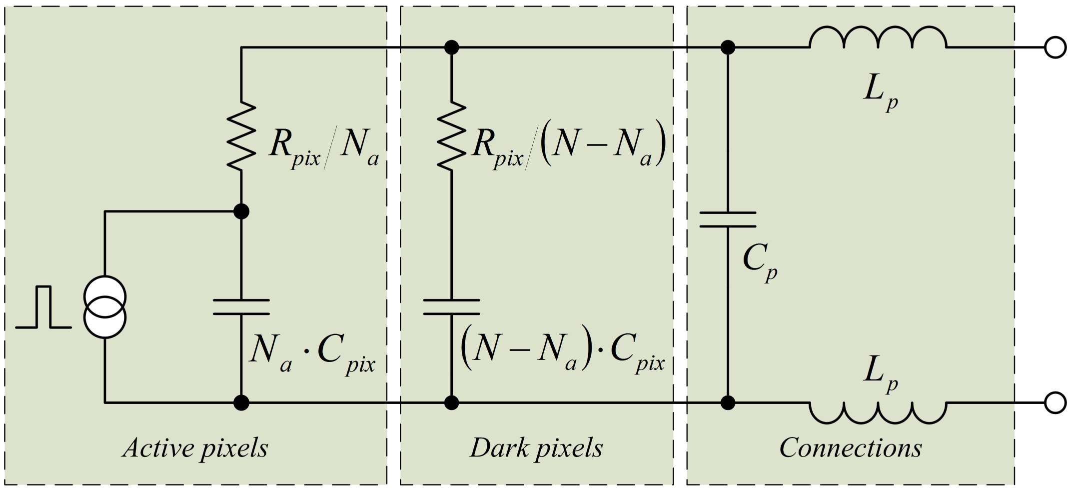

Figure 2.7: The small-signal model of the MAPD with parasitic elements. N_A is the number of active pixels. Charge generation is simulated by a current source producing a short pulse with total charge of $N_A \cdot C_{pix} \cdot \Delta V$. C_{pix} and R_{pix} are the parameters of a single pixel. N is the total number of pixels. C_p and L_p describe the parasitic capacitance and inductance associated with the terminals

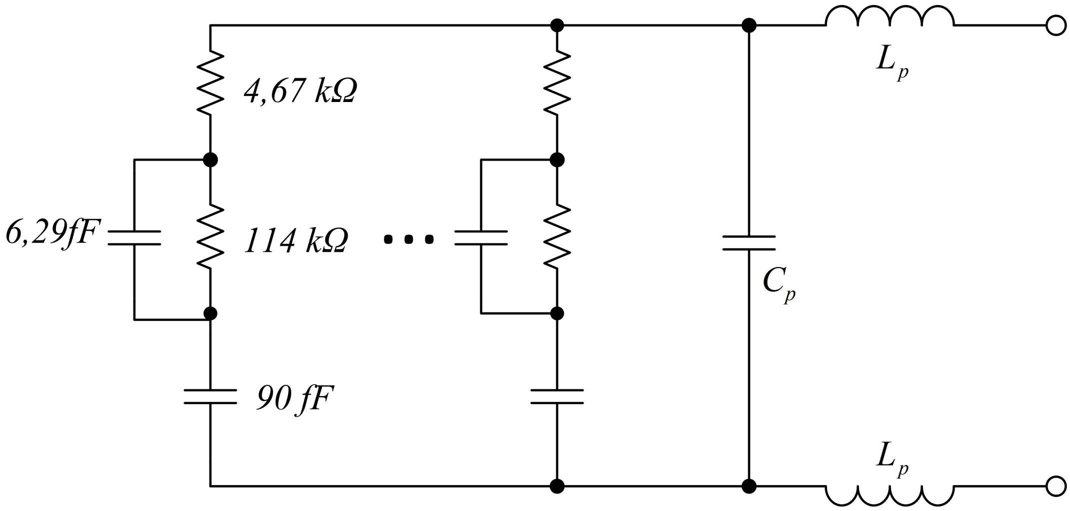

Figure 2.8: More accurate MPPC electrical model taking into account the parasitic capacitance of the quenching resistors, based on the measurements performed at the Warsaw University of Technology. The values of the elements are related to a single pixel.

The basic model shows the MAPD as a number of diodes with their serial resistors. Since the diodes are reverse polarized under normal conditions, they are usually reduced to junction capacitances (figure 2.7). The resulting circuitry can be treated as MAPD small signal model.

In order to analyze the response of the device to an avalanche, all pixels of the MAPD are usually divided into two groups – a group of pixels, in which the discharge has occurred, and a group of pixels, in the resting state ('dark' pixels). The avalanche discharge is usually represented by an appropriate current source.

Due to the linearity of the model, the absolute value of the voltage on the capacitor is not important. Often the value of V_{br} is subtracted from the bias voltage and one operates only with the value of ΔV.

If more precise model is needed, some parasitic elements are added – the terminal capacitance and inductance of the leads (due to the small values of these parameters, it is important to take into account corresponding parasitic elements in the measurement system). An interesting parameter is the parasitic capacitance of the quenching resistors [8]. Figure 2.8 presents an MPPC model with element values found basing on the time characteristics of the output pulses and a spectral impedance characteristics measured using a vector impedance meter.

Physical phenomena models

Physical models allow an analysis of the processes associated with the development of the electron avalanches and describe all of their sources (photoelectric effect, dark generation, crosstalk and afterpulses).

Figure 2.9 shows a basic diagram for simulation of the basic phenomena occurring in the MAPD. Each of the blocks shown on the diagram requires a separate description. In practice, so far, first of all behavioral models are used, which, while not going into the essence of the phenomena, allow them to be easily simulated. Examples are the PDE or CT+AP models used in the simulations [25] defining these values in relationship to the overvoltage. An example of a model based on physical evidence will be presented later in section 6.2, with the analysis of the phenomenon of dark pulses.

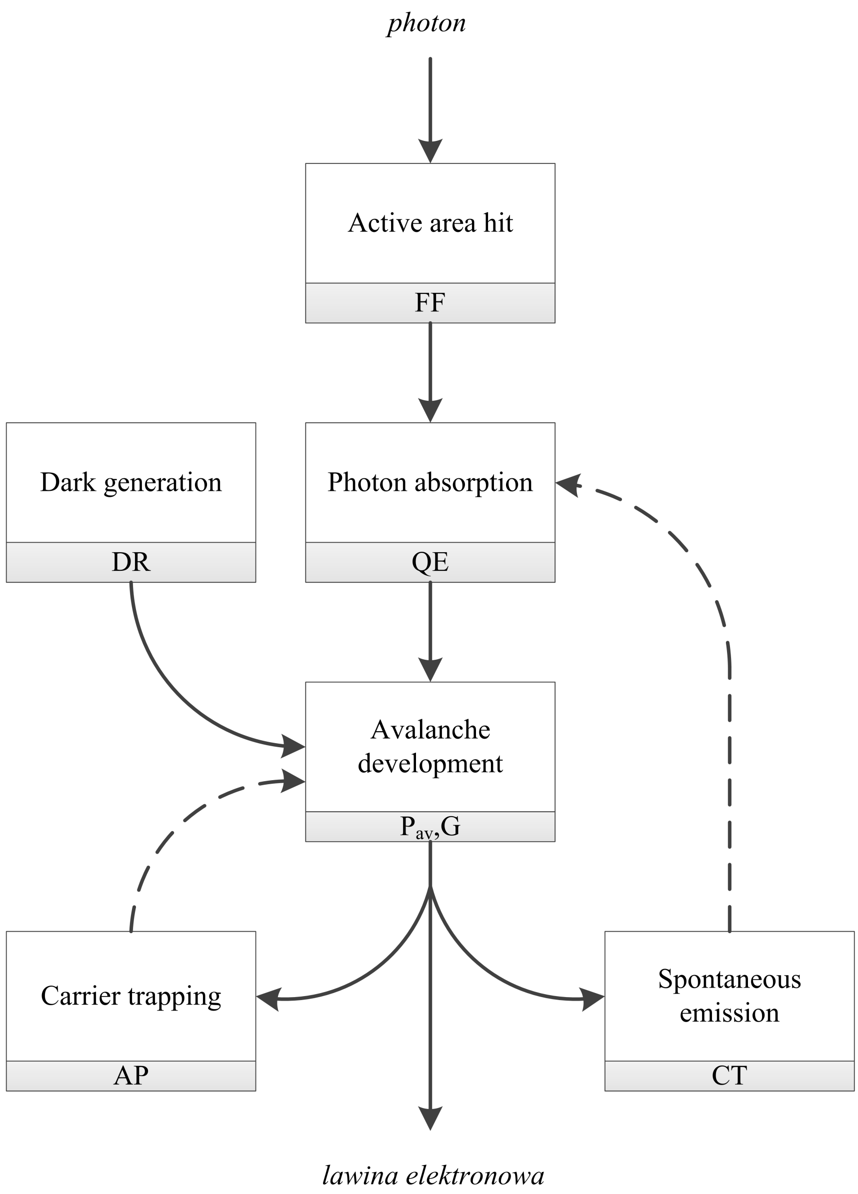

Figure 2.9: General scheme of physical phenomena modelling, responsible for a single pixel, with the basic parameters describing different phenomena. There are at least two feedback loops in the model (shown by dashed lines); they are responsible for correlated noise, which has a form of the formation of secondary avalanches – appearing in other pixels or later. Note that some of the parameters depend on bias voltage, so their values will vary during pixel recharging after an avalanche discharge

2.5 Market offer

Multipixel avalanche photodiodes are now produced at least by a few companies around the world, including Hamamatsu [29][15], Amplification Technologies [4], AdvanSid [1][2], SensL [23][24] and Voxtel [27], but Hamamatsu seems to be the only big company among them. MAPDs are available under various market names (the most common – SiPM – Silicon Photomultiplier or MPPC – Multi-Pixel Photon Counter – in the case of Hamamatsu[20]). There is a very fast progress observed in the offered solutions, both in terms of refining existing technologies, as well as creating entirely new ones. The most interesting ones include Micro-Pixel Avalanche Photodiodes without quenching resistors, developed in JINR (Dubna) [7], which were already mentioned. Of course, the rapid progress makes serious difficulties for the presentation of the current state of development of this technology and the latest knowledge related to MAPD research and modeling.

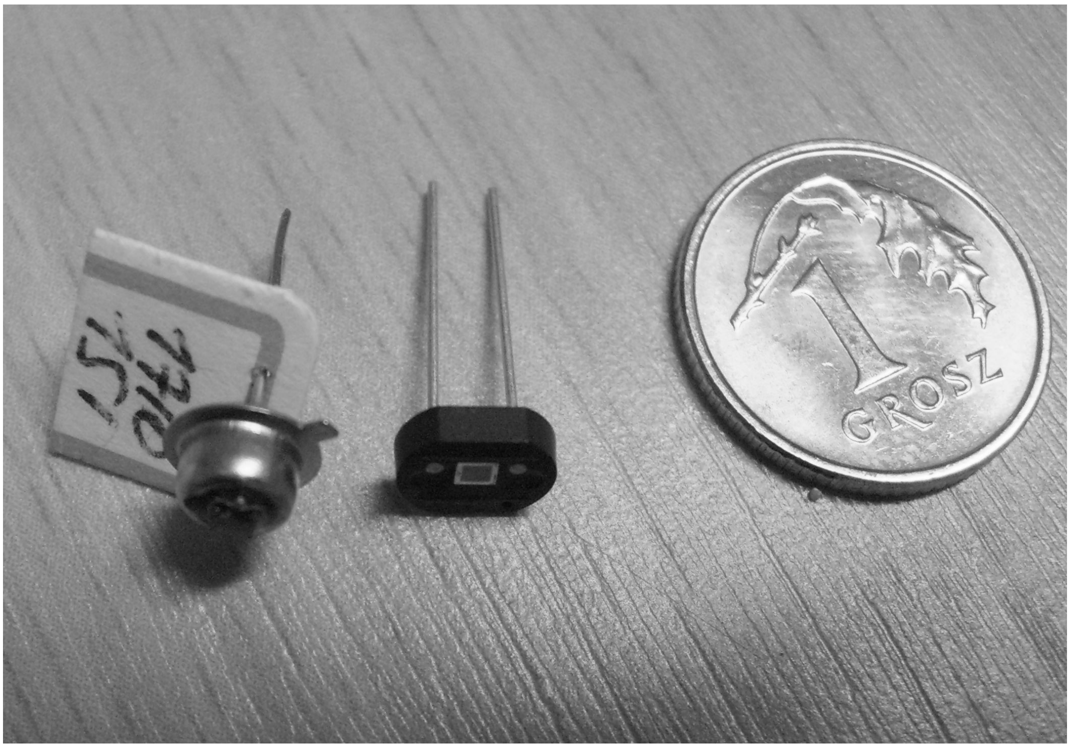

Figure 2.10: Two types of MAPD photodiodes: prototype series created in Dubna – Sipm in a metal housing (left), and Hamamatsu MPPC in a ceramic housing with flexible window (right)

[20]The vast majority of the experience of the Author with MAPDs concerns Hamamatsu product. In this book, MAPD and MPPC abbreviations will be used interchangeably – depending on whether it refers to MAPD as such, or to a particular Hamamatsu product.

Chapter 3

MAPD measurements

3.1 MAPD measurements description

The aim of the study

The introduction of a new type of item (in this case the MPPC for the T2K experiment, or generally the MAPD) to a wide market requires its characteristics to be accurately investigated. Manufacturer's data are often insufficient, incomplete, and most of all they are unverified. For this reason, the use of MAPD in new devices, especially to a large scale as in the case of the T2K experiment, requires a series of tests, which are independent of the manufacturer's data. In addition, these studies should be conducted simultaneously by several institutions to eliminate any mistakes[1]. On the other hand, the lack of trustworthy information on the reliability of the product and the quality of mass-production requires at least a rough testing of each element intended for installation in the target application.

Detailed and screening measurements

Referring to the main objectives of measurements, there appears a natural distinction between detailed measurements (deep and accurate, for a small number of items) and screening (coarse, but involving the entire production series). This distinction does disappear with some measurements (eg, distributions of individual parameters can be regarded as the result of detailed measurements, but it is difficult to get reliable results here without testing a large number of items).

[1]Some measurements carried out for the T2K experiment preparation used a selected sample of few tens of MPPCs, which were exchanged between involved institutions. In addition, the statistics of a greater number of elements were compared, as well as the final results.

Detailed measurements are carried out to accurately examine the device characteristics, such as the dependence of various parameters on the supply voltage and temperature. A strict control of working conditions of the MAPD and changing them within reasonable limits are needed to perform specific measurements.

The detailed measurements are essential in the creation of the models of the device, allowing determination of their parameters, as well as a general verification of correctness of these models. In addition, the ability to control the operating conditions in an appropriately wide range allows to determine practical limits of the applicability of a given type of tested solution.

A characteristic property of the detailed measurements is the large number of tests performed with a single specimen under various conditions, allowing further determination of the characteristics of the device. Hence, the automation of the measurement process is highly desirable.

Screening measurements are performed to verify proper operation of units to be installed in the target application, or getting information on basic parameters (for MAPD the important parameter is, for example, the breakdown voltage – V_{br}). In contrast to the detailed measurements, the time-consuming examination of the dependences between various parameters is replaced by only one or few measurements under specified conditions. These conditions usually correspond to the operating conditions in the target application.

The screening measurements contribute to the study of the detailed properties of the element in a way – they provide information on characteristics such as production dispersion and reliability.

Due to the huge amount of measurements, the throughput of the measurement system and a high level of automation are particularly important, during the measurement as well as at the stage of data processing. Typically, the devices for screening tests are built as multi-channel systems, enabling simultaneous testing of several elements [30][31]. This allows to increase throughput, mainly due to paralleling most time-consuming process throughout the measurement procedure – setting the temperature of the structure after installing the element on the test bench. Also the reduction of the number of operator's interventions is not negligible – the whole batch is replaced every few minutes or even few hours instead of a continuous changing of single specimens.

Measurement methods

The characteristic features of the MAPD (first of all, very small fluctuations in electron gain) have become a base for a unique method of measuring of a plenty of various parame-

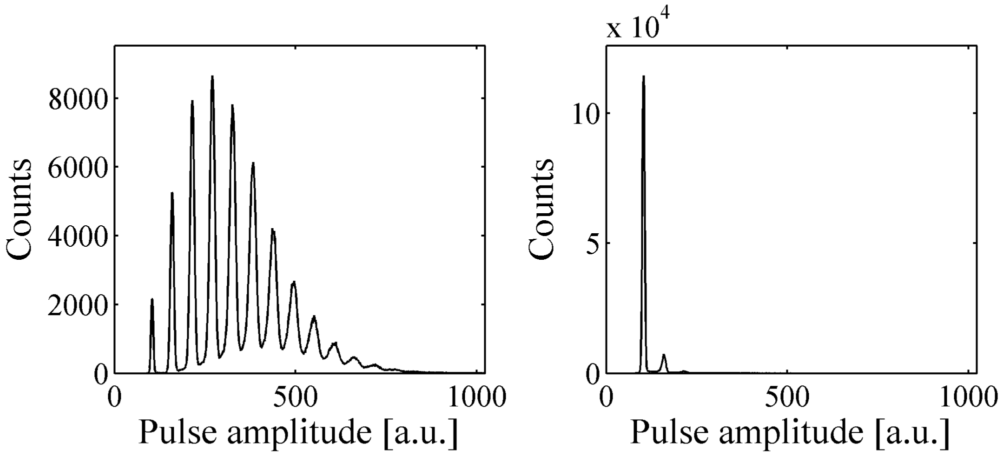

Figure 3.1: Pulse amplitude histogram obtained in low light conditions (left) and in darkness (right). $\Delta V = 1.09$V, $T = 25°$C. Hamamatsu MPPC was measured.

ters. A key element of this method is to build a histogram of the amplitudes of the pulses generated by the MAPD in the dark or when illuminated by low-level pulsed light (fig. 3.1). The resulting histograms, acquired in proper conditions, allow one to specify, among other parameters, the value of gain, dark rate, photon detection efficiency and correlated noise level. In practice, more 'classical' measurement methods (such as direct measurement of junction capacitance or series resistance of the device) are important rather as a complementary measurements or for verification of the data obtained from histograms.

Test conditions

Both histogram-based measurements and the majority of supplementary tests require precise control of the operating conditions, in particular the supply voltage of the MAPD and the ambient temperature. The limits presented below are estimated basing on the Author's experience with the MPPCs (Hamamatsu), but can be regarded as representative also for the devices offered by other vendors.

Supply voltage (V_{op}) should be stabilized with an accuracy not worse than 50 mV. Larger fluctuations, through the mechanism of change of the gain, cause blurring of the histogram peaks and deterioration of their separation. This has a negative impact on the accuracy of the calculation of virtually all parameters. The required adjustment range of the V_{op} value includes voltage from V_{br} to a value higher by few volts.

Ambient temperature requires a stabilization with an accuracy not worse than 1°C. With a standard slope of the $V_{br}(T)$ dependence, the change in temperature of 1°C corresponds to a change of voltage of about 50 mV (for MPPC). Determination of the temperature characteristics of the device requires the ability to control the temperature in the range of at least $\pm 10°C$ around a standard operating temperature.

Incident light intensity should be controlled with an accuracy of about 1% for photon detection efficiency (PDE) measurements. This will be further described in section 3.2. For another measurements, this parameter is not crucial.

3.2 Histogram-based measurements

Measurements with various light levels

Depending on the parameters to be determined, the histogram-based measurements are performed either with no light (these measurements are commonly called 'dark measurements') or with pulsed light illumination ('light measurements').

Dark measurements are performed without any external light source. In this case, the only source of the MAPD output signal is the thermal generation and the phenomena responsible for the correlated noise. Under these conditions, one can obtain valuable informations concerning not only the dark rate, but also the fraction of the correlated noise, and (with limited precision) the electron gain.

With no light, the MAPD output signal has a form of pulses appearing at random time, whose amplitude typically (but not always) corresponds to a single photon.

Light measurements are performed with low-level pulsed light illumination of the MAPD structure. A single pulse contains from few up to tens of photons emitted in a time not exceeding a few nanoseconds. Such conditions are imposed by a desire to obtain a histogram with possibly large number of well-separated peaks. Insufficient lighting will reduce the number of peaks, and too strong one – merging them into one shape. Pulse duration should be (if possible) significantly less than the τ_r value of the MAPD.

The main purpose of light measurements is to determine the electron gain and the PDE value[2]. The measurement performed with at least two properly selected operating voltages allows one to find the V_{br} value.

The signal from the illuminated MAPD consists of pulses with an amplitude corresponding to the number of photons[3], correlated in time with the light pulses, and an overlapping dark signal.

Obtaining the histogram

In the dark or low-light conditions, the MAPD signal has always a form of a series of pulses, which are usually clearly separated in time. The histogram is created by measuring the amplitudes (or more often integrals) of these pulses, representing the distribution of the charge generated by single events.

For the light measurements, the MAPD signal is gated synchronously with the operation of the light source to eliminate the dark pulses from the statistics as much as possible; the dark pulses would otherwise be a great majority of counts – a typical light pulse frequency during the measurement is of the order of a few or tens of kHz, and the dark rate is at $10^5 - 10^6 \mathrm{s}^{-1}$.

With dark measurements, the signal gating is also used, but this time it's more a side effect of the measurement method, which comes firstly from the unification of the apparatus, and secondly from the limit of its throughput (usually registering of hundreds of thousands of pulses per second is not possible). Usually a random trigger (ie uncorrelated with the signal) is used to open the gate. In more advanced solutions, it is possible to use the MAPD pulse for self-triggering (this will be described in section 3.2).

Regardless of lighting conditions, a philosophy, 'one gate – one measurement' is used – the signal, which is collected within the gate open period, is treated as a single pulse. This means that it is not possible to distinguish a number of pulses occurring in a very short time. If the signal is integrated, registered value of the integral is the sum of all pulses. In the case of a peak converter in place an integrator, the amplitude readout will be strongly dependent on the time delay between the pulses[4], which will result in a deterioration of the quality of the histogram (blurred peaks).

[2]The correct measurement of the PDE also requires a dark measurement to determine the dark rate and fraction of CT+AP (correlated noise). This will be described in more detail when discussing the data processing algorithms.

[3]We will use a notation n p.e. (photoelectrons) whenever we talk about pulse amplitude corresponding to n original electrons – regardless of the source of their generation. In this context, identifying them with photoelectrons is basically wrong, but the acronym is generally accepted and the Author is not going to change it.

[4]Because of the effect of pulse pile-up.

Electron gain and breakdown voltage calculation

The electron gain (defined according to the definition given in section 2.1) can be calculated basing on the distance between the histogram peaks (fig. 2.5).

In the simplest case, the distance between the peaks corresponding to 0 p.e. and 1 p.e. can be used, as they are the sharpest ones. In practice, a greater accuracy can be achieved with more distant peaks[5]. Before determining the positions of individual peaks, the histogram is usually smoothed or approximated by series or Gaussian functions.

The gain measurement has a relative character. To obtain the absolute value of the gain, the measuring device needs to be calibrated. This calibration turned out to be a complex and quite inaccurate process[6].

The determination of the breakdown voltage requires the gain measurement for at least two voltages which will be higher than the expected V_{br}. Since the dependence of $G(\Delta V)$ is almost linear, simple interpolation of the two points with a straight line should be sufficient to find the breakdown voltage. Unfortunately, the histogram data are of poor value for low gains (the peaks are close and unclear, which causes problems with their automatic recognition and accurate determination of their position) and measurements at relatively high ΔV have to be used for the determination of the V_{br}. However, under these circumstances, the method of finding of the V_{br} is ill-conditioned and very sensitive to variations in the input data. As a result, to obtain a precise measurement of V_{br}, it is useful to take more measurements.

Dark rate measurements

As it has been mentioned, high dark rate is the main drawback of the MAPD. The operation of any system using the MAPD with a signal threshold less than 1 p.e. is basically impossible. This is one of the reasons why the manufacturer's specifications provide two dark rate values: the basic rate of all counts and the rate of dark pulses with an amplitude exceeding 1.5 p.e., that means, at least two-photon pulses.

At this point, one must remember the nature of the two-photon (and higher) dark pulses. Their appearance is not only a result of accidental coincidences of single dark counts, but first of all, comes from crosstalk and afterpulses. This means that the distribution of registered dark pulses will not have the expected Poisson distribution, like for

[5] The distance between 0 p.e. and 1 p.e. may be subject to systematic error introduced by the baseline restorer, which is often used in the signal path of the measurement system (see section 4.3); in this case it is better not to use the 0 p.e. peak to calculate the gain.

[6] The absolute gain values presented by Hamamatsu have not been clearly verified as yet, and the data presented by various research centers differ often by more than 20%.

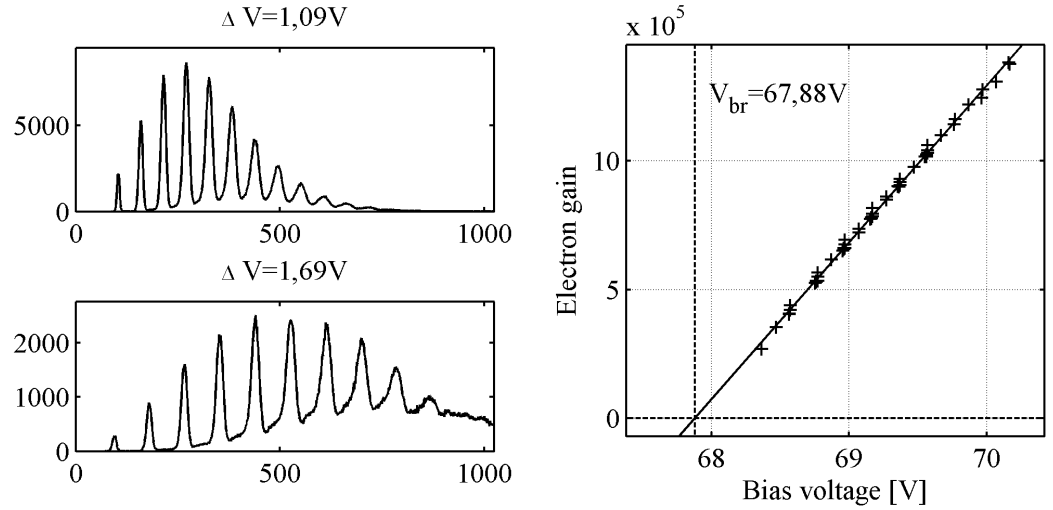

Figure 3.2: With the bias voltage increase, the electron gain does change, which is reflected in the distance between the peaks on the pulse amplitude histogram (left). Extrapolation of the data points on the $G(V_{op})$ plot can lead to the breakdown voltage (V_{br}) determination. The plot (right) shows 53 measurement points, but usually only two or three measurements ar used for ordinary measurements of V_{br}

independent events. Giving the 1.5 p.e. dark rate is important, as its value can not be simply deduced from the knowledge of the dark rate for the threshold of 0.5 p.e.

The measurement of the dark rate can be done in two ways: 'classically', with discriminator and scaler, or basing on the histogram coming from a dark measurement. These two methods are theoretically equivalent, although the differences between them will show up at higher dark rates.

The discriminator-scaler method. The classical method uses a discriminator with a threshold set to 0.5 or 1.5 p.e., depending on which of the two characteristic rates one wants to measure. This method requires the *a-priori* knowledge about the level of the thresholds to be set. These values can be determined by two methods:

– By measuring the frequency counts several times, gradually moving the discriminator level. The obtained curve (fig. 3.3[7]) is a 'backwards' integrated dark histogram. The level of 0.5 p.e. is located in the region of the first plateau. This method is reliable, but requies multiple dark rate measurements, so it's relatively time-consuming (about one second for each point on the plot).

– By determining the thresholds directly basing on the positions of the pulse histogram valleys, with the histogram coming from a dark or light measurement. In this case,

[7]This figure should be regarded as an illustration only. The data from the discriminator and the ADC came in fact from various measurements and are set together only to illustrate the method of calibration.

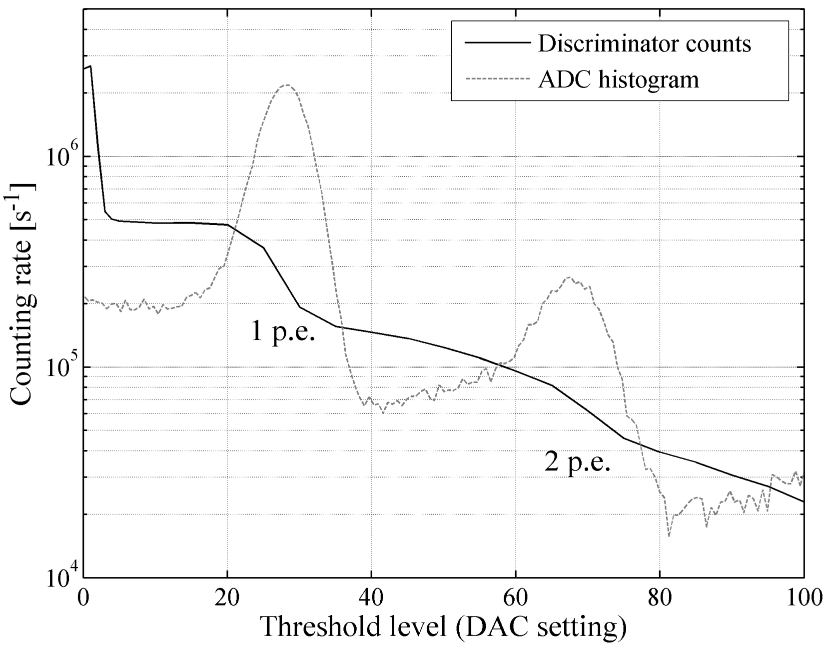

Figure 3.3: The dependence of the dark rate on the discriminator threshold. Every sharp drop in the number of counts corresponds to one peak in the pulse amplitude distribution. Theoretically, one can get the distribution of peak amplitudes by differentiating the dark rate on the threshold value; in practice, however, the quality of these data is quite poor. Amplitude histogram shown in the plot was obtained with the ADC

it is necessary to cross-calibrate the discriminator and the pulse amplitude readout system. This operation is performed just once during instrumentation setup.

The histogram-based method. The dark rate can be also calculated on the basis of the histogram coming from a dark measurement. In this case, the total number of the collected measurements (total counts) multiplied by the gate time is the time of measurement. The number of counts above the selected threshold (0.5 or 1.5 p.e.) corresponds to the number of dark counts. We can get the dark rate by dividing the number of counts above the threshold by the total measurement time.

In practice (not only for the the dark pulses analysis) it is convenient to transform the histogram into a discrete form, in which the amplitude of the pulse is rounded to the nearest full photoelectrons; the thresholds between particular numbers of p.e. can be determined using one of two methods:

– at the valleys (local minima) of the histogram,

– halfway between neighboring peaks.

None of these methods can be considered impartially better, and the choice depends on the characteristics of the measuring apparatus[8], although the second one is better suited to the definition of noise at 0.5 and 1.5 p.e. If some peaks are not clearly distinguishable (which takes place for a greater number of photoelectrons), an information about well-defined peaks is used and extrapolated for the remainder of the histogram (if the measurement device's signal path is linear, all the peaks should be equally spaced).

With both described methods of dark rate measurement, one should always remember about two phenomena, causing that the measurements from various sources can be significantly different:

– If no adjustments are made, the measured dark rate includes also the pulses generated by crosstalk and afterpulsing phenomena, so the measured value can not be strictly understood as the rate of thermal generation. A measurement which is free of this error is is possible under proper conditions; the details will be described below, in the section regarding the correlated noise.

– Depending on the pulse shaping time constant (or integration time), two separate pulses, which are close in time, can be recorded as the two pulses, or as a single pulse of higher amplitude. Obviously, this will affect the results of the measurements for the threshold of 0.5 and 1.5 p.e. This effect will be dependent on the parameters of the measuring apparatus – in particular on the shaping of the pulses. For this reason, the target readout system parameters should be taken into account when performing measurements.

  At the same time, thanks to the analysis of the dependence of the count number on the discriminator threshold level and integration time (or discriminator dead time), one can get some information related to the correlated noise [25].

Photon detection efficiency

Direct measurement of the photon detection efficiency (PDE) requires a fairly complex equipment based on nonlinear optics [9] and is performed very rarely[9]. Typically, the measurement of the PDE is done indirectly, by comparison with a detector with known quantum efficiency (usually with a calibrated photomultiplier). For screening measurements (and usually for the detailed measurements, too) the knowledge of the absolute

[8]For example, under certain conditions, the histogram peaks have asymmetric tails, resulting in significant displacement of local minima, and with different settings the tails are symmetrical.

[9]This is true not only for MAPD, but all photodetectors in general.

PDE value is generally not required – it is sufficient to compare the results of various measurements.

A naive method of PDE measurement can rely on summing up the counts in each histogram peak for a light measurement[10]. Unfortunately, such an approach is charged with an error associated with the correlated noise, the same as in the case of the dark rate measurement. However, it turns out that the PDE value can be determined from the amplitude of the 0 p.e. and 1 p.e. peaks; this approach will be described in chapter 5.

There is also an alternative method for PDE measurements, based on the measurement of the MAPD current with relatively strong steady lighting. This method requires a prior measurement of the electron gain, CT+AP fraction and the knowledge about non-linearities occuring due to saturation effects. The advantage of this method is that it's theoretically less affected by random errors getting from the correlated noise (paid with an additional gain and linearity measurement error).

Correlated noise

The correlated noise consists of two phenomena: the crosstalk and the afterpulses. Both of these phenomena have similar effects and are often treated as a whole, as a fraction of CT+AP, although they are based on completely different mechanisms. The measurement of the CT+AP fraction is particularly important because of its influence on the measurement results of the dark rate and the photon detection efficiency.

The measurement of the correlated noise is based on the histogram obtained during a dark measurement. If the described effect didn't exist, the distribution of the pulse amplitudes (after a quantization with the bin size of a 1 p.e.) would have a Poisson distribution. The correlated noise modifies this distribution, moving it towards larger number of counts (some of the single-photon pulses become two-photon ones, two-photon ones become three-photon etc.). The only value that is not affected by the correlated noise is the number of zero-photon counts (no crosstalk nor afterpulse appears without a primary pulse)[11]. It turns out that the ratio of the 0 p.e. counts to the total count number is sufficient information to calculate the expected value of the theoretical Poisson

[10] The problem of the histogram discretization was described on page 40.

[11] In fact, with a large fraction of AP, it can happen quite often that a dark pulse will occur before the opening of the integration gate, and the accompanying afterpulse will be inside of the gate window and will be registered. In this case, the number of 0 p.e. counts is of course affected. In fact, there is no method that would determine whether a particular pulse is a result of the dark generation or the afterpulse.

distribution. This distribution is described by the equation:

$$P_k = \frac{e^{-\lambda}\lambda^k}{k!} \ . \tag{3.1}$$

By substituting $k = 0$, we can calculate the dependence of P_0 and λ:

$$P_0 = e^{-\lambda} \text{ or } \lambda = -ln(P_0) = -ln\frac{N_0}{N_{tot}} \ , \tag{3.2}$$

where $N_0$is the number of 0 p.e. counts and N_{tot} is the total number of counts in the histogram. The knowledge of the expected value of the distribution allows to calculate the actual value of the dark rate (coming only from thermal generation) at a given threshold. The ratio of 1 p.e. events in the real histogram and in its Poisson equivalent allows to specify the probability of CT+AP events:

$$P_{(\mathrm{CT+AP})} = 1 - \frac{N_{1cnt}}{N_{1poiss}} \ , \tag{3.3}$$

where N_{1cnt} is the actual number of registered avalanches with an amplitude of 1 p.e. and N_{1poiss} is the same number obtained on the basis of a theoretical Poisson distribution. $P_{(\mathrm{CT+AP})}$ is the probability to generate at least one, additional avalanche, which is the requested fraction of correlated noise.

Theoretically, it should be possible to determine the correlated noise basing on the histogram from the light measurement (in this case the discrete representation would have a Poisson distribution too, if the phenomena of CT and AP didn't exist). In practice, however, for small values of P_0 (large λ) this method is ill-defined and the equation 3.2 gives quite random results.

Dedicated testing devices

All the above measurements can be performed with a single, properly constructed apparatus (fig. 3.5).

The MAPD is closed in a housing which functions as a thermostat and provides an optical isolation from the environment. A pulsed light source, used for light measurements, is installed in the same housing . The signal from the MAPD is pre-amplified and shaped, and then converted to a digital form. For this latter task one of the three devices can be used:

- Integrating ADC (or QDC, charge-to-digital converter). The integration of the signal takes place in a time window of a fixed length and is triggered by an external signal. The use of the MAPD output pulse as a trigger signal requires a delay line in the ADC analog signal path.

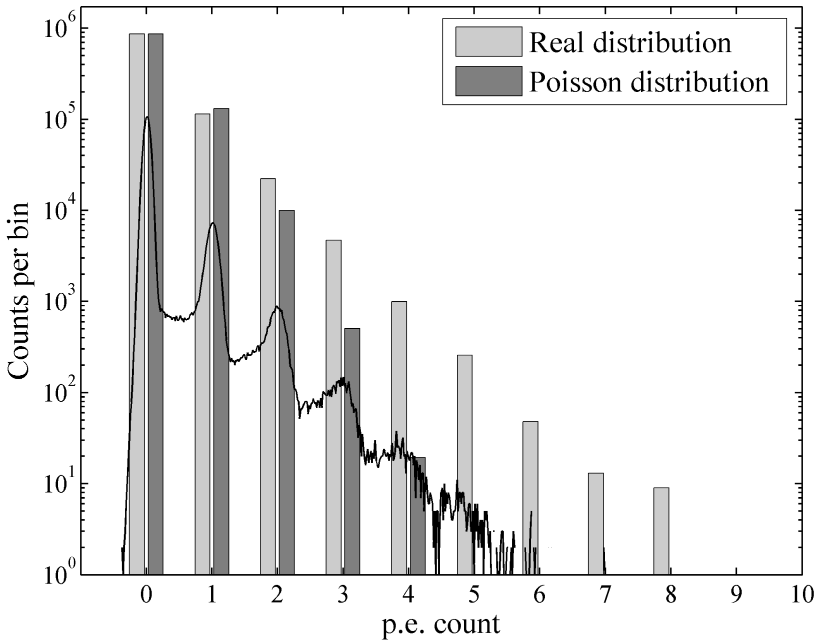

Figure 3.4: The actual distribution of dark pulse amplitude (before and after the histogram discretization) and theoretical Poisson distribution for the same dark generation rate. The effects of CT+AP will shift the distribution of dark counts towards higher amplitudes

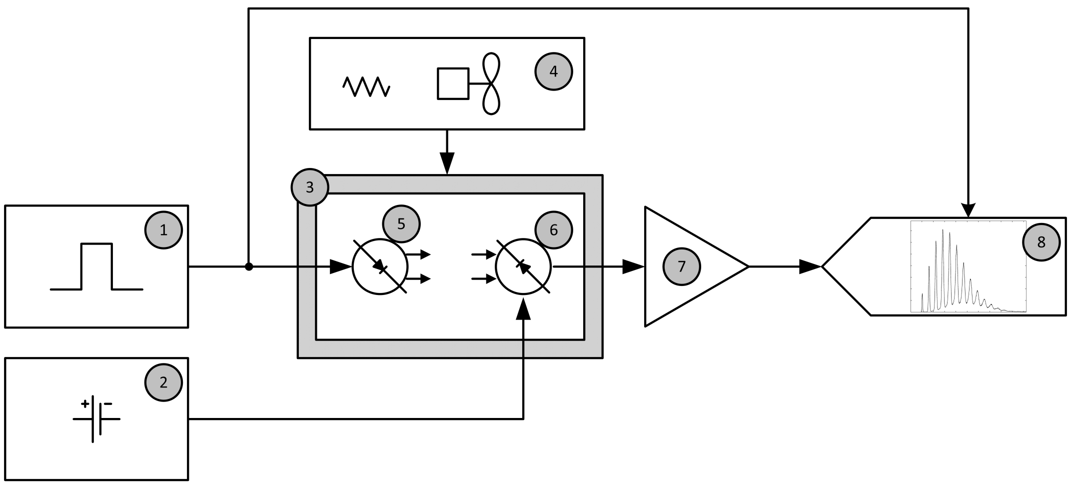

Figure 3.5: A diagram of an apparatus for measuring the basic parameters of the MAPD by means of the histogram analysis. 1: pulse generator, 2: regulated power supply for the MAPD, 3: light-proof housing, 4: temperature control unit, 5: pulsed light source, 6: the MAPD, 7: preamplifier, 8: multichannel amplitude analyzer (MCA)

– Peak converter. This is a simplified version of the previous solution. The signal at the input of the converter usually requires gating. With low gate times, the obtained results are consistent with the results obtained using the integrating ADC, and with a long gate both solutions will behave differently due to the different response to multiple pulses.

– High speed sampling ADC, which collects at least few samples for each pulse. This solution theoretically does not require the trigger signal, but in practice it is still used because of the extremly high data rate produced by the converter operating in continuous acquisition mode. In terms of its functionality, the sampling converter can replace both previously described converters. The operation of pulse integration or peak recognition can be done digitally. In addition, the sampling ADC does not require a delay line if the signal itself is used as trigger source, because the delay can be implemented at the stage of digital signal processing.

The sampling ADC is the most flexible solution among the others and gives the greatest benefits. Its main advantages are:

– A possibility of emulation of the two previous solutions. The same measurement can be used to determine both pulse integral and peak value.

– Freely selectable integration time within the time window acquired by the converter. If all the data flowing from the converter is beeing saved, the choice can be made in off-line mode, several times for the same data.

– The possibility of recording the data which is coming before the trigger pulse. This can be useful when registering dark pulses (in the role of the trigger signal, the signal from the discriminator may be used, so the system is triggered on the pulse itself).

– The possibility to observe the signal shape (limited by the analog path bandwidth and sampling frequency). This feature is particularly useful for the analysis of afterpulses, although thorough analysis of this phenomenon requires a sampling rate of at least 1 GHz.

One of the basic disadvantages of the described solution is very large amount of data being generated (the converter is required to operate at a sampling frequency of about 100 MHz to several GHz, depending on the desired frequency response and device's functionality) and a relatively high price. In practice, most of the existing equipment for MAPD measurements uses pulse converters.

In parallel with the converter's signal path, a discriminator can operate, allowing measurements of dark rate, and possibly serving as a trigger source for the converter for registration of dark pulses. The discriminator's signal path includes a comparator with adjustable threshold and a counter (scaler).

The whole electronic equipment is typically made of pre-designed modules for nuclear electronics (NIM, CAMAC or VME standards). The only exception here is the preamplifier, which usually is constructed specifically for the MAPD signals reception. Sometimes, solutions basing on systems used in the experiments (such as Trip-T chip [26]) are used. The equipment is typically supervised by one or more PCs.

3.3 Another measurements and tests

Despite the high versatility of measurements based on the histogram, there is a number of parameters that can not be measured using the apparatus described above. The most important ones are listed below.

Direct measurement of capacitance and quenching resistance can be performed using a vector impedance meter and an additional circuitry to bias the MAPD with the required voltage. The total capacitance of the MPPC as a function of bias voltage is shown, for example, in [25]. It should be noted that such a measurement gives us the parameters of the whole MAPD structure (that is all pixels in parallel and also the parasitic elements).

Quenching resistance measurement can be accomplished also by polarizing the diode in forward direction – basing on $\mathrm{d}I/\mathrm{d}U$ function slope. Like the junction capacitance, the result of this measurement will be distorted by the existence of parasitic, serial resistances.

Afterpulses measurement is always done basing on a detailed analysis of the time intervals between pulses. This analysis may be performed in two ways:

– Directly on the basis of the shape of the MAPD signal in time domain [21]. This method is particularly useful for short time constants (up to 100 ns). In order to improve the performance of the method, the time signal is deconvoluted with a standard pulse response of the MAPD, allowing better separation of the pulses, even if they appear with a delay less than τ_r. Then the distribution of the length of intervals between pulses is observed. The measurement is performed for dark pulses, without any light.

– Using the measurements with the discriminator. In this case, the measurement is also carried out in the dark, and the basic data is the dark rate. By gradually changing the discriminator's dead time, one can determine the distribution of the time delays between pulses. This method is best with the analysis of longer time constants.

The study of crosstalk requires the use of specific instrumentation allowing the illumination of only one pixel. Since a single pixel is able to generate only 1 p.e. response, all higher-amplitude pulses (collected in a sufficiently short time gate, which efficiently excludes afterpulses) will be the result of stimulation of adjacent pixels through the mechanism of crosstalk. Properly designed optics allows to move a well-collimated beam of light on the surface of the structure in order to study the phenomenon in various places over the MAPD area [25].

Saturation of the MAPD under high intensity of light can be described by observing the MAPD's current dependence on the light level (similar measurement can be done with pulsed light). This measurement requires an information about electron gain and PDE, in addition to the intensity of light. Direct observation of the phenomenon basing on the histogram peaks is not possible, because the characteristic picture of peaks and valleys disappears completely at about 20 p.e. due to the gain differences between particular pixels.

The measurement of saturation effects in the pulse mode is theoretically possible using the equipment described in section 3.2, but it requires a very large dynamics range (in practice – the possibility of switching between two relatively calibrated ranges and a very wide range of light intensity adjustment).

Chapter 4

A device for automated MPPC measurements

4.1 Initial assumptions

As part of the preparations for the the T2K experiment, a team from the Warsaw University of Technology has designed a specialized, automated apparatus for measuring the parameters of the MPPC photodiodes [11]. The author was one of the creators of this unit (see paragraph 4.5).

The goal application of the device

The main task of the designed device was to measure about 1200 MPPCs for the SMRD subdetector of the T2K experiment[1], which were to be tested by the Warsaw team. Furthermore, the device had to have possibly wide capabilities of performing some detailed measurements.

The demands regarding the functionality

In the first phase of the design of the device, several primary requirements were defined on the functionality of the equipment and the quality of the data. These requirements, listed below, were the basis for the selection of specific technical solutions in the design of the unit.

[1]The total number of more than 4000 photodiodes for SMRD was divided into three parts examined by various institutions, although the initial plan was to examine all the units at one place.

Optimization for the measurements of MPPC-type elements. Since the device was constructed to measure one specified model of the MPPC photodiode, the specification of this element (both mechanical and electrical) was the base for the design of the apparatus. To determine the expected performance range of the MPPC, the data provided by the manufacturer were studied, and then subject to a preliminary verification using a quick-and-dirty measuring system made of several CAMAC modules and equipped with a custom-designed preamplifier with an analog integrator.

At the same time it was assumed that the structure of the target device should be as far as possible able to be be easily modified for use with another types of MAPDs. The device should work with both 660-pixel MPPC model used in the T2K (inaccessible at the time of the construction of the apparatus), as well as the 400-pixel prototype – S10362-11-050C, without any modifications to the hardware of the device. This last condition is easy to meet as both MPPC models have identical case, and their electrical parameters should vary only slightly.

The ability to perform screening measurements. It was assumed that the minimum throughput of the device for screening tests would have to be about 100 specimens per day. The operation of putting the tested components into the device should be done as rarely as possible, by whole batches – the size of a single batch was proposed to be 32 specimens. This allowed to reduce the number of the operator interventions to about three times per day, assumed that the measurement of whole batch would take 4-8 hours (during the operation, we managed to significantly reduce this time, which allowed to carry out even six batches a day[2]). There would also be the ability to control the device remotely, including remote power off in case a failure or finish of the measurements.

The ability to obtain the detailed MPPC characteristics. To provide an ability to do the tests in a wide range of working conditions of the MPPC and with high accuracy, a number of requirements for the control of operating conditions were defined:

- MPPC bias voltage should be adjustable in the range of 60 to 80 V and stabilized with an absolute accuracy not worse than 25 mV, with a quite small output current (average current during the measurement of the MPPC does not exceed tens of nA). The finally achieved absolute accuracy of the voltage regulation was 10 mV.
- The temperature range for the MPPC should be 10-40°C, with an absolute accuracy not worse than 1°C. We obtained an accuracy of 0.1°C for temperatures close

[2]In addition, during the night shift, some longer measurements at several temperatures were performed.

to room temperature and about 0.5°C for temperatures less than 10°C. The actual temperature range was much wider than expected and reached from 0 to at least 70°C. The assumed time to change and stabilize the temperature is 30 minutes; this requirement was also achieved with an excess.

– Light pulses for illuminating the MPPC structure should not be longer than about 5 ns and the spectral characteristics of the light should correspond to the light generated by WLS fibers used in the T2K experiment (to ensure this condition, it was decided that there would be exactly the same WLS fiber in the optical path of the device as in the ND280 detector of T2K). The intensity of light reaching the structure should be controlled in the range of from about 10 to about 100 photons per pulse, with a precision of ca 1%. Due to the strong dependence of the light intensity of LEDs (used as the primary light source to drive the WLS fiber) on the temperature, we decided to equip the device with a reference measurement system to monitor the mean light intensity.

The repeatability of the results. The main disadvantage of various multi-channel measurement systems is a potential problem with providing the same parameters (especially gain and light intensity) for all channels. Such devices require periodic calibration, which is a quite time-consuming and laborious process. Therefore, we rejected this concept and decided to design a device with a single, high-performance measurement channel, working with an automatic specimen feeder. Such a solution requires a single source of light and only one signal path, and the only part to change is the tested MPPC itself. Such a solution – as it turned out – has a number of other advantages in addition to the elimination of the problem of differences between the channels:

– The existence of only one electronic signal path allows for its significant increase of complexity, without having to make any compromise solution due to price or space needed. This allows one to achieve good performance of the device and high quality of the data received without a significant increase of the costs.

– The absence of the light distribution system, which is characteristic for multi-channel solutions, provides a significant reduction in size of the device. It should also be noted that the light distribution system, made in a form of a bundle of fibers, is quite suspect to mechanical damage. The micro-ruptures appearing in the fibers can lead to a reduction of light intensity and to the need to recalibrate the equipment.

– The throughput of the proposed solution is not lower than with the multi-channel devices. In fact, the time of the test of a single MAPD is dependent on the temperature stabilization time and the throughput of the system for data acquisition and processing (this causes that the data in a single channel system is collected much faster than data from a single channel of a parallelled system). Because of the ease of replacement of the tested photodiodes and efficient data processing procedures, the designed device was even faster than other competitive multichannel solutions.

– An effective reduction of the the amount of electronic circuits in single-channel solution leads to improvement of the reliability.

Portability. There was a presumption that one may need to re-test at least some MPPCs already in Japan, immediately prior to their installation in the detector, as in the design phase of the equipment there were not any unquestionable informations available on their reliability. It was therefore decided that the unit should have a possibly compact design for easy transport. It should also be able to work in a non-laboratory conditions (instable ambient temperature, electromagnetic interference). As it turned out, the device constructed in Warsaw was the only portable system of this type (though fortunately the MPPCs are so far working fine[3], and on-site tests were not needed).

High immunity to electromagnetic interference. The experiments with the early quick-and-dirty MPPC testing system have shown that it is essential to shield the whole entity from interference, and in particular, pay attention to the interference appearing between individual sub-systems. Therefore, a few assumptions have been made in the design phase:

– All sub-systems have been divided – depending on the signals they were processing – into four groups: fast analog, low-frequency analog, digital and power circuits.

– Each group has its own grounding system and a separate power supply. Particular attention was paid to the proper selection of connection points between the grounds.

– All long-distance lines transmitting high-frequency signals (MPPC output signal, trigger signals) are implemented as symmetrical lines.

[3]The ND280 detector survived without major damages the Japan's strongest earthquake (11 March 2011) and a few weeks of downtime with no air-conditioning, at one hundred percent relative humidity and water condensing on the electronic components.

– Switching power supplies were completely eliminated out of the design. All voltage regulators and power supplies are made as linear systems, with full awareness of the consequences of this solution (such as the need to dissipate heat from the losses of the 500-watts power supply).

– Two-stage voltage regulation was used in the power supplies for all analog circuits – the first regulator stage is located in the power supply, while the other is placed directly on the printed circuit board of particular module.

Possibility of expanding the functionality of the device. The design of the device assumed the possibility of its expansion, increase of the functionality, as well as adapting to measure other types of MAPDs. This was achieved mainly through the design of most of the electronics in the form of interchangeable modules (see paragraph 4.2). The device's case has some free space for additional modules left, and power supply is designed with significant excess of capacity.

4.2 The design of the device

The mechanical design, MPPC feeder

All components of the unit were deployed into two enclosures connected via a bundle of cables in order to create a compact, portable design (see figure 4.1).

The electronics box is a standard 19" 3U crate. It contains the vast majority of electronic systems; most of them have a form of an euro-card and are connected together via a common motherboard. The elements which dissipate large amounts of heat (power supply components, the power stage of the temperature control system) were placed on a common, highly-efficient cooling module equipped with a fan.

The feeder box contains the specimen feeding mechanism, the preamp, the light source and some elements of the temperature control system. Due to the possibility of a significant temperature difference between the feeder and the environment, the case has been fitted with a polyurethane foam insulation. The whole unit is mounted in a plywood outer casing.

Figure 4.1: The complete device during normal operation. The feeder box (on the right) is connected to the electronics case (on the left) with a wiring harness. There is an opened pack of MPPCs on the top of the electronics box

Modular electronic circuitry

The whole electronic equipment has been divided into a number of sub-systems due to their functions :

- a light source, coupled with an integrated photodetector and an amplifier for feedback and control;
- analog signal processing circuit, which stays in the electronics box (except for the preamp installed in the feeder box);
- sampling ADC with accompanying digital circuits;
- dual discriminator with counter;
- slow-control circuits, responsible for maintaining the desired temperature, MPPC bias voltage, light intensity, controlling the feeder tray position and cooling fans;
- accompanying systems such as the communication interface and the power supply.

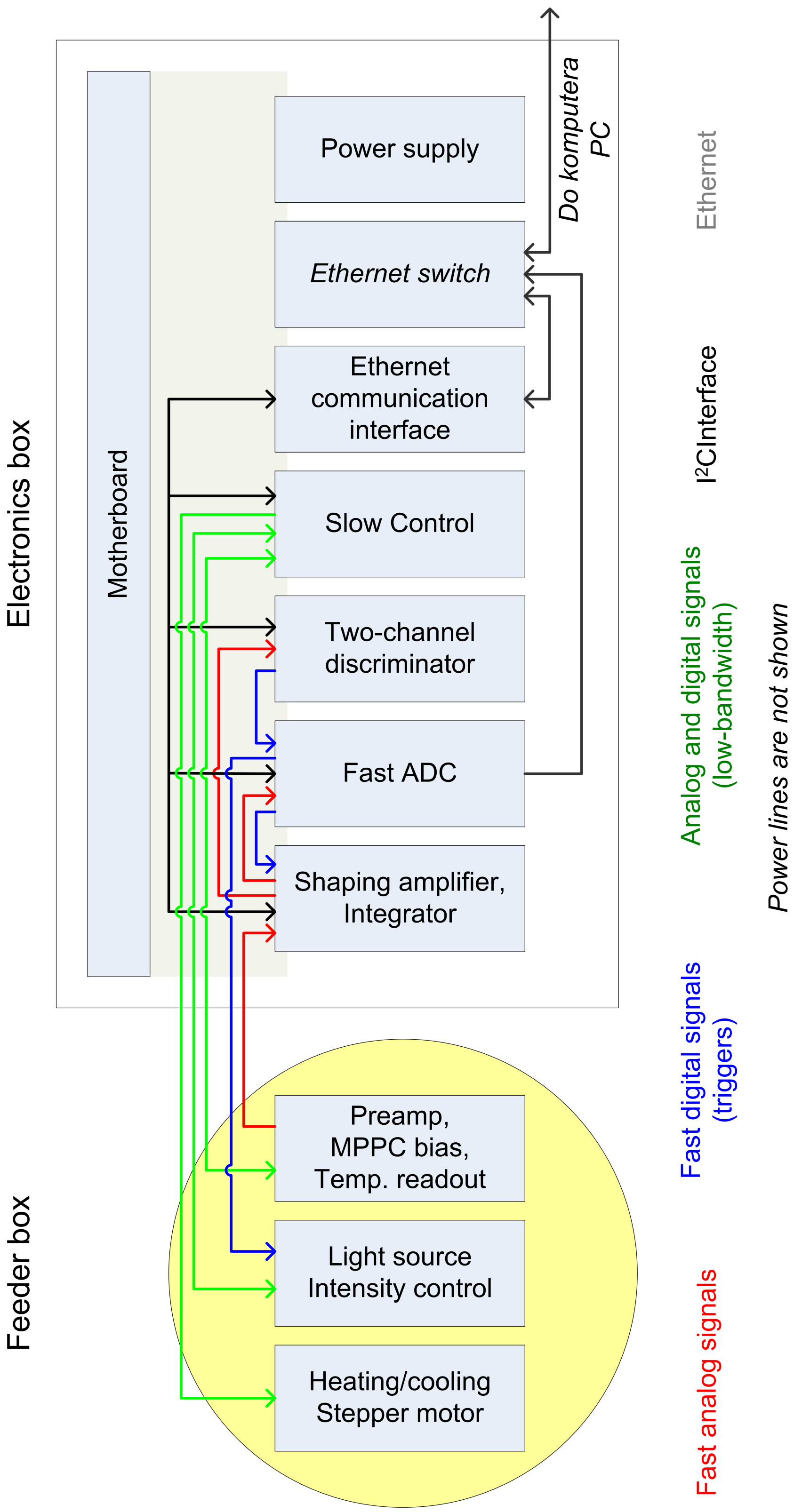

Figure 4.2: A block diagram showing various electronic components and their interconnections [11]

All blocks that require the digital control are connected with the communication interface via an I^2C bus. The support for individual modules is providd by 8-bit AVR microcontrollers: ATmega88 or ATmega128, depending on the resources required. Each of the euro-card modules has its own microcontroller to monitor and control its operation.

Communication with the PC and data acquisition

The communication of the device with the controlling computer is provided via a single Ethernet connection. This enables operating with virtually any computer (including laptops) without installing additional expansion cards or interfaces. A public network can be used to exchange the data between the device and the computer, however it is desirable to use a dedicated connection because of the large data flow (about 80 Mbit/s).

The software designed for the device is able to perform the most laborious operation – the digital integration of pulses – in real time. Some operations such as the construction of the histograms and calculating the gain are also carried out during the measurements. More complex operations can be performed after the measurement, on the operator's demand. The data from any stage of processing (except for the raw data from the ADC) can be exported to disk files, and then processed by other tools. Recording of the raw data can be performed in parallel with normal processing, but on a separate computer, equipped with an array of hard disks of sufficient capacity.

In addition to the data processing, the software also provides a clear data management system that allows to manage over a large number of different measurements of many MPPCs, supporting data archiving, as well as comparing the results. The management system is a relic of a world database of MPPC data for T2K experiment, which was planned but never built.

4.3 Detailed technical solutions

The feeder with integrated electronic circuits

The design of the MPPC feeder is shown in figure 4.3. Its main element is a rotating tray with sockets for 32 MPPC-type photodiodes, placed in a cylindrical housing. The positioning of the tray is provided by a stepper motor and a worm gear (the wormwheel's rim is mounted directly on the tray). The zero position of the tray system is determined by an optical sensor (sensor's transmitter is located in the cover of the housing and the receiver is placed on a PCB mounted directly on the tray).

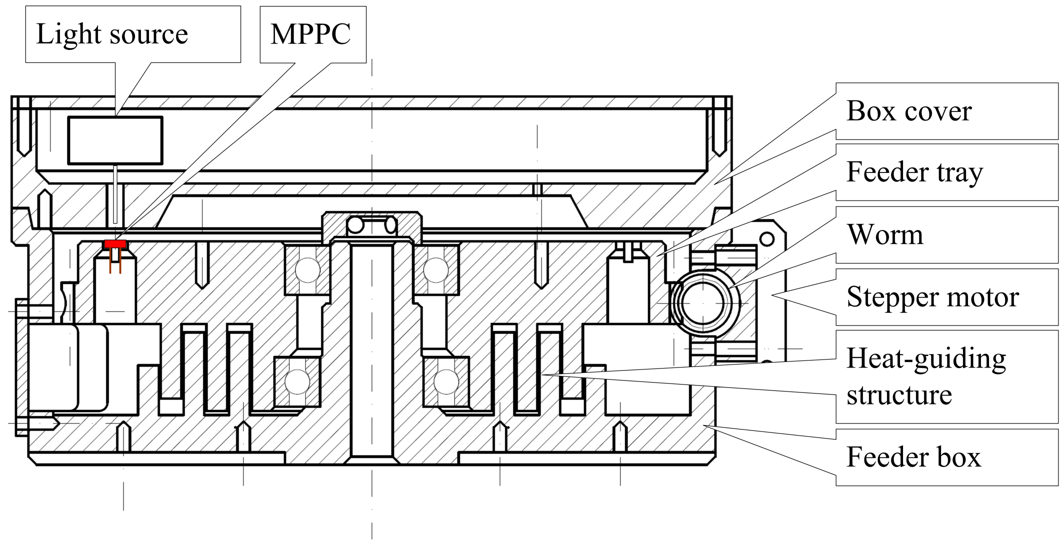

Figure 4.3: Cross-section through the feeder box with basic components. The temperature stabilization of the feeder tray is achieved by cooling and heating elements placed directly under the bottom of the housing

The accuracy of the MPPC position setting during the measurement is mainly determined by the precision of the placement of the MPPC in its socket.

The MPPCs are installed in sockets located on the circumference of the tray. The socket design provides repeatable position of the inserted specimens (± 0.2 mm) and a large area of thermal contact with the feeder tray, ensuring good heat exchange. Electrically insulating elements of the sockets are made of polyamide-6 – a material characterized by a relatively easy mechanical processing, good insulating properties and low piezoelectric effect.

The existence of a rotating feeder excludes a direct, continuous electrical connection between the tested specimen and the preamplifier. Instead, a solution similar to a commutator of a DC motor was used. The leads of the MPPCs are connected, through the sockets, to a slip ring on the underside of the feeder's tray. There is a brush system directly under the tray, providing electrical contact between the slip ring with photodiodes and the preamp. This provides a very short signal route between the diode and the preamplifier (about 20 mm) and eliminates the need for a connecting cable whose impedance would determine the input impedance of the amplifier. Less important cables which provide connections to some electronic circuits mounted on the tray, are routed by a hollow pivot of the feeder and provide the possibility of the tray rotation up to $360°$.

Figure 4.4: The feeder box after removing the cover. The MPPC sockets with inserted specimens are arranged on the circumference of the tray, Also the position sensors, stepper motor, and the foam coating providing thermal insulation from the environment are visible. The vents for cooling fans are placed at the bottom of the outer plywood case

Temperature control of the whole feeder box is provided by heaters (power transistors are used in this role) and cooling elements (Peltier cells), both located at its bottom. The heat removal from the Peltier cells is ensured by aluminum cooling module with integrated fans. The maximum power delivered to the heating and cooling elements can reach 200 W. To ensure good thermal contact between the feeder tray and the box, a finger-shaped, cylindrical structure was prepared (shown in figure 4.3), increasing the contact area. The space between the two parts is filled with a grease. This ensures a sufficient heat transport to change the temperature of the tray by 10 °C within 10 minutes. The temperature readout is provided by 3 PT-1000 sensors: two (with a tolerance class A) are located directly on the feeder tray, and the third (additional, with B-class tolerance) is installed on the bottom of the case.

The feeder box has a removable cover, with the light source installed inside for light measurements of the MPPCs. Good thermal contact with the main part of the box ensures maintaining a constant temperature of the cover. After closing, the whole case is optically tight and additionally acts as a shielding against electromagnetic interference.

All mechanical components, with the exception of the worm gear elements subject to friction, are made of duralumin (PA-6). The wormwheel ring is made of brass and the worm from stainless steel – this guarantees a long life of the gear, and most importantly, does not require grease, which could contaminate the MPPCs or electrical connectors inside the box.

Light source

The heart of the light source is a so-called Kapustinsky flasher [16]. This is a simple and cheap device which generates short pulses of light (from about 1 to a few nanoseconds) using an LED. A schematic diagram of the circuit used in our device is presented in figure 4.5. The main components are two transistors connected in a manner providing positive feedback. Their key task is to quickly close the circuit composed of a LED and a capacitor, which acts as the source of power. The peak current running through the LED after turning on the switch is over 1 A and decreases as the capacitor discharges. To reduce the pulse tail, there is an inductor placed in parallel with the diode. It has a form of a small coil of wire, of several nH in inductance, experimentally selected for minimizing the pulse length while maintaining a sufficient quantity of light generated. Because the recharging of the capacitor is performed by a resistor whose resistance must be relatively high, the circuit can usually operate at trigger frequencies up to several kHz. In our device, the Kapustinsky circuit is additionally equipped with an LVDS trigger signal receiver, made of discrete components.

The light intensity can be adjusted by changing the capacitor charging voltage, but the relationship between these two values is highly non-linear (fig. 4.6). In addition, there is a strong dependence between the LED efficiency and temperature. For this reason, it is necessary to control the amount of light emitted by the flasher. It is provided by a PiN photodiode (BPW-34), which is located close to the LED. The amplifier for the photodiode is equipped with a low-pass filter with large time constant to measure the average light intensity.

A WLS fiber tip is inserted between the LED and the PiN photodiode. The fiber acts as a source of photons illuminating the structure of the MPPC. The length and location of its tip is chosen to ensure an adequate number of photons reaching the MPPC with possibly high intensity of the light coming from the LED (a strong beam of light can be more precisely measured by the PiN photodiode and the flasher is generally more stable at high intensities). The measured waveform of the light pulse is shown in figure 4.7.

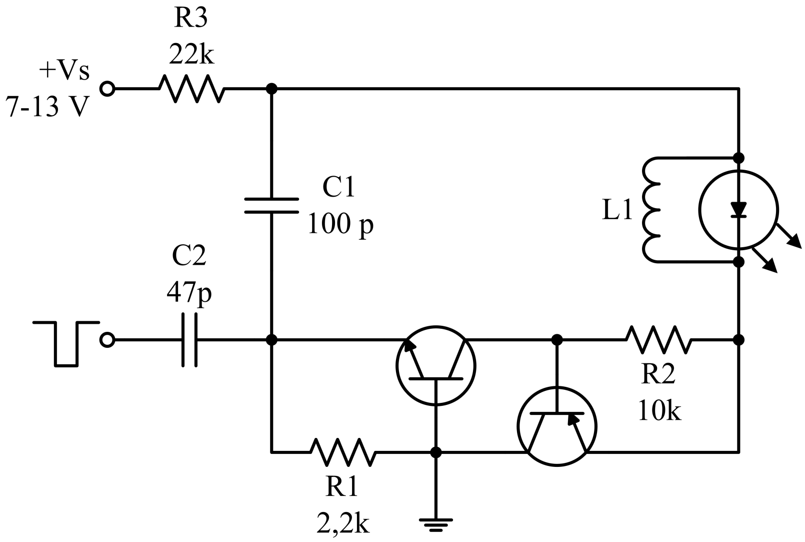

Figure 4.5: The Kapustinsky flasher used in the MPPC measuring device (without the LVDS receiver). The pulse provided to C2 capacitor leads to triggering of the transistor switch and further to discharge of the C1 capacitor through the LED. After discharging, the transistor switch goes into the open-circuit state, and the capacitor is re-charged through R3 resistor. The coil inserted in parallel to the LED can significantly reduce the pulse length

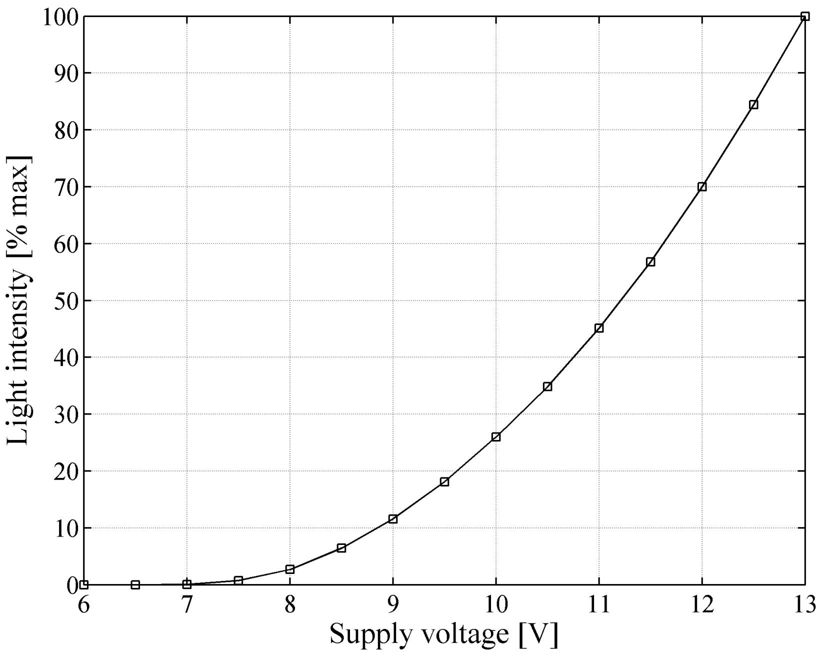

Figure 4.6: Voltage characteristics of the Kapustinsky flasher

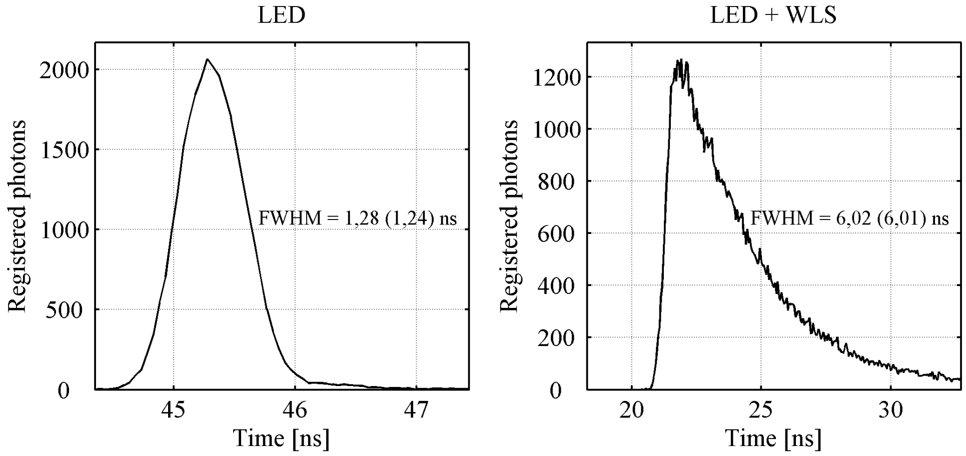

Figure 4.7: The shape of the light pulse from the built Kapustinsky circuit working with WLS fiber (right) and without fiber (left). A photomultiplier tube was used for this measurement. The values of pulse duration (FWHM) given in parentheses takie into account the PMT's time spread (310 ps FWHM). Different numbers on the time axis are due to the propagation time of signals in the apparatus

Analog signal path

The purpose of the analog signal processing circuitry is to amplify the signal from the MPPC and bring it to an optimal form for the analog-to-digital converter. The analog circuitry can be divided into several sub-components:

- the preamplifier, which is mounted in the feeder box,
- the line receiver with the main amplifier,
- the baseline restorer (BLR),
- the pulse shaping circuitry,
- the analog integrator,
- the switching and buffering circuits.

All stages were built using integrated operational amplifiers. The only component with discrete transistors is a pair of current sources of the baseline restorer.

The preamplifier

The preamplifier circuit is placed as close to the tested photodiode as possible, in the feeder box, just under the feeder tray. It is based on a current-feedback op-amp, namely AD8000 [6] by Analog Devices, working as a non-inverting voltage amplifier, which is the

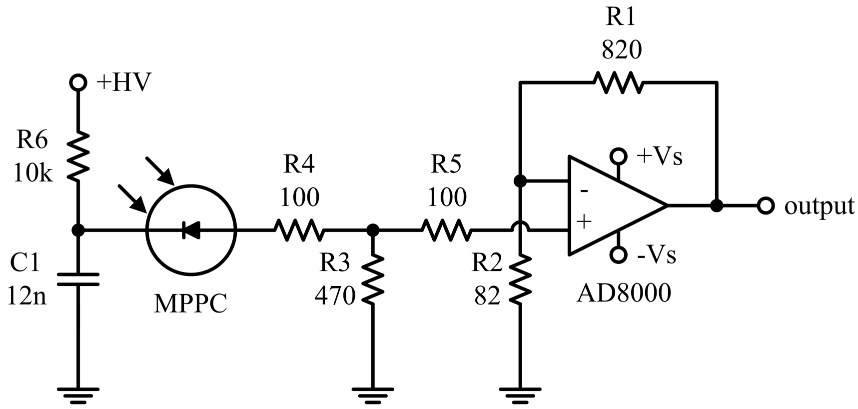

Figure 4.8: Simplified schematic diagram of the first stage of the preamplifier. R1 and R2 define the amplifier's voltage gain, R3 is the load resistor of the diode, and R4 and R5 are inserted to increase the stability of the amplifier and avoid ringing. R6 and C1 form a low-pass filter for the photodiode supply

natural configuration for this chip. Compared with the more common solutions based on discrete transistors, the circuit based on an op-amp has more stable parameters (strong feedback) and should give less trouble in the debug phase[4], which is paid by slightly worse parameters (primarily higher noise) compared to a well-designed amplifier based on discrete transistors.

A resistor acting as the MPPC load is inserted in parallel with the input of the op-amp. The gain of the first amplifier stage is 5.2 kV/A[5] (for low frequencies). The parameters of the output pulse depend on the capacitance of MPPC; for the tested diodes, the 1 p.e. pulse had an amplitude of about 1 mV, and tail time constant of about 25 ns.

Immediately after the first stage of the amplifier, the DC component is removed by a high-pass filter with cut-off frequency of about 2 kHz. The last element in the preamp's signal path is a symmetrical line driver (for a twisted pair with impedance of 100Ω), whose task is to transfer the signal to the next stages of the device, which are placed in the main electronics box. The upper frequency limit of the preamp is 300 MHz.

Preamplifier noise. The preamplifier noise level has a significant impact on the quality of the results. Figure 4.9 presents a schematic of the preamp with most significant sources of noise. Due to the subsequent process of signal shaping and integration, the lower-frequency components of the noise are most significant, for which the serial resistance of the photodiode is cut off by its capacitance and does not affect the operation of the

[4]In retrospect, this assumption needs to be considered as false.

[5]The ability to switch between the input resistance of 220 and 470 Ω with a CMOS switch was planned to change the gain. During tests, however, this solution was abandoned, due to the distortion of the frequency characteristics introduced by quite large capacitance of the CMOS switch.

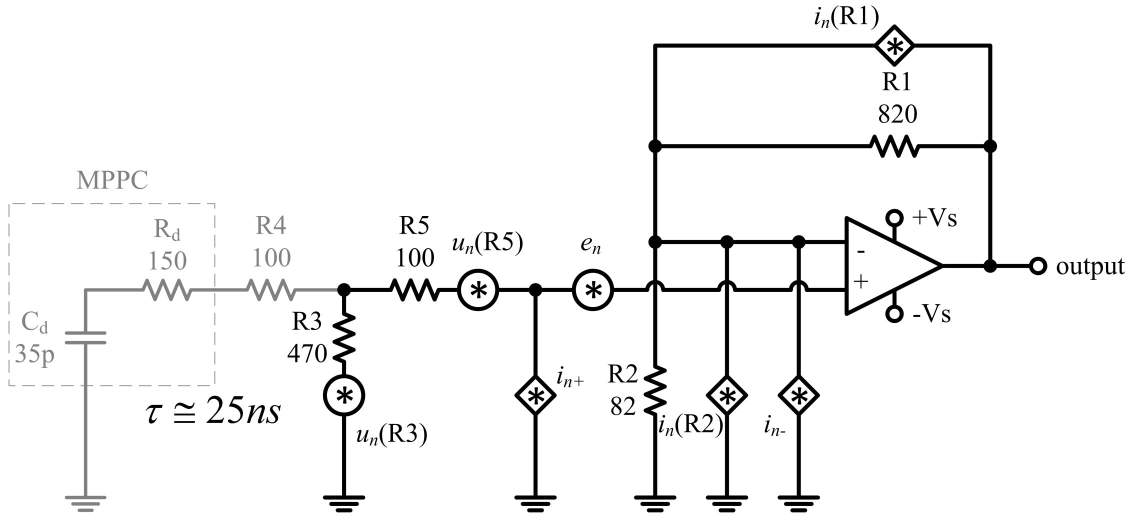

Figure 4.9: Small-signal schematic of the preamp with its noise sources. The values of i_{n+}, i_{n-} and e_n describe the noise of the operational amplifier. The noise of R3 and R5 resistors can be reduced to $u_n(R3, R5)$ relating to the resultant resistance of 570 Ω.

system (the elements marked as gray in the figure). In this case, the total noise of the preamp can be expressed by the equation:

$$u_n^2 = u_n^2(R3, R5) + e_n^2 + i_{n+}^2 \cdot (R3 + R5)^2 + [i_n^2(R2) + i_{n-}^2 + i_n^2(R1)] \cdot R_-^2 \cdot \left(\frac{k_{u-}}{k_{u+}}\right)^2 , \quad (4.1)$$

where $\frac{k_{u-}}{k_{u+}} = (1 - \frac{R2}{R1+R2})$ is the ratio of the amplifier gain for the inverting and non-inverting configuration and R_- is the equivalent resistance connected to the opamp's inverting input. The individual components of the noise are distributed as follows:

Input resistors:

$$u_n(R3, R5) = \sqrt{4kT \cdot 570\Omega} = 3.0 \text{ nV}/\sqrt{\text{Hz}} . \quad (4.2)$$

Op-amp's non-inverting input:

$$u(i_{n+}) = i_{n+} \cdot 570 \ \Omega = 3.4 \text{ pA}/\sqrt{\text{Hz}} \cdot 570\Omega = 1.9 \text{ nV}/\sqrt{\text{Hz}} , \quad (4.3)$$

$$u(e_n) = 1.6 \text{ nV}/\sqrt{\text{Hz}} . \quad (4.4)$$

Feedback loop:

$$u_n(FB) = \sqrt{\frac{4kT}{R2} + \frac{4kT}{R1} + i_{n-}^2} \cdot R_- \cdot (1 - \frac{R2}{R1 + R2}) =$$
$$= \sqrt{(10.8 + 108 + 375) \cdot 10^{-20}} \cdot 0,9 = 2.0 \text{ nV}/\sqrt{\text{Hz}} . \quad (4.5)$$

The input resistance for the inverting input of the op-amp is not directly given by the producer, but it has no influence on the noise calculation nor the amplifier's gain.

The noise of the amplifier's input resistor network is a gently dominant component. It should however be borne in mind that the value of these resistors (or even the desirability of their use – as in the case of R5) are the result of a number of requirements, including in particular the amplifier's stability.

The total noise referred to the amplifier's input is estimated to be 4.1 $nV/\sqrt{Hz}$. With the signal bandwidth of about 5 MHz (resulting from the time constants of the filters used in the following signal path), the RMS value of the noise is about 10 μV. However, it must be kept in mind that directly referencing the noise to the pulse amplitude (around 1.5 mV/p.e.) is problematic due to the complex signal processing operations in the next stages of the signal path, including its final integration in a given time window. For these comparisons, the signal RMS value calculated in the integration window seems to be better better. This RMS value is of about 30% of the amplitude. The measured RMS value of the equivalent noise charge (ENC) (together with interference) of the entire device is about 5.6 fC, which is 3.5×10^4 e and is slightly higher than that expected from the estimates presented above. It corresponds to about 5% of the standard MPPC single-photon response (in relation to the level of about 2.5% estimated basing on the presented theoretical calculations).

Main amplifier

The key elements of the main part of the amplifier are the twisted-pair line receiver, the pole-zero compensation circuit and the voltage amplifier.

The line receiver is based on an AD8130 amplifier operating at a gain of 2 (150 MHz bandwidth). The CMRR of this amplifier is 70 dB at 10 MHz and 40 dB at 100 MHz, which ensures sufficient immunity to any common-mode interference appearing in the cable from the preamp.

The task of the pole-zero compensation circuit is to shorten the tail of the MPPC pulse. The system's transmittance has a zero at a frequency of 3 MHz, corresponding to the approximate time constant of the MPPC pulse tail of 50 ns and introduces a new pole which is located at the frequency of around 30 MHz. It should be noted, that although the use of the pole-zero compensation reduces the pulse tail, the quality of its operation depends on the matching of the pole of the coming signal and the corresponding zero of the circuit. Since the position of this pole depends on the capacitance of MPPC, this circuit can not be treated as a panacea that could eliminate the influence of a relatively large MPPC load resistance on the shape of the signal. However, it shortens the pulse,

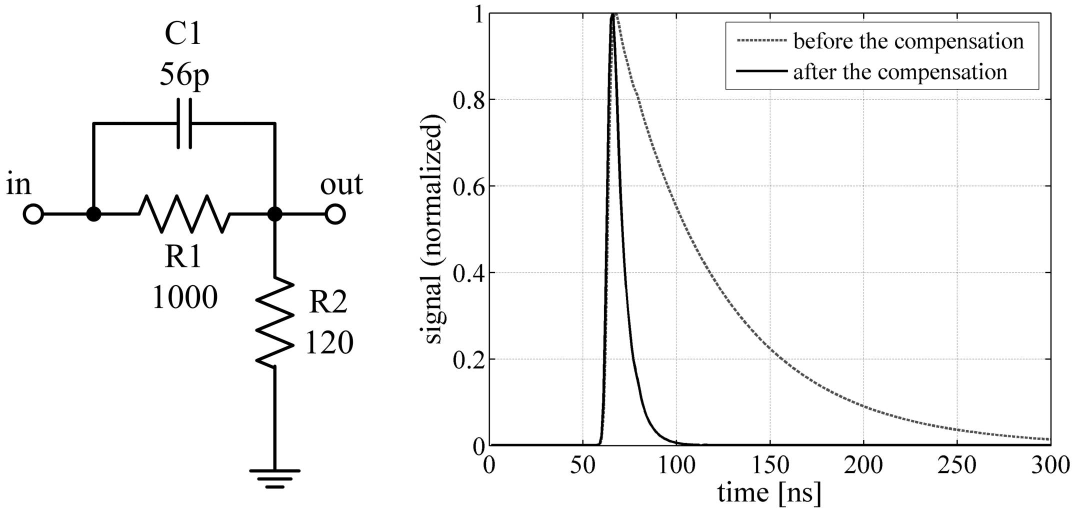

Figure 4.10: The schematic of the pole-zero compensation circuit (left) and the effect of its operation (right) – the shortening of the pulse tail. The plot is drawn on the basis of computer simulation.

which is desirable for the baseline restorer proper operation, as well as for better signal shaping for the ADC.

The voltage amplifier has a single stage with an AD8009 chip[6], operating at a gain of 10. Its bandwidth is 320 MHz.

Baseline restorer

A baseline restorer (BLR) – a typical component of nuclear electronic systems – was used for the reconstruction of the DC component of the signal (the DC has been previously cut off in the preamplifier to avoid problems with saturation).

A circuit based on two current sources of 0.1 and 0.2 mA was built (fig. 4.11). The choice of the current value is the result of a compromise between the minimization of two effects: the baseline shift at high pulse rates and distortion that affects the distance between the peaks of 0 p.e. and 1 p.e. on the histogram. A small 'duty cycle' of the signal (ie, the mean interval between the pulses must be large compared to the pulse length) is required to meet both of these requirements. This is the reason why the baseline restorer is located before further shaping stages, but after the pole-zero compensation circuit.

There is a voltage follower based on an AD8057 amplifier at the output of the BLR, with a 325 MHz bandwidth. Up to this point, all stages have a relatively high bandwidth,

[6] Just as in the case of a preamplifier, CMOS switches were installed here to change the gain. Due to problems with switch capacitance and a lack of real need to change the gain, finally the switches were completely removed.

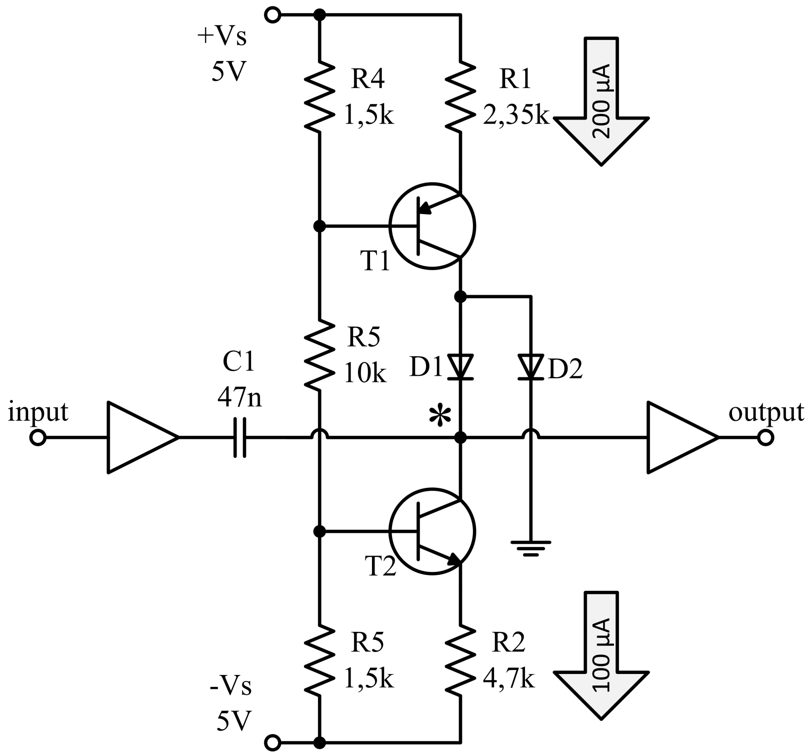

Figure 4.11: The baseline restorer (BLR) used in the device. At the point marked with an asterisk, the steady state occurs when the total incoming current is equal to zero. This occurs only when the current from the source based on the T1 divides equally over the two diodes (D1 and D2), which means that both have the same voltage drop, and the point marked with an asterisk has a potential equal to zero. If this state of equilibrium is lost (also when a pulse occurs) a difference between the currents from the two sources will occur, leading to reloading of the C1 capacitor and bringing the potential back to zero. Because the differential current is essentially constant and almost independent on the value of the deviation, the BLR circuit does not significantly affect the useful pulses which are short and have a rather high amplitude

with a single, dominant pole at a frequency of 30 MHz, which is introduced intentionally. Another poles resulting from the parameters of the amplifiers used are located at frequencies of at least 150 MHz. This allows one to form the frequency response of the signal path quite easily, without any regard to the parameters of the op-amps. In addition, the bandwidth margin enables one to quite freely increase the gain if needed.

Pulse shaper

The signal from the baseline restorer is provided to two separate circuits: the pulse shaper and the integrator.

The pulse shaper is an active, 4th order Butterworth filter, which is built using AD8057 op-amps. Its structure provides so-called quasi-Gaussian pulse shaping. The time constants of individual shaper stages (3.3 or 3.6 ns) give a pulse response of 17.5 ns FWHM and a bandwidth of 18 MHz (-3 dB). The signal attenuation for the Nyquist frequency of the ADC used (100 MHz) is 38 dB. For the frequency of 150 MHz, by which the 50-MHz component of the signal would have been distorted by aliasing, the filter has an attenuation of 52 dB (the frequency of 50 MHz is already quite significant in terms of useful signal bandwidth). It has been experimentally verified that the parameters of the shaper allow one to reproduce the sampled signal in the time domain with good-enough quality.

The main aim of the pulse shaper is to act as an anti-aliasing filter for the ADC. From this point of view it may seem to be a strange decision to use the Butterworth filter, since there are solutions with narrower spectral characteristics. The reason is the specificity of the signal processing in nuclear electronics: the object of interest are primarily timing parameters of the pulses. From this point of view, the best signal shape means short total time and no waving at fast slopes. Therefore, the quasi-Gaussian shaping is the most popular solution in this area, which means just a response of a multi-stage Butterworth filter.

The described pulse shaper is a signal source for both the ADC and the discriminator.

Analog integrator

The integrator provides an alternative signal path, which does not require the digital integration of the signal. An often encountered solution with a capacitor and CMOS switch in the feedback loop of an op-amp was implemented. To maintain a positive polarity of the signal, the circuit is equipped with an additional inverting amplifier. The signal from the integrator does not require any additional shaping and can be addressed directly to the ADC.

Due to the fact that the analog integrator was finally not used in the measurement, it will be not further described.

Switching and buffering circuits

The last stage of the analog signal path is the signal switching and buffering sub-system. It provides source selection for both ADC and discriminator (the pulse shaper or the analog integrator can be selected as a source) and buffers the signals for both the ADC and discriminator[7]. These signals are further transmitted through motherboard connections, due to the short distance no differential transmission is required[8].

[7]The signal selection feature for the discriminator was significant only in the debug phase, when an oscilloscope was connected instead of the discriminator module. Normally, the discriminator always uses the signal from the shaping amplifier.

[8]In the case of the ADC connection, a quasi-differential approach is utilized – the ADC has a differential input, but one of the wires is grounded by a serial terminating resistor on the side of the transmitter.

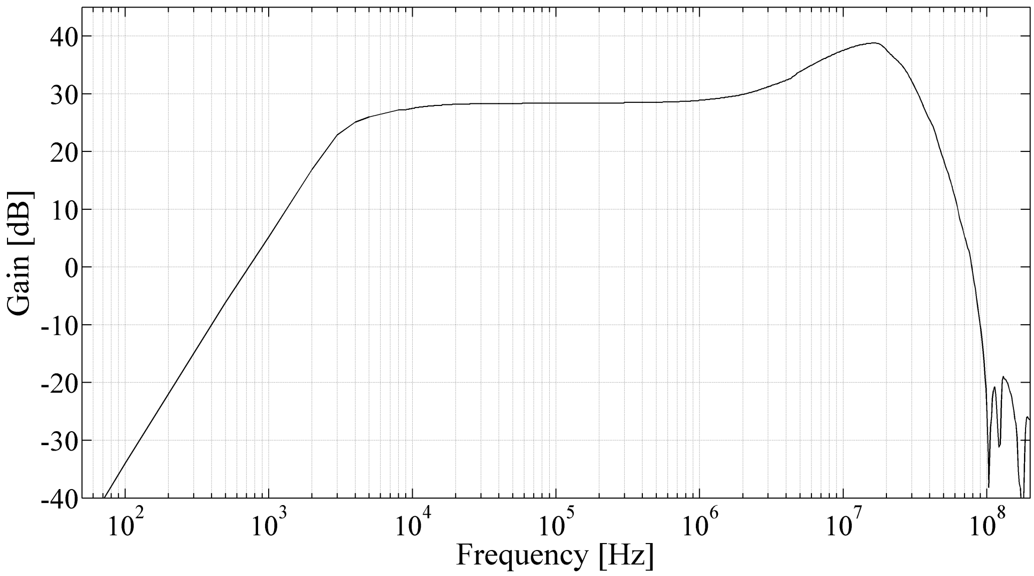

Figure 4.12: The frequency response of the whole analog signal path. The suppression of low frequencies ($40^{dB}/_{dec}$) is caused, among others, by the BLR circuit, which is non-linear – therefore the presented characteristic will depend on the amplitude of the signal. The visible raise of gain in the range of 10-20 MHz is the effect of the pole-zero compensation. The measurement of the characteristics up to 10 kHz has been made with a function generator and an oscilloscope, and for higher frequencies a vector analyzer was used

Sampling analog-to-digital converter

The analog-to-digital converter (ADC) is a key element responsible for the data acquisition. A 10-bit AD9601-200 chip, operating at a sampling frequency of 200 MHz, was used for this task. The data from the converter is processed by an FPGA chip from Xilinx Spartan 3E family, namely XC3S500E. It provides data reception and caching, and then it transfers them to a computer. The data is sent over Ethernet network and the high bandwidth (10 MB/s) was achieved through a completely hardware implementation of the transmission protocol. While maintaining full compatibility with Ethernet standard, the protocol has been simplified – in fact, the communication takses place only in one direction, without acknowledging, using only the basic Ethernet frame. The higher layer protocols, such as UDP or TCP/IP, are not used at all. As a result of such an approach, it is not possible to collect the data beyond the local network – this is the price paid for a relatively simple, but efficient solution based on the FPGA. The control of the FPGA is possible via a microcontroller, coupled with the other elements of the device by the internal I^2C bus (see paragraph 4.3).

The data acquisition is performed in triggered mode (just as it is in digital oscilloscopes), and enables the measurements to be performed at a repetition frequency of 20 kHz, with buffer length of 256 samples per measurement. The triggering signal is generated internally by the FPGA. Theoretically, external triggering with the discriminator output is possible – the ADC works continuously and the data is stored in a circular buffer, so all three common schemes of triggering might be used: pre-, mid- and post-triggering. This feature was provided for dark pulse registration, but it turned out that a relatively long buffer of recorded data is capable of accidentally coming across a dark pulse, so dark pulses acquisition with a random trigger is possible. In addition, the determination of the dark rate based on the histogram requires the use of a trigger which is uncorrelated with the MAPD dark pulses.

The discriminator-counter module

Although the measurement of dark rate can be achieved on the basis of the histogram, the device has been fitted with a discriminator and a pulse counter to provide an independent method of dark rate measurement.

The discriminator is made using a fast comparator: AD96687 with ECL-level output. The digital pulses are then extended by a monostable ECL flip-flop. The flip-flop provides a possibility to set the discriminator's dead time, which is independent of the input pulse length. Than the pulses are converted to TTL logic levels and counted using a two-stage counter. The first stage is a 4-bit TTL counter, while the second is based on a built-in counter of the Atmega88 microcontroller. This solution allows counting the pulses with the average rate of about 5 MHz, but a dead-time correction is required above about 1 MHz.

The comparator level is set digitally by means of a digital-to-analog converter (DAC) with 10-bit effective resolution. A proper calibration (see page 39) allows one to set the threshold in order to measure the dark rate at desired level (e.g. 0.5 p.e.), according to the previously measured MPPC gain.

The discriminator PCB contains two independent measuring channels with individually adjustable thresholds, allowing simultaneous measurement of dark counts at two levels (for example, 0.5 and 1.5 pe). This feature has more to do with the capabilities of integrated circuits used (dual comparator, dual flip-flop, etc.) than with the intention of accelerating the measurement, which takes only 1-2 seconds.

The slow-control system

The control of all slowly-varying parameters defining the conditions of the measurement is done by a dedicated controller. The device is equipped with an Atmega128 micro-

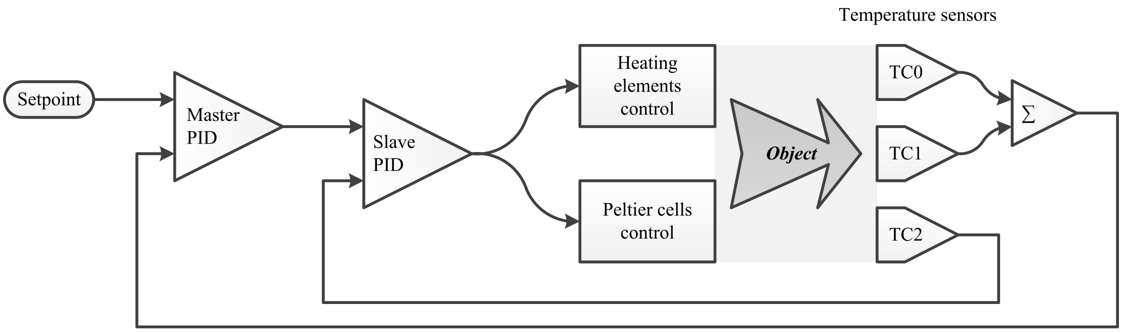

Figure 4.13: Temperature stabilization of the feeder tray. The inner (slave) loop controller uses the TC2 sensor placed on the bottom of the feeder box, close to heaters and Peltier modules. The outer (master) loop controls the inner one basing on the readouts of the TC0 and TC1 sensors placed on the tray, near the measured photodiodes. The controllers, marked as PID, in fact use only the proportional and integrating blocks (PI)

controller, with a number of external analog-to-digital and digital-to-analog converters. Among them, a key role is played by a 24-bit $\Delta-\Sigma$ ADC converter – AD7718. It's a specialized, precision converter with a built-in preamplifier and 10-channel multiplexer, allowing direct acquiring signals from various sensors which normally require a sensitive preamplifier (thermocouples, thermistors, strain gauges, etc.). This converter is responsible for temperature measurements as well as MPPC bias voltage monitoring and light intensity control. The whole system is supplemented by accompanying analog circuits (mostly input and output buffers).

The detailed tasks of the controller are:

- temperature control of the feeder tray and MPPCs,
- MPPC bias voltage control,
- pulsed light intensity control,
- feeder position setting,
- control over cooling fans for various high-power-dissipating elements,
- performing the procedure of remote switch-off of the device.

Feeder tray temperature control is performed via a two-stage, cascaded proportional-integrating controller (PI), whose block diagram is shown in figure 4.13.

The inner control loop sets the heaters or Peltier modules to bring the temperature of the feeder box to the requested value. This control is possible thanks to the PT-1000 temperature sensor placed on the bottom of the box. Depending on the sign of the error signal, the controller enables warming or cooling systems, and the power supplied to them is continuously adjusted by means of an 8-bit DAC.

The outer loop is to maintain the desired temperature of the MPPC feeder by adjusting the temperature in the inner loop. To measure the temperature of the tray, two precision class A PT-1000 sensors are used. The tolerance of the elements used allows to measure the temperature with an absolute accuracy of 0.2°C without any calibration.

The use of two cascaded controllers improves the stability of the control loop and ease of tuning, while providing quick response to changes in the temperature setpoint.

An experimental circuit was built-in into the device to allow estimatng the temperature of the MPPC structure, basing on the voltage drop across the forward-polarized junction of the MPPC. While the determination of the absolute temperature of the structure using this method might be problematic, it could measure the voltage drift, showing if the junction temperature has been stable enough to start the measurement. This system, however, has never been used, as it was easier to monitor the stability of the temperature of the die by periodically measuring the MPPC gain.

MPPC bias voltage control. The regulation of the high voltage used to bias the MPPC is done in two stages. The first stage is a power supply providing constant voltage of 92 V. The second stage provides a control mechanism with digital feedback loop. This solution gives a very accurate control, but due to the large time constants (software feedback loop and an accurate but slow ADC) requires prior stabilization and filtering of the input voltage to eliminate the voltage ripple.

The output voltage can be continuously adjusted in the range from 30 to 80 V, while maintaining an absolute accuracy of 10 mV. There are some simple security elements at the output of the controller: a relay, which cuts off the power when the feeder box is open or the voltage limit is exceeded, and a serial resistor of 10 kΩ to protect the photodiode in case of putting it in the socket in reverse position (it would cause forward polarization of the junction). The voltage drop across the resistor during normal operation is a fraction of mV and has no effect on the obtained results.

Light intensity control is provided by a cascaded PI controller, as in the case of the temperature control system. The inner loop is responsible for setting the supply voltage for the Kapustinsky circuit. The outer loop stabilizes the average light intensity by changing the desired voltage. Due to the almost-exponential dependence of the light level from the supply voltage (figure 4.6), the input data for the regulator is the logarithm of the measured light intensity[9]. This allows the controller to operate with higher gain (which means it's faster), while maintaining the stability in a wide range of setpoints.

Feeder position setting is carried out by means of a stepper motor and the previously mentioned optical sensor. The motor is controlled with half-step resolution; due to the low power and moderate clocking frequency it is not required to stabilize the winding current, or to gradually accelerate and break the motor during movement.

The position sensor has two independent channels (two photodiodes at the opposite sides of the tray surface), which is important for its reliability. Since a free movement of the feeder could lead to a damage of the cable connections for temperature and position sensors, there is a number of software mechanisms to prevent such a situation: the sequence of both channels activation is detected, and moreover, the drive is automatically stopped if no sensor is detected after turning the tray by more than 180° (the angle is calculated basing on the number of steps done). The tray will also stop automatically if the feeder box is opened.

Control of the fans. The whole unit has three independently controlled groups of fans: for the feeder box cooling, for power supply cooling module and for entire electronics box. The fan speed in each group is independently controlled by modified proportional controllers[10]; it's set basing on thermistor temperature sensors located in different locations within the device. The fans are controlled via an 8-bit DAC and power elements located in the power supply.

Communication with PC – the Ethernet connection

A 100-megabit Ethernet link was chosen to exchange the data with the controlling computer, which is an essential part of the measurement system. This solution was chosen due to several important advantages:

- virtually all modern computers are equipped with the Ethernet adapter;
- this solution provides sufficient throughput;

[9] Calculated in an approximate way by straight lines.

[10] For each group a minimum operating voltage of fans is determined, below which they are switched off. In addition, the fans for the feeder cooling system are automatically stopped when heating elements are activated. The main fans of the electronics box are never completely switched off, but only slowed-down to a minimum speed.

– it provides galvanic isolation between the device and the PC, so there is no risk of the appearance of undesired ground loop – which would be a problem for example in the case of USB connection.

The device contains two modules equipped with Ethernet interface. One is the high-speed ADC. The second one is the communication interface that provides the interconnection between the computer and the internal I^2C bus of the unit, which is responsible for the control of individual components. A solution with two separate interfaces (for device control and data acquisition) is due to the design of the ADC interface – excessive expanding of the functionality of the interface based on FPGA is difficult. A better solution was to use a separate μP-based controller, which is quite slow compared with a purely hardware solution (FPGA), but provides an incomparably greater flexibility and ease of programming. The communications module uses an ATmega128 microcontroller and a dedicated *Wiznet* W-3150 chip which supports the network connection with the TCP/IP protocol.

In order not use two separate cables for communication, a standard 4-port Ethernet switch was installed in the device. An additional advantage of its operation is that it eliminates possible network conflicts that the ADC module could cause.

The power supply

The power supply, featuring a total power of about 500W, provides a number of voltages required for the operation of the device:

– +5 V for digital circuits (other voltages, if required, are made directly on the PCBs of the individual modules)

– ±7.5V for high-speed analog (this voltage is reduced to ±5V by the local voltage regulators of individual modules)

– ±18V for other analog sub-systems (this voltage is also locally reduced – to ±15V)

– +92V for the MPPC supply,

– +12V and +24V for high-power systems such as heating and cooling

– +5V for power supply's internal logic (this is a standby voltage which remains active after the device is turned off).

In addition to the DC voltage regulators, the power supply unit contains all power elements of the regulators responsible for maintaining the temperature and fan control.

Due to high power and big capacitance of the power supply's filtering capacitors, a soft-start circuit with a fixed-value power resistor was used. After start-up, the resistor is shorted by a relay.

The idea not to use switching regulators in the power supply results in significant power losses, reaching about 200 W. To dissipate this heat, all high-power elements have been placed on a common, high-performance cooling module in a form of tunnel-type heat sink with a fan.

Due to the sophisticated grounding system, some parts of the power supply were designed to have floating ground. The various ground subsystems of the device (there are five, at all) are connected in few different places. Since some of these connections are placed on removable modules, whose removal would result in a loss of integrity of the grounding, which is potentially dangerous to the electronics, there is a ground-control system on the motherboard, which monitors the difference in potentials between particular grounds. If any of the grounds differs from the case shield potential by more than 200 mV, the device is automatically switched off.

The power supply includes a number of security systems, which include, besides the ground control system, the monitoring systems of different voltages and currents in each circuit. Although the power supply's logic is quite complex, it is not connected with the rest of the device via the I^2C bus. Instead, it has a simple user interface with an alphanumeric LCD display, providing the monitoring of all the power supply voltages and corresponding currents, temperature in various places, as well as diagnostic information – available even after the emergency switch-off.

4.4 MPPC gain calibration

Measuring the real value of the MPPC electron gain requires a prior calibration of the measurement circuitry. Theoretical determination of the gain of the entire signal path proved to be virtually impossible due to the complexity of the system – all attempts ended with fairly random results, whose accuracy was far from satisfactory. An attempt to determine the characteristics of the signal path using the vector analyzer also did not give satisfactory results due to the difficulty of interpretation – the coupling of the preamp input with 50-ohm cable of the analyzer is different from the coupling with the MPPC.

Finally, an appropriate matching circuit was used to calibrate the system – a simple device which emulates the MPPC in terms of electrical parameters (with an accuracy limited by our knowledge on MPPC parameters and the tolerance of small capacitors used in this matching circuit), and allows the injection of a specified charge into the

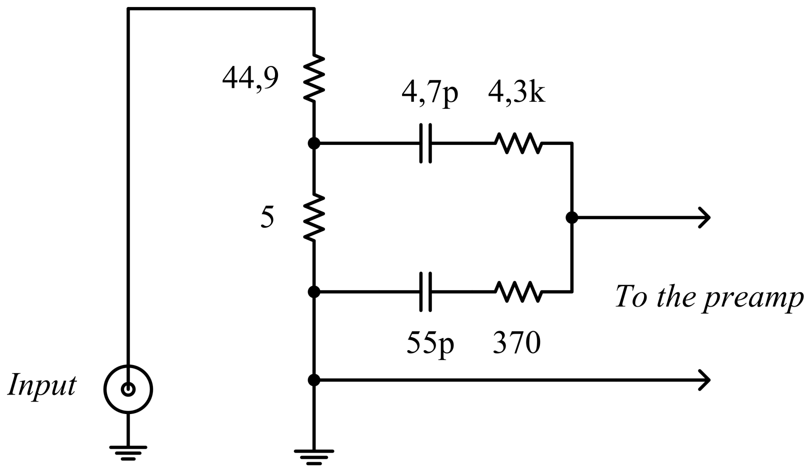

Figure 4.14: The matching circuit used to calibrate the device.

preamplifier. This approach has eliminated the need of the analysis of input preamplifier circuit by ensuring that it will be operated under the same conditions during calibration as during MPPC measurements.

The schematic diagram of the matching circuit is shown in figure 4.14. The charge injected into the preamp is determinded by the amplitude of the pulse applied to the input voltage divider. The divider is used to increase the immunity to interference – when connecting the matching circuit to the preamp, a ground loop is formed, and it is important that the signal sent through the cable has a relatively high amplitude to maximize the overall SNR. In addition, the existence of the voltage divider reduces the impedance of the voltage source which drives the output. As shown by *Spice* computer simulation, the exact frequency compensation of the divider is not needed, because its possible variations only slightly affect the shape of the output signal, and completely do not affect the overall charge. The experiments have shown that the shape of the signal did not have a noticeable effect on the final result of the calculated charge.

The whole process of the device calibration has led to the following conclusions:

– Although the results obtained by calibration using the circuit mentioned above were repetitive and computer simulations showed no obvious influence of the components tolerance to the final gain measurement (with the exception of the input voltage divider resistors), the accuracy of calibration can be carefully determined at 20%[11].

– MPPC parameters, in particular the total capacitance, have an observable impact on the shape of the system response (this has been shown with 400-pixel MPPC

[11]Undoubtedly, many unsuccessful attempts to calibrate the device, similar failed attempts of other teams have an impact on such a conservative estimate. Of course, a simple error calculation gives much lower values than 20%, but it does include unexpected error sources.

measurements: the pole-zero compensation circuit, which was tuned for diodes with 667 pixels, in the case of smaller structures gave a negative overshot in the pulse tail). At the same time, no impact of the change in the pulse shape on calculated integral was observed, which in a way confirms the linearity of the measuring system. Therefore, once the calibration is carried out, it's valid for structures of various sizes (different number of pixels).

4.5 Author's participation in the construction of the device

The designed device, despite its compact size, is in fact a complex measurement system, which required many technical problems to be solved and a number of basic questions about the methods of measurement to be answered. Its construction took over a year (not including the initial phase of planning and research with a prototype system) to a four-people team. In this job, the Author was responsible for the following tasks:

- development of the concept of photodiode feeder, design of the feeder with its housing and mounting of the whole unit;
- design, construction and commissioning of the preamplifier and whole analog circuitry;
- design, installation, programming and commissioning of the discriminator unit;
- design, installation and commissioning of the pulsed light source;
- design, installation, and commissioning of the slow-control system and associated elements (with the exception of power end-stages);
- design and installation of the motherboard with the ground control system;
- development of the grounding system.

In addition, the Author invented the concept of a single measurement channel cooperating with feeder tray, direct temperature measurement of the structure and the digital integration of the signal. He is also the creator of the aforementioned prototype testing system (with the exception of the temperature controller).

Chapter 5

Measurement data processing

5.1 Data flow

The data processing algorithms are essentially an inherent element of the presented device. The data from the ADC (256 samples per pulse) are transmitted via Ethernet to the computer for processing[1]. There, in real time, the signal is integrated within specified time window, and integrals of the individual pulses create a pulse amplitude histogram. This is the basic data for further calculations, which can take place at a time when data acquisition is not carried out (semi-on-line, eg when changing the position of the tray, or completely off-line, at any later time).

Thanks to the pulse integration at the very beginning of the processing, the data flow is reduced from 10 MB/s to about 40 KB/s, which does not require large computing power requirements for further calculations (a single PC with 1.5 GHz processor was successful to perform all the tasks in real-time).

5.2 Pulse integration and histogram creation

In the designed device, the signal integration can be performed by the analog integrator, or digitally, at the stage of digital data processing. Analog integrator has been provided primarily as an 'emergency exit' only if it turns out that the digital integration does not work well. A very high quality of the results obtained from the digital integration was confirmed already in the initial testing phase, so the analog solution has never been used – in all measurements the signal was integrated by means of software.

The pulses are pre-selected prior to the integration – these cases are rejected, where the range of the ADC is exceeded, or an accidental pulse tail is found at the beginning of the

[1] As mentioned, they can be simultaneously transmitted to the disk array for archiving.

integration window. Then, the signal within desired time window (typically 48 samples, which comprise the entire pulse) is summed, and the result is scaled to the range of 0-1023. A 1024-bin histogram is then formed basing on the integral values.

Theoretically, it would be desirable to pre-filter the signal to cut-off high frequency components, where the influence of aliasing effect is quite strong, (quite low attenuation of the analog filter) and useful information is negligible. This operation would increase the signal-to-noise-ratio (SNR). In fact, the process of signal integration acts as a low-pass filter, and additional filtering would involve considerable computational effort, which could be a major problem regarding the high data flow, and at the same time it would only slightly increase the data quality.

Before proceeding to the description of the next stages of data processing, it should be mentioned that the operations described below were performed in most cases twice. For the first time – automatically during the measurements, allowing to quickly check the parameters of measured MPPCs (these calculations were often a necessary stage in the measurement process – for example a dark count rate measurement requires the prior knowledge of electron gain to set the discriminator threshold). For detailed measurements, including the purposes of this elaboration, these operations have been performed for the second time, basing on archived histograms, using a number of procedures written in Matlab environment. This approach enabled a careful selection and optimization of various data processing procedures to obtain results of possibly highest quality. Since most of the results presented in this study were obtained basing on this second path, the following paragraphs will describe the algorithms and procedures developed in Matlab, which were in some cases different from these used by on-line processing.

5.3 Electron gain calculation

The key operation to calculate the electron gain of the MAPD is the exact finding of the positions of the histogram peaks, because the distance between them defines the value of the gain. In order to find the peaks, an approximation with a number of Gaussian distributions (one for each histogram peak) is commonly used. The expected values of particular Gaussian functions are treated as the position of relating peaks. This method works quite well even with poor data statistics and allows to find peak positions with a resolution better than the width of the histogram bin, however it has some drawbacks:

– It is a source of systematic errors if the actual peak shape is not symmetrical. The asymmetric shape of the peaks actually appears for some device settings, which, on the other hand, guarantee the smallest width of the peak, ie the best resolution.

- It was noted that a simple iterative algorithm of peak fitting with Gaussian functions could lose convergence in some cases, which resulted in incorrect results on the one hand, and on the other in a substantial loss of time on unproductive calculations.

- In general, the process of approximation of the whole histogram takes a relatively long time, which was also observed by other institutions working on MPPC measurements.

Due to the described problems, we finally decided to use a completely different philosophy of peak searching, which is based on the filtering of the histogram with a FIR Gaussian filter with adaptive width. The task of the filtering process is to smooth the histogram to the extent that there are no random local maxima caused by statistical fluctuations in the number of counts in particular bins. By the way, the interpolation filter allows to increase the resolution of the histogram. In order to ensure a better quality of filtering, it is performed twice – the process of gain calculation is as follows:

- The first pass of the filtering algorithm is processed by a filter whose width is defined by the variance of the data in the histogram, which is a very rough measure of the average distance between the peaks.

- All peaks and valleys of the histogram are located. The search is based on the analysis of the histogram's derivative, which is calculated as a convolution of the histogram with a differentiating filter of the form:

$$f(x) = \frac{x}{4.5}\sqrt[3]{\frac{\pi}{2}}cos^2(\frac{\pi}{2 \cdot 4.5^3}x^3) \ , \tag{5.1}$$

  whose shape is shown in figure 5.1[2]. The overall width of the differentiating function defines the minimum distance between the peaks to be detected by the algorithm.

  The value of the derivative can be calculated for any argument – there is no limit to the discrete points defined as a histogram bin centers. This means that the positions of the peaks and valleys can be found with a resolution better than the histogram bin width – the same as in the case of a Gaussian approximation. In order to determine whether the extreme is a maximum or minimum, the sign of the second

[2]The presented form of the filter was determined experimentally. The advantage of the presented function is missing of any sharp edges, so that differentiation is less sensitive to noise contained in the histogram, and on the other hand, a brief, analytical form of the function allows its calculation for any specified point. At this moment, the Author is not able to explain, why simply a derivative of Gaussian function wasn't used.

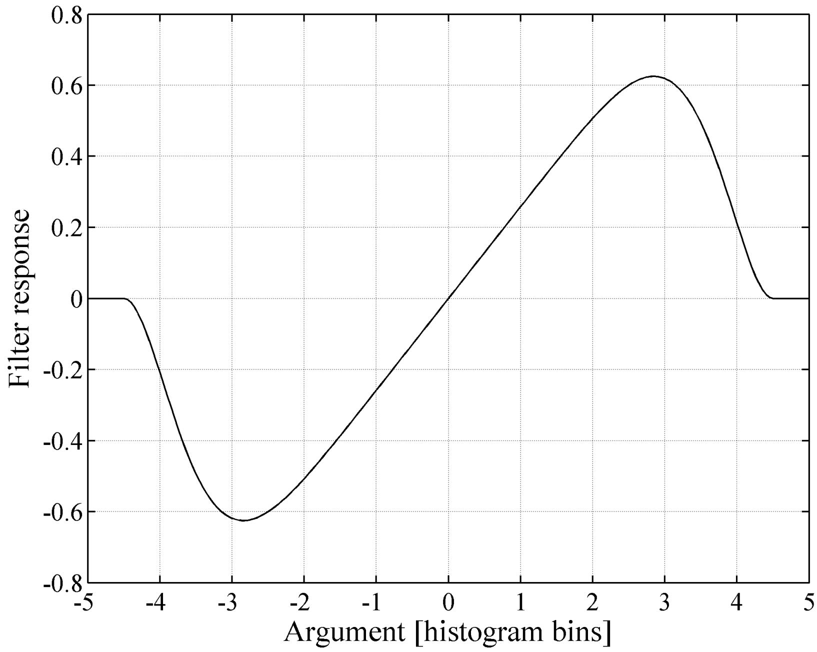

Figure 5.1: The differentiating filter impulse response.

derivative of the histogram is tested – the same differentiating filter is used for the second time to calculate the second derivative.

- The raw histogram is again subjected to the Gaussian smoothing filter, but this time, the width of the Gaussian function is adapted to the average distance between the peaks found in the previous iteration.

- Again, histogram peaks are located (using the same algorithm as in the previous pass). 'Flat' peaks and valleys are eliminated from the set of found extrema, because their position usually can not be determined with high accuracy, and consequently their inclusion in further calculations would reflect negatively on the accuracy of the final determination of the gain.

- The average distance between the peaks is then measured, while the set of distances is iteratively decreased to reject those distances that differ too much from the average (in practice, this means rejecting the outer peaks related to high p.e. number, and sometimes the 0 p.e. peak; the position of the 'inner' peaks does not affect the average distance).

- The average distance between the peaks, after a proper scaling, is a measure of the MPPC's electron gain.

Another issue is the estimation of the gain calculation errors. This problem will be further described in section 5.5.

5.4 Dark rate measurement

The basic measurement of the dark rate is performed by the discriminator and the counter and, as such, does not need special data processing, except for the introduction of the discriminator's dead-time correction. However, in most of the measurements the dark rate was independently determined using the histogram obtained in the dark. This is done in several steps:

- The thresholds of 0.5 and 1.5 p.e. are determined by the position of the 0 p.e. peak on the dark histogram and the electron gain, which was previously calculated;
- The dark rate is given by the total number of counts above the specified threshold divided by the total gate time (defined as the product of the number of counts and a single integration window width);
- The dead-time correction is optionally applied.

Both methods of the dark rate measurement provide the 'resultant' dark rate, which consists of both dark generation and afterpulses, if no correction is applied. However, the histogram analysis can also help determining the actual rate of thermal generation, excluding the effects of the correlated noise. This can be done basing on equation (3.2) from page 43. To obtain the rate in s^{-1}, the resultant value of λ is divided by the length of the pulse integration window.

The further data processing provides an estimate of the error of the dark rate measurement, taking into account such factors as the accuracy of determining the threshold of 0.5 p.e., the accuracy of bias voltage setting and MPPC temperature, and the statistical distribution of pulse count.

5.5 Breakdown voltage calculation

The MAPD breakdown voltage (V_{br}) is determined as the intersection of the extrapolated characteristics of $G(V_{op})$ with the x axis (figure3.2). This characteristics (determined on the basis of several measurements for different V_{op}) was approximated using one of three functions:

– A linear function: $G = A \cdot V_{op} + B$. The assumption of such a model means, in fact, that we assume that the junction capacitance is constant and the electron gain depends only on ΔV.

  The fit is performed using the least-square method to minimize the $G(V_{op})$ variations.

– A quadratic function, so that a linear change of the junction capacitance versus bias voltage is taken into account. Again, the same least-square fitting method is used.

– A quadratic function with changed fitting criteria, which this time do not concern the electron gain, but the junction capacitance. If the capacitance changes with the voltage, the electron gain can be described as:

$$G(V_{op}) = \frac{1}{e} \int_{V_{br}}^{V_{op}} c_j(V) dV \ , \tag{5.2}$$

  where e is the electron charge, and $c_j(V)$ defines the dynamic capacitance of the junction. Let's introduce a *quasi-static* capacitance:

$$C_j(V_{op}) = \frac{1}{V_{op} - V_{br}} \int_{V_{br}}^{V_{op}} c_j(V) dV \ ; \tag{5.3}$$

  now the gain will be expressed simply as $\frac{1}{e} \cdot C_j \cdot (V_{op} - Vbr)$.

  The aim of the fit is to find such a value of V_{br}, where the dependence of $C_j(V)$ is as close to linear function as possible (by the way, this is a function of a possibly constant value). It turns out that the assumption of bad V_{br} results in a significant 'bending' of the $C_j(V)$ dependence.

  This method was developed for verification purposes during the data analysis using a quadratic fit and should give the same results.

The result of a determination of V_{br} may be affected by a large error when measurement points are quite away from the value of this voltage. Therefore, the error of the V_{br} was every time estimated using data bootstrap method, which is a very powerful statistical tool, especially when error distribution is not known [12].

5.6 Correlated noise analysis

The phenomena related to afterpulses and crosstalk were not analyzed in detail in the study presented, but the total fraction the correlated noise (CT+AP) was determined. For this purpose, a dark histogram is used.

The process of calculating the fraction of CT + AP is realized in the following steps:

– The histogram is brought to a discrete form (see page 40).

– The probability of 0 p.e. (p_{0pe}) and 1 p.e. (p_{1pe}) pulses is calculated.

– Basing on p_{0pe}, the actual rate of dark generation is determined. Knowing the expected value of the theoretical Poisson distribution, one can determine the theoretical value of (p_{1pe}).

– CT+AP fraction is determined by the equation (3.3) – see page 43.

5.7 Photon detection efficiency estimation

The measure of the photon detection efficiency (PDE) is the average number of photons recorded in the light measurement (of course while maintaining a constant level of illumination), with an obvious correction for the CT+AP fraction. The mean number of photons, which is the theoretical expected value of the Poisson distribution of histogram peaks, can be calculatd basing on the 0 p.e. peak amplitude, just as in the case the dark rate estimation. This method, however, has encountered a technical problem of the dynamic range of the testing device. At high electron gains (eg for high overvoltage), the histogram's tail exceeds the limits (see figure 5.2), making it impossible to determine the total number of counts (N_{tot}). Further, neither the determination of the value of p_{0pe}, nor the distribution's λ value is possible.

For this reason, the amplitudes of 0 p.e. and 1 p.e. peaks are used. It's easy to notice, that for the Poisson distribution, $\lambda = \frac{p_{1pe}}{p_{0pe}}$, which means that the ratio of the number of counts for the first two histogram peaks is enough to find the expected value of the distribution. The information on the total number of counts is not required, but one should be aware that the amplitude of the 1 p.e. peak is disturbed by the events associated with correlated noise and requires a correction for the CT+AP fraction. This value is normally determined by means of a dark measurement.

Finally, the average number of photons recorded in a single time gate in the light measurement can be calculated as:

$$\lambda_{light} = \frac{N_1}{N_0} \cdot \frac{1}{1 - P_{(\mathrm{CT+AP})}} - \lambda_{dark} \ , \tag{5.4}$$

where N_0 and N_1 are the numbers of counts corresponding to 0 p.e. and 1 p.e, $P_{(CT+AP)}$ is the total fraction of crosstalk and afterpulses (see equation 3.3) and λ_{dark} is the probability of a thermal generation in a single time gate.. The calculated value of λ_{light} is a direct measure of the PDE.

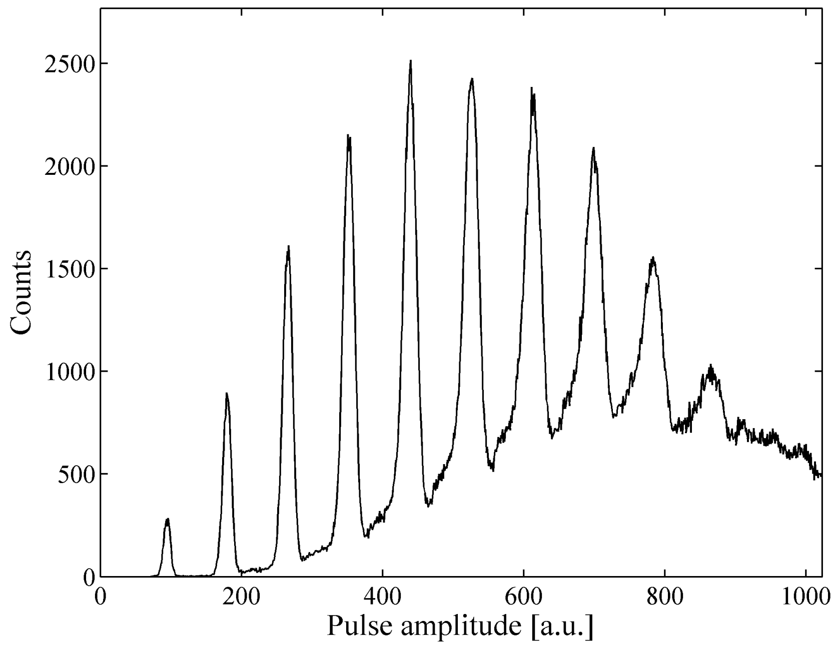

Figure 5.2: An overranged histogram of pulses from a light measurement. Determining the average number of registered photons is still possible thanks to an analysis based on the amplitude of the 0 p.e. and 1 p.e. peaks

Chapter 6

Results of the Measurements

6.1 Introduction

Some results of the measurements were already presented in the previous sections as examples to illustrate various issues and ideas. Also, some of the MPPC properties, already presented, have been deduced on the basis of obtained results (waiting for them up to this point would create uncomfortable insinuations, especially in the chapters regarding the MAPD operation). In this chapter, more emphasis will be put on the completeness of the results and their wide representation. Some topics will be described more accurately, such as the issue of interpretation of the junction capacitance measurement.

Some of the results presented below correspond to the data presented in the publication [25]. It is because the results presented in both papers come from the same measurements.

6.2 Measurement results – MPPC characteristics

Measurement series

All the data presented in this chapter come from three series of measurements:

– The first series of screening measurements. These measurements were performed for a total number of 1206 MPPCs, usually at one temperature (25°C) and one supply voltage (determined by the nominal value of V_{op} given by the manufacturer). Some specimens were tested at several voltages and several temperatures. The advantage of this series is that the dark count rate was measured using the two methods. The biggest drawback is the fact that the measurements were carried out before some test equipment modifications to increase its accuracy. Minor corrections to the device, made during these measurements, also resulted that the data are not always consistent, and usually require a pre-selection before presenting the results based on them. The results based solely on this measurement series can be found in the early studies of the MPPC, for example [11].

– The supplementary series of screening measurements after device modifications – these were mainly the changes in the pulse shaping and integration window length. 221 MPPCs were examined at a constant temperature (25°C), but with a number of supply voltages (usually 7 values, covering the range of 800 mV around the nominal V_{op}). This series enables one to determine the breakdown voltage of the diodes. Unfortunately, the histograms for dark measurements were not acquired, which makes this series hardly useful in terms of determining the parameters associated with the MPPC noise.

– The series of detailed measurements. 7 MPPCs have been studied – one 400-pixel prototype (1x1 mm structure) and 6 specimens of the final 667-pixel model (1.3 x 1.3 mm) with serial numbers TA8092, TA8120, TA8160, TA8584, TA8744 and TA9314. The measurements were carried out for 11 temperatures from 0 to 50°C and bias voltage distributed in the range of approximately 2V (about 50 values), which is virtually the entire useful range for these elements. A great number of measurements, even redundant ones, allowed to eliminate random errors to a great extent.

Electron gain, breakdown voltage and junction capacitance

Electron gain. The electron gain dependence on the bias voltage for a single diode and several different temperatures is shown in figure 6.1. The extrapolation of the characteristics down to the intersection with the x axis ($G = 0$) allows to determine the breakdown voltage of the diode (V_{br}) for a given temperature. The calculation of V_{br} allows one to plot a new characteristics of gain, this time as a function of ΔV[1] (fig. 6.2).

It is easy to note, that in this coordinates, the gain is strictly dependent on ΔV, and at least at first glance, independent of the temperature.

[1] $\Delta V = V_{op} - V_{br}$.

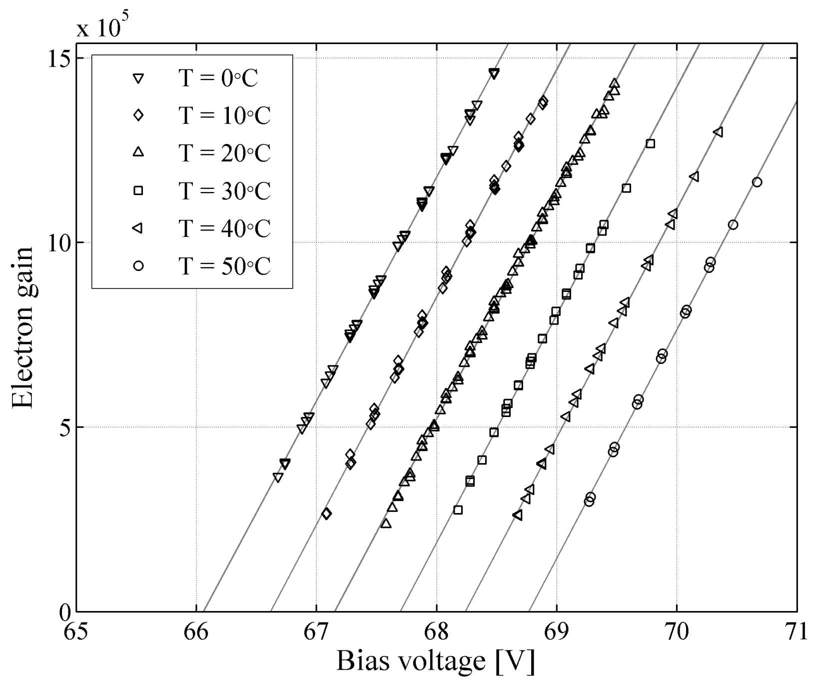

Figure 6.1: The dependence between the electron gain and the supply voltage for one MPPC measured at different temperatures. An extrapolation (here – linear) of the measurement series to the x-axis indicates the breakdown voltage for each temperature

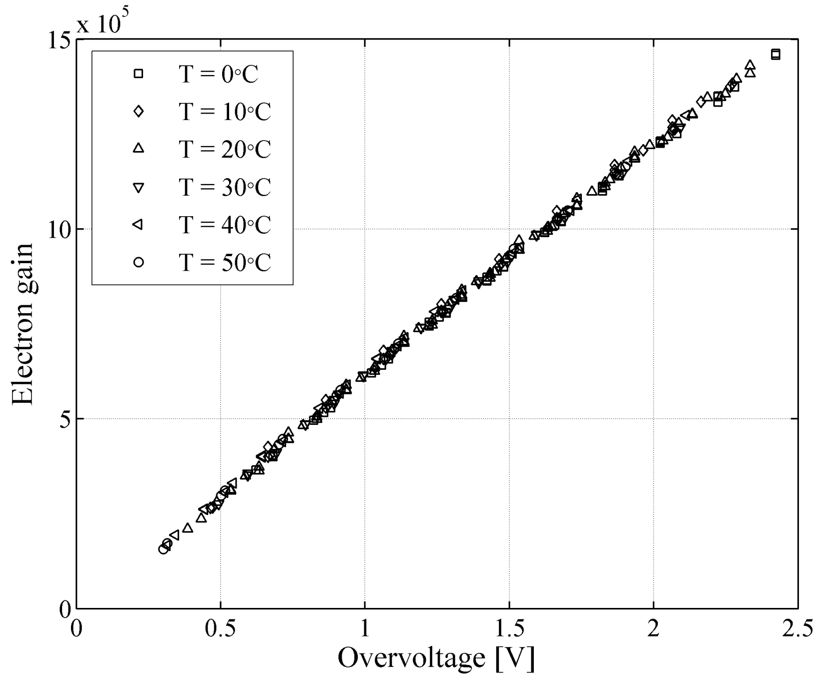

Figure 6.2: A typical dependence of the electron gain and overvoltage. No noticeable effect of temperature change on the characteristics can be observed

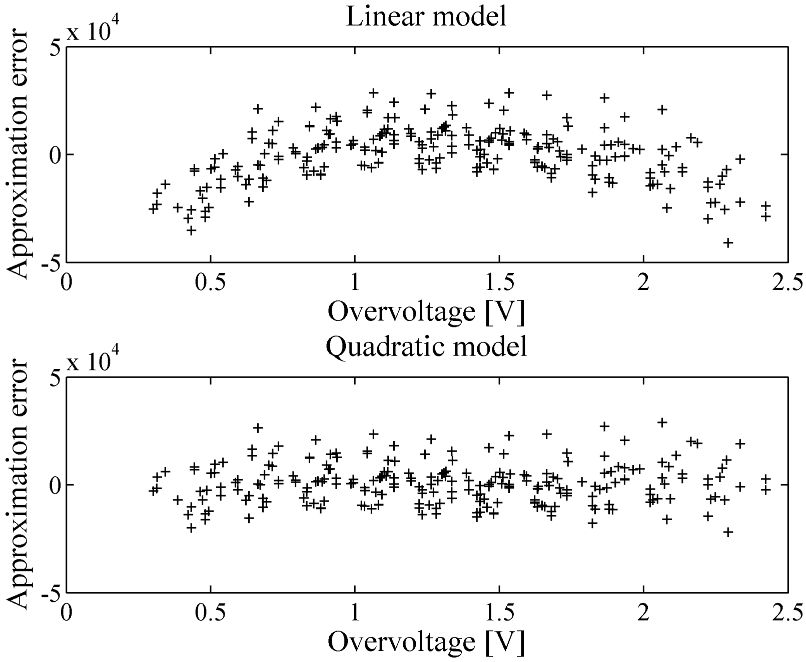

Figure 6.3: The residua (deviations of the measured values from the approximated curve) for the linear and quadratic model of the $G(V_{op})$ dependence. The vertical axis is scaled in electron gain units

The dependence between the electron gain and ΔV can be considered linear with satisfactory precision, but a quadratic function gives a better approximation[2] (figure 6.3), as it takes into account the changes in capacitance as a function of the junction bias voltage. For typical operating voltages[3] ($\Delta V = 0.5 - 2V$), the electron gain values are estimated to be 3×10^5 to 1.2×10^6. The nominal value given by Hamamatsu, which is 7.5×10^5, was reached for the ΔV of about 1.3 V.

Breakdown voltage. As shown in Figure 6.1, the value of the breakdown voltage is a function of temperature. This dependence can be considered linear in the observed temperature range (Fig. 6.4); the temperature growth of 1 °C leads to an increase of V_{br} by about 54.5 mV. The described effect can be explained by a relationship between temperature and the mean free path of carriers in silicon (the mean free path generally decreases with the temperature; the slope of this function is variable and depends on the temper-

[2]Although the fit with a quadratic function is more accurate than a linear one, it requires high-quality data; otherwise the value of V_{br} determined on its basis has a relatively high dispersion. The practice has shown that it should be considered every time, which function to use to obtain reasonable results of V_{br}, remembering about the systematic error made by linear fit on one hand and the dispersion associated with a quadratic fit on another hand. An example, how the errors made by bad fit look like, is presented in section 6.2.

[3]An attempt to determine the optimal supply voltage is shown on page 103.

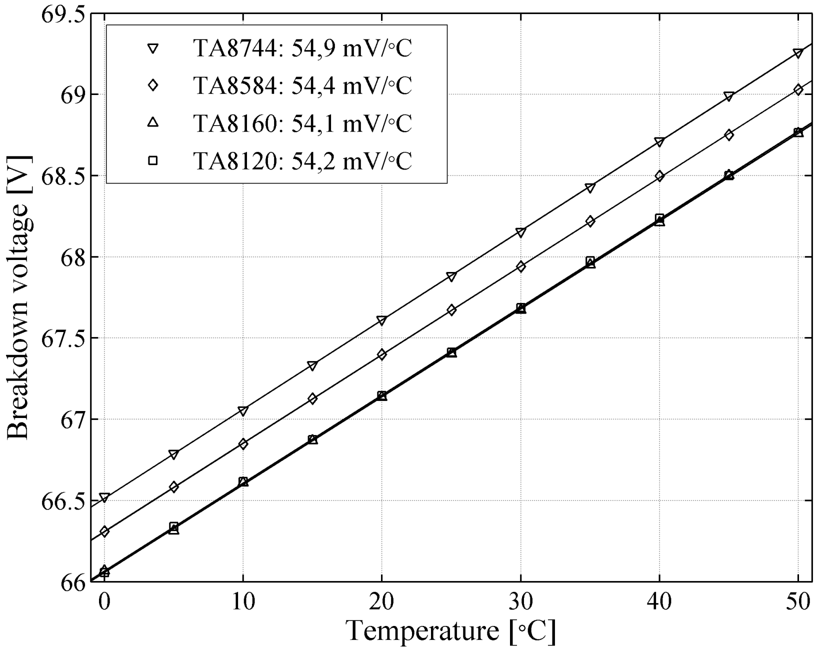

Figure 6.4: The dependence between the breakdown voltage (V_{br}) and the temperature for a few specimens of the MPPC. The slope (about 54.5 mV/°C) can be considered as fairly universal value and applied to all MPPCs

ature and dopants concentration [28]). Figure 6.5 shows the distribution of the V_{br} value at a constant temperature of 25°C for 64 photodiodes.

Given that the practical range of the MPPC operating voltage is of about ±0.5V around the nominal voltage, a spread in V_{br} of almost 2 volts means that the supply voltage of various MPPCs must be independently set in the final application. If the unit operates in a wide temperature range, it may be necessary to constantly tune the supply voltage to maintain constant electron gain.

Junction capacitance. The slope of the $G(\Delta V)$ function can be considered as a measure of the capacitance of the junction (section 2.1).

If the gain of the testing device is absolutely calibrated, it is possible to determine the value of the junction capacitance. On the basis of the performed calibration (section 4.4), it can be stated that the value of the pixel capacitance of 90 fF, given by the manufacturer, is reasonable. Due to the limited accuracy of the calibration, presenting any numbers appears to be pointless at this moment.

A detailed analysis of the gain dependence on temperature and junction bias voltage lets one to pay attention to two phenomena:

– The fact that the dependence of $G(\Delta V)$ is approximately quadratic, means that

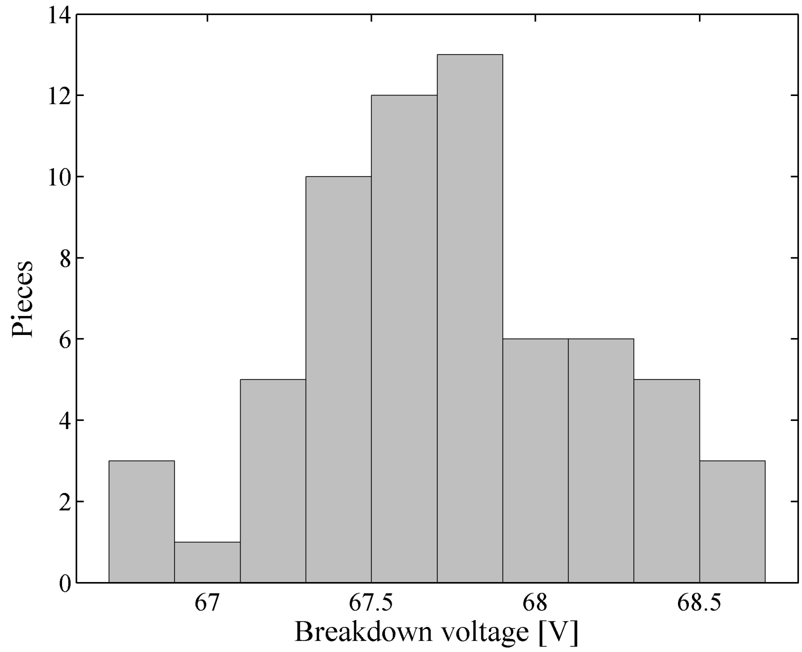

Figure 6.5: The breakdown voltage histogram for 64 photodiodes. The distribution has truncated, tails, suggesting a rejection of the units with extreme values of the V_{br} by the manufacturer

there is a linear dependence of the junction capacitance on the bias voltage. Indeed, it appears that the correlation is surprisingly strong – a relative change in capacitance as a function of the voltage is approximately -10%/V. Such a large change can not be explained by changes in the width of the depleted region. Instead, we should state that the model in which the electron gain depends only on the ΔV and the junction capacitance, is imperfect – in fact, the gain depends on some other factors[4]. However, as the simple model we use is very convenient, the Author proposes to stay using it, noting that the size which was previously called simply 'junction capacitance' will be called, from now on, the 'effective junction capacitance'.

As shown in figure 6.6, the measured voltage drift of the effective capacitance is dependent on the temperature and varies almost twice in the temperature range of 0 to 50 degrees. A more accurate description of this dependence can not be determined due to quite high dispersion of the data.

[4]Unfortunately, at the present stage of research, the author is not able to provide an alternative model, which would have physical background. At this point one should to take into account the limitations of the used model, and use use the experimentally determined quadratic dependence to accurately determine the gain.

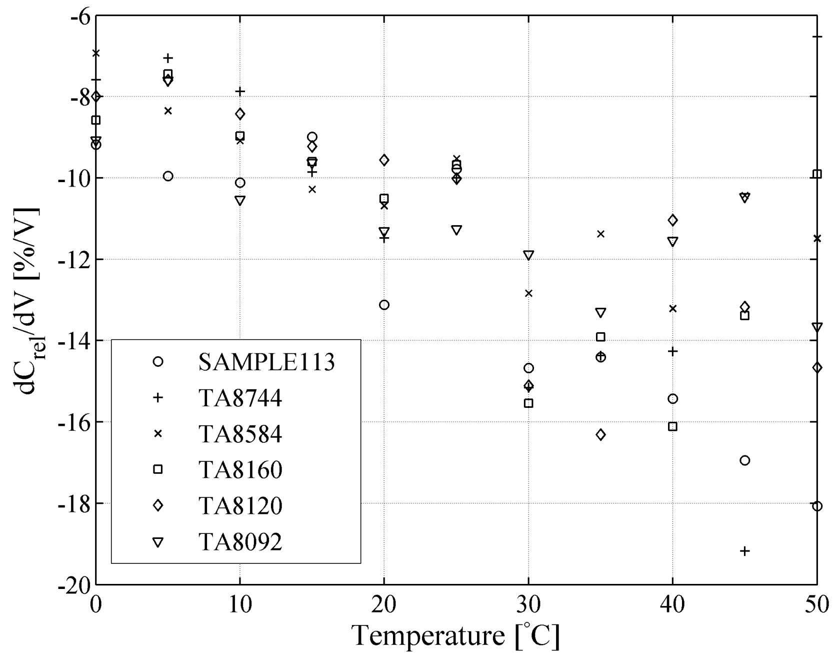

Figure 6.6: The change of the effective capacitance for one Volt (relative, given for ΔV=1.5V) for different temperatures. It can be carefully assumed that the dependence is growing with temperature increase. The dispersion of the data does not permit any modeling of this dependence

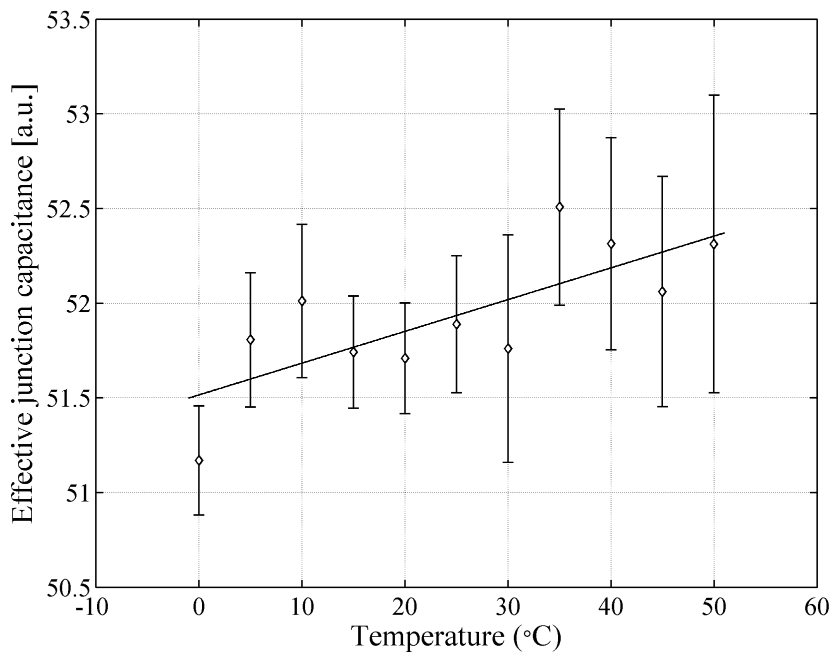

Figure 6.7: The dependence of the effective junction capacitance (given in arbitrary units) versus temperature for a constant ΔV (which means in essence various bias voltages) measured for a single MPPC (TA8120)

Finally, it should be noted that the results have been repeatedly verified, in particular the linearity of the testing device over its whole dynamic range was checked very carefully.

– One can expect a drift of the junction capacitance with the temperature, as a result of changes in dielectric permittivity of silicon [17]. Unfortunately, any attempts to measure this dependence gave the results of a large dispersion, which do not allow to verify this hypothesis for sure.

  Although some consistent results were obtained in a long series of measurements carried out for one MPPC and specific measurement conditions (presented in [25], also shown in fig. 6.7), a similar analysis for a larger number of specimens gave quite random results. The author is of the opinion that the issue of capacitance dependence on the temperature requires additional measurements[5].

Dark pulses

Measurement of the the dark rate (DR) could be carried out by two techniques, as already mentioned – using a discriminator and a counter or basing on the histogram (an example of a dark pulse histogram is shown in figure 6.8). Figure 6.9 illustrates a comparison of the results obtained with both methods. Although these results are highly correlated, they have quite clearly different values. It turns out that due to afterpulsing, the dead time of the measuring system has a strong influence on the measured dark rate (a system with lower dead time will record more afterpulses) and this effect occurs in a very wide range of measured count rates. One should keep this in mind when comparing results obtained by different methods and with different devices (in particular, it is difficult to compare the values measured by different labs.)

The dependence of DR on the voltage. Figure 6.10 shows the dependence of the real dark generation rate on ΔV for several temperatures. It's easy to observe that the dependence can be described by a linear function for reasonable values of ΔV. The distortion of the characteristics visible at higher voltages is an apparatus effect – along with the overvoltage increase, more pulses in the integrator time window begin to appear, which are not actual dark counts, but the afterpulses coming from the dark pulses which appeared earlier. This artifact can not be eliminated with used measurement metho d.

[5]Probably, the determining of the dependence of the *real* junction capacitance on the bias voltage, and thus creation of a new, improved MPPC gain model will be needed, because the temperature drift of V_{br} leads to the inability to measure the capacitance always at the same voltage.

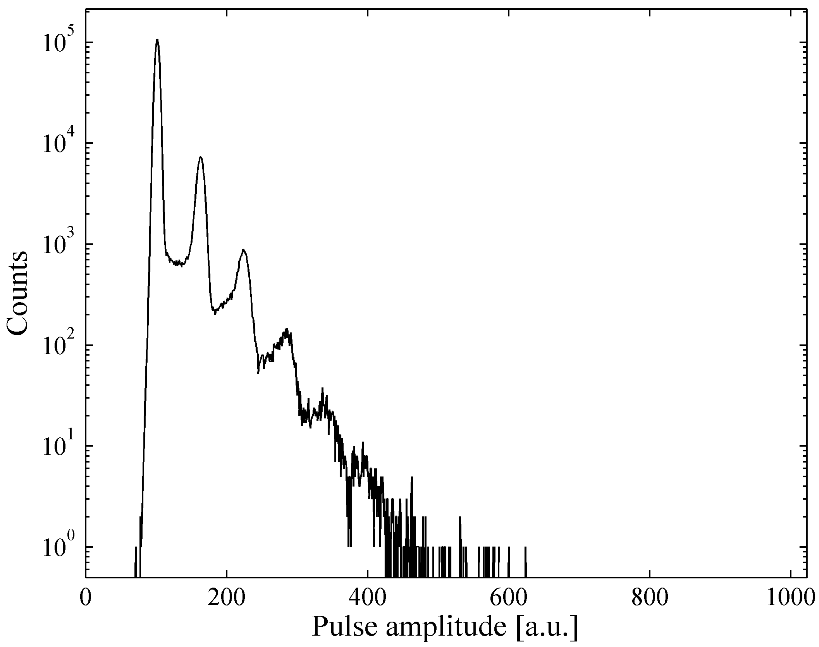

Figure 6.8: A histogram of the dark pulses for MPPC s/n: TA8744 at 20°C and $\Delta V = 1.19$V

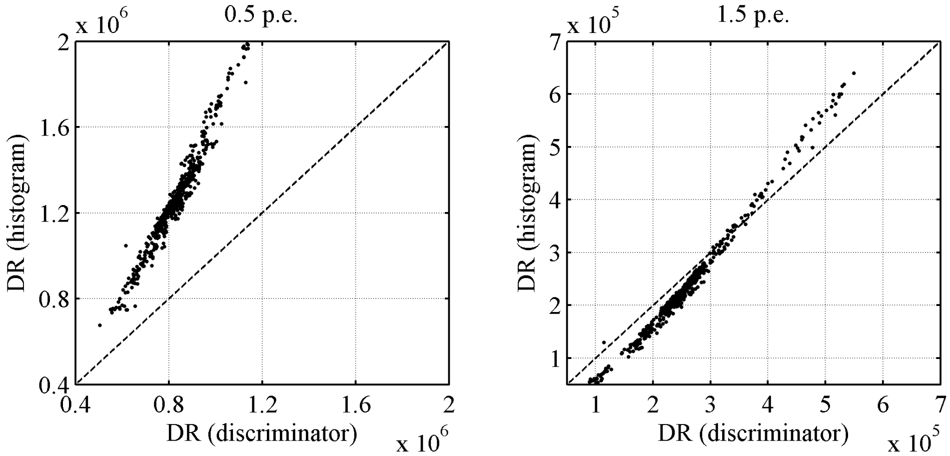

Figure 6.9: The mutual dependence of the dark rate measured by two methods (using data from the discriminator or histogram) for two thresholds (0.5 and 1.5 p.e.). The data come from the early measurements – some outliers can be seen, especially for the threshold of 0.5 p.e. The differences in the count rates measured by two methods due to the different dead times are clearly visible

The chart points out that a simple extrapolation of the dependence of $DR(\Delta V)$ does not converge at $\Delta V = 0$, as could be expected[6] – but at another point. This is the result of systematic errors in the calculation of V_{br} on the basis of gain-voltage characteristics, resulting from the imperfection of the function used to approximate the measurement

[6]See also page 102.

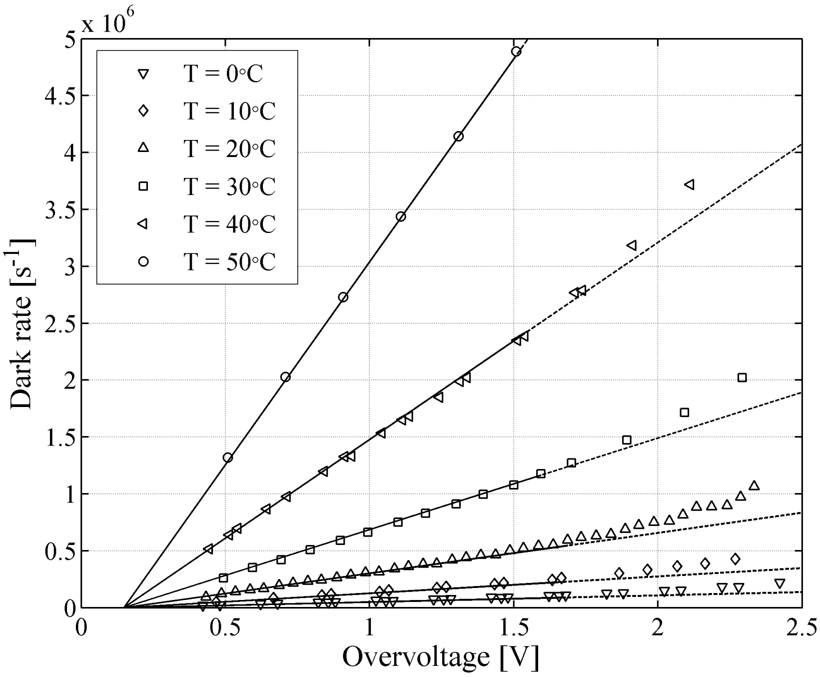

Figure 6.10: The dark generation rate dependence on ΔV for different temperatures. The lines approximating the data are determined according to equation (6.8) and are assumed to intersect at one point. Due to systematic errors in the breakdown calculation basing on the gain-voltage characteristics, this intersection does not agree with the found value of V_{br}. The normally-linear dependence of DR(ΔV) is affected by the effects of CT+AP for high overvoltages.

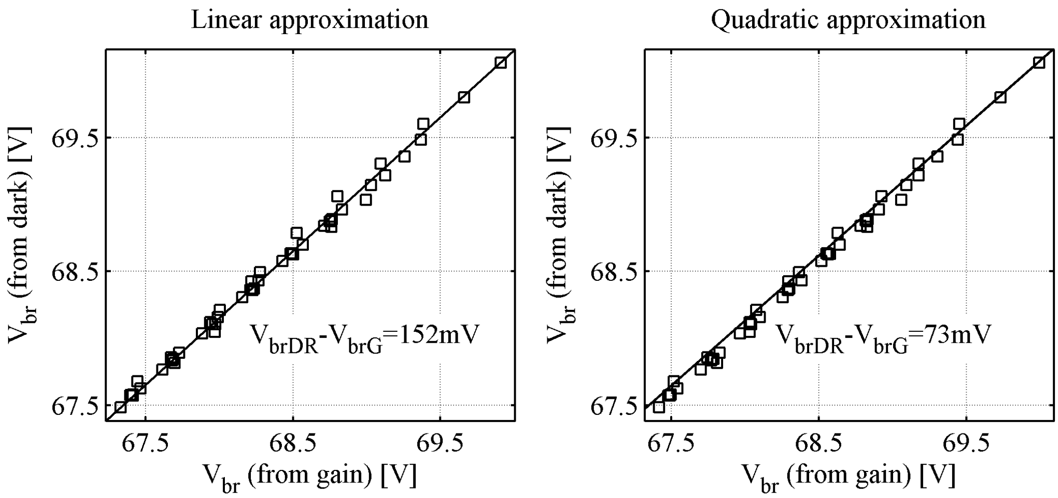

Figure 6.11: Comparison of determining the breakdown voltage (V_{br}) with two methods for 7 MPPCs in various temperatures. The results come from a series of detailed measurements and the value of DR is determined by means of histogram. The value of V_{br} from gain characteristics was based on linear (left) or quadratic fit (right). To find the V_{br} from the DR characteristics, a linear extrapolation was used in both cases

points. This phenomenon has been quite thoroughly analyzed, and some results are shown in figure 6.11. Basing on the DR dependence on (V_{op}), the breakdown voltage (V_{br}) can be defined – in the same way as basing on the dependence of $G(V_{op})$. Then both V_{br} values can be compared and the average difference between the results can be calculated. The measured value of the difference is quite random – for other test series (in which the apparatus was set up slightly differently) the difference between the V_{br} values calculated by two methods were quite different. Figure 6.11 shows such a comparison using a linear and quadratic model of $G(V_{br})$. The value of the difference is quite random – for the other test series (in which the apparatus settings were slightly changed) the difference between the V_{br} calculated by two methods were quite different.

Another issue to be noted is that the dependence of the dark rate on voltage[7] should be at least roughly consistent with the corresponding dependence for the PDE[8]. Basically, the dark rate is defined by the rate of thermal generation of carriers, and the probability of generating an avalanche. Thermal generation rate of primary carriers depends only on the temperature, and the resulting change in the total dark rate is a function of the voltage-related change of avalanche generation probability – the same factor, which determines the dependence of PDE on ΔV (see page 19). It can be assumed that there should be a linear dependence between the DR and the PDE (of course, one should keep in mind the above-mentioned problems of measuring the real DR at large values of ΔV). The actual shape of the measured dependence is shown in figure 6.12.

The dependence of DR on the temperature. Figure 6.13 shows the dependence of the dark rate on the temperature for several bias voltages. In contrast to previously presented voltage dependence, which was associated with PDE, the changes of DR with temperature are directly related to changes in the rate of thermal generation of carriers in the depletion layer[9]. The measurement points are arranged on a curve, whose general form can be determined theoretically, but this requires some understanding of the mechanisms of thermal generation in the semiconductor.

In silicon, the dominant mechanism of generation and recombination is the generation/recombination with traps due to the indirect bandgap of the semiconductor. The recombination (or generation) rate is given by the following equation:

---

[7] We are talking about the real dark generation rate, ie after the corrections of the measurement results for CT+AP.

[8] The dependence of PDE on voltage is described in section 6.2.

[9] A second factor that could affect the dark current – diffusion of minority carriers from the boundaries of the depleted area – is negligible in silicon.

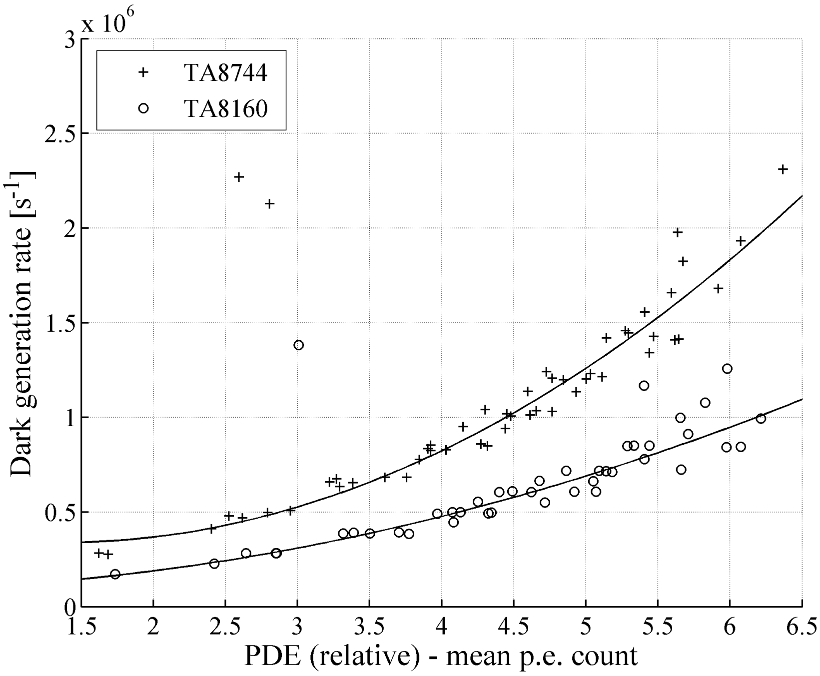

Figure 6.12: The dependence between DR and PDE (T = 25°C), which was supposed to be linear. Fairly strong deflection of the characteristics under extreme conditions (high ΔV, large values of PDE and DR) is due to the fact that the influence of the afterpulses can not be fully eliminated. It may happen that an afterpulse coming from an unregistered dark pulse will be recorded at the beginning of the integration window and treated as a 'true' dark pulse. This phenomenon happens quite often with large values of ΔV, and unfortunately it can not be detected in the context of a single event

$$R = \frac{np - n_i^2}{\tau_p(n + n_1) + \tau_n(p + p_1)} \ , \tag{6.1}$$

where n and p are carrier concentrations (electrons and holes, respectively), n_i is the intrinsic carrier concentration, τ_n and τ_p are the minority carrier lifetimes (they're constant for a given material), and the coefficients denoted as n_1 and p_1 are defined as follows:

$$\begin{aligned} n_1 &= n_i \cdot e^{\frac{E_T - E_i}{kT}} \\ p_1 &= n_i \cdot e^{\frac{E_T - E_i}{kT}} , \end{aligned} \tag{6.2}$$

where E_T where is the energy level associated with trapping centers, and E_i is the intrinsic level of the semiconductor.

Making two assumptions:

– the concentration of free carriers in the junction area is very small (strong electric field immediately removes all carriers)

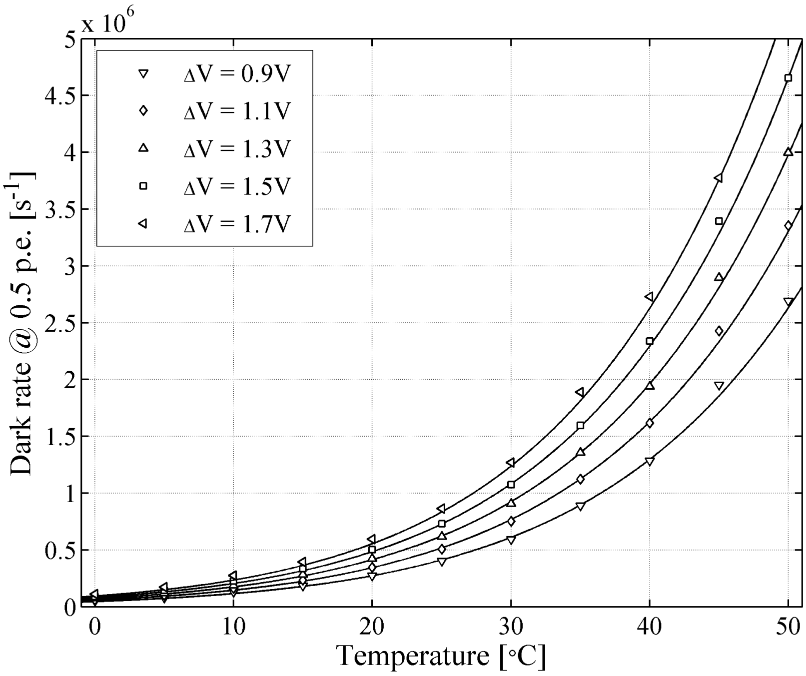

Figure 6.13: The dependence of the dark rate on temperature for several values of ΔV and one particular MPPC

– the trap level is located near to the middle of the bandgap (this level is the most effective from the point of carrier generation)

we can transform equation (6.1) to:

$$R \approx -\frac{n_i^2}{\tau_p n_1 + \tau_n p_1} = -\frac{n_i^2}{\tau_p n_i e^{\frac{E_T - E_i}{kT}} + \tau_n n_i e^{\frac{E_T - E_i}{kT}}} = \\ = -\frac{n_i^2}{\tau_p n_i + \tau_n n_i} = -\frac{n_i}{\tau_n + \tau_p} \ . \tag{6.3}$$

In general, the value of R may be positive or negative – in the latter case, this means that we have to deal with the carrier generation. In our case, the value of R is actually negative, so we're talking about generation. Since the minority carrier lifetimes are constants, the generation rate will depend only on the changing intrinsic concentration – n_i. This is given by the equation:

$$n_i = \sqrt{N_c N_v e^{\frac{E_g}{2kT}}} \ , \tag{6.4}$$

where E_g is the bandgap energy. Effective density of states in the conduction band (N_c) and valence band (N_v) are defined as:

$$N_c = 2\left(\frac{2\pi m_n^* kT}{h^2}\right)^{\frac{2}{3}}$$
$$N_v = 2\left(\frac{2\pi m_p^* kT}{h^2}\right)^{\frac{2}{3}}, \tag{6.5}$$

where m_n^* and m_p^* are the effective masses of carriers, constant for a given material, and h is the Planck's constant. Since all other parameters are fixed, the values of N_c and N_v depend only on the factor of $T^{2/3}$. Finally, the equation 6.3 can be shown as:

$$R = -\alpha \cdot T^{\frac{2}{3}} \cdot e^{\frac{-E_g}{2kT}} , \tag{6.6}$$

where α is a constant factor for a given material.

The dependence of the dark generation rate on the temperature at a constant voltage will have the same shape as the given R value. Finally, the dependence of the dark rate on the voltage and temperature can be described as:

$$\mathrm{DR} = A \cdot \Delta V^* \cdot T^{\frac{2}{3}} \cdot e^{\frac{-E_g}{2kT}} , \tag{6.7}$$

where $\Delta V^* = V_{op} - V_{br}^*$, while V_{br}^* is the breakdown voltage defined by means of the dark rate characteristics, T is the temperature in Kelvin, and A is a fixed factor determining the noise level of the MPPC, different for each specimen.

In the T2K workgroup an idea has been raised to present equation (6.7) in a slightly modified form:

$$\mathrm{DR} = \mathrm{DR}_{norm} \cdot \Delta V^* \cdot \left(\frac{T}{298}\right)^{\frac{2}{3}} \cdot e^{\frac{-E_g}{2kT} - \frac{-E_g}{2k\cdot 298}} . \tag{6.8}$$

In this case, DR_{norm} denotes the dark rate at $T = 25°\mathrm{C}$ (298K) and $\Delta V = 1\mathrm{V}$.

Analyzing equation (6.7) one can see that the dependence of $\mathrm{DR}(T)$ should be presented (in a reasonable temperature range) as an almost straight line on the plot in which the horizontal axis is the inverse of temperature, and the vertical axis – the logarithm of the dark rate. This form of presentation of this dependence is shown in figure 6.14.

Two coefficients should be found in order to properly fit the theoretical curve to the data points: DR_{norm} and E_g, where the value of E_g should agree with the known bandgap energy for silicon, unless a mistake was made. Actually, for a sample of five carefully measured MPPCs, the average bandgap was estimated to be 1.127 eV, with the value given by literature of 1.1 eV.

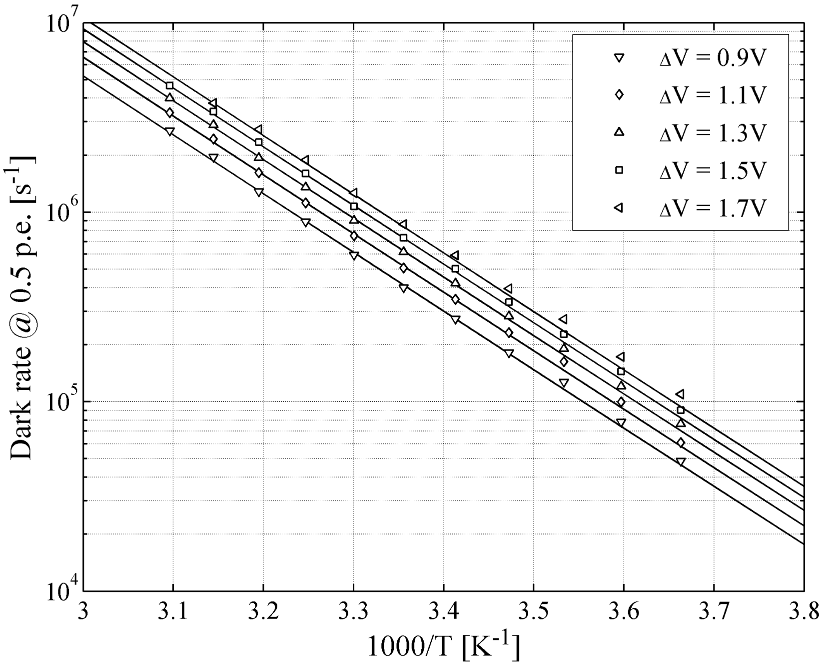

Figure 6.14: The dependence of the dark rate on the temperature as used to be shown in T2K: $\log(\mathrm{DR}) = f(1000/T)$

Production dispersions. Figure 6.15 shows the actual dark rate dependence on ΔV for a few specimens of the MPPC, highlighting significant production dispersion. For statistical purposes, the dark rate was measured for all tested elements (first screening measurement series, more than 1200 pieces). Unfortunately, after analyzing the data, it turned out that they were useless for this purpose.

The problem is shown in figure 6.16 – the measurement data shows two distinct mean level changes during the data taking and it could not be found if they are the result of changes in the Hamamatsu's technology (this is unlikely – the changes occur in the middle of the production series) or from accidental changes in equipment calibration (more likely – some minor changes to the software were made during measurements). For this reason, another series of measurements was used to see the statistics (this was the second screening series, more than 200 pieces, of which 58 could be used for this purpose). Figure 6.17 shows a histogram of dark rate at 0.5 p.e., normalized to $\Delta V^* = 1$V, at a temperature of 25°C (ie, the histogram presents the DR_{norm} values). As one can see, the distribution appears to be 'cut' at higher dark rates. This is probably an intentional action of the manufacturer, who eliminated the pieces with the dark current exceeding a particular value.

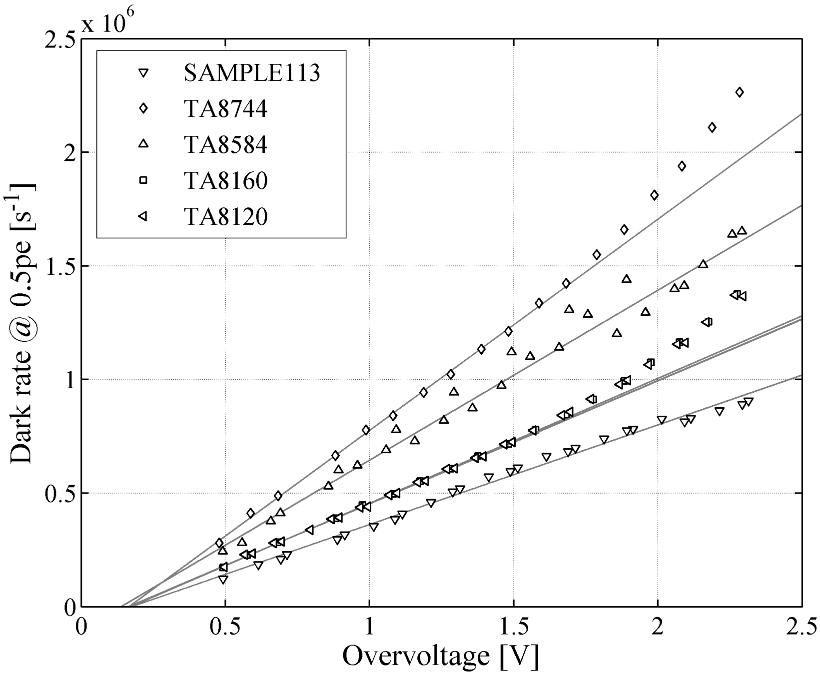

Figure 6.15: The dark rate as a function of voltage for a temperature of (25°C) and several photodiodes. The value of V_{br} has been calculated on the basis of gain characteristics – hence the difference in the point of intersection with the abscissa

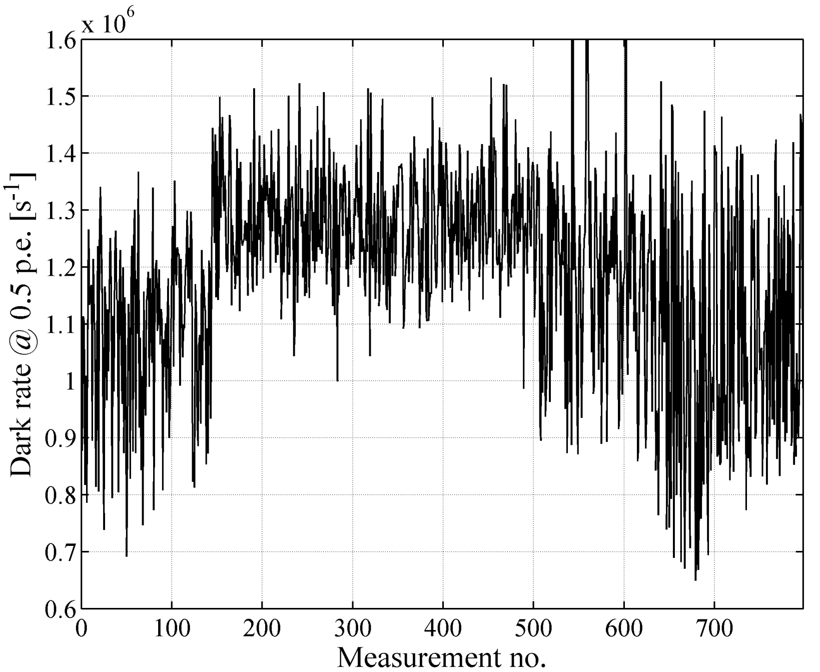

Figure 6.16: Dark rates ordered in time when the measurements were performed; two significant changes in the mean value of the measured frequency can be observed

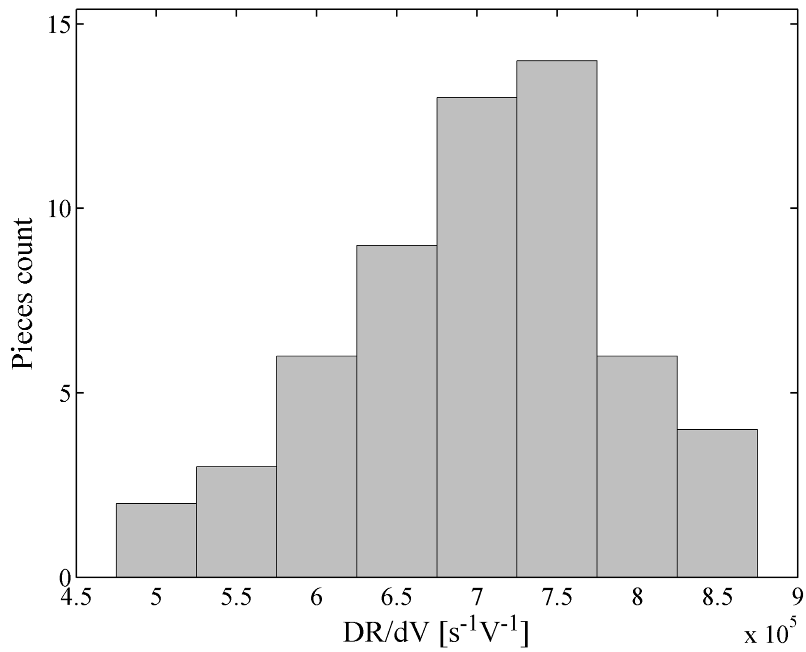

Figure 6.17: The distribution of the dark rate (0.5 p.e.) normalized to ΔV at V_{br} calculated on the basis of DR(V_{op}) – determined basing on measurements of 58 specimens of the MPPC at $T = 25°$C. The parameters of the distribution: $E = 7.0 \times 10^5$, $\sigma = 8.5 \times 10^4$, $\sigma_{rel} = 0.12$

Correlated noise – CT+AP

The dependence of the fraction of CT+AP on ΔV is shown in figure 6.18. The plot is based on the data for one MPPC tested at 6 different temperatures. The data is fairly consistent (in particular showing no CT+AP dependence on the temperature), and the dependence of CT+AP(ΔV) is close to quadratic in the initial phase, and at higher values of ΔV it becomes almost linear. One can find an arbitrary analytic function to fit the presented data, it seems better, however, to look for a reason for this particular shape.

The CT+AP fraction is dependent on two phenomena:

– The generation of primary electrons (photoelectrons generated by photons from neighboring cells for crosstalk, or electrons released from the trapped state for afterpulses). The number of electrons generated is directly proportional to the total number of charges in the primary avalanche, so the whole fraction of CT+AP should be linearly dependent on the electron gain.

– The probability of triggering the avalanche by these electrons (P_{av}) – so again there is a dependence on the PDE.

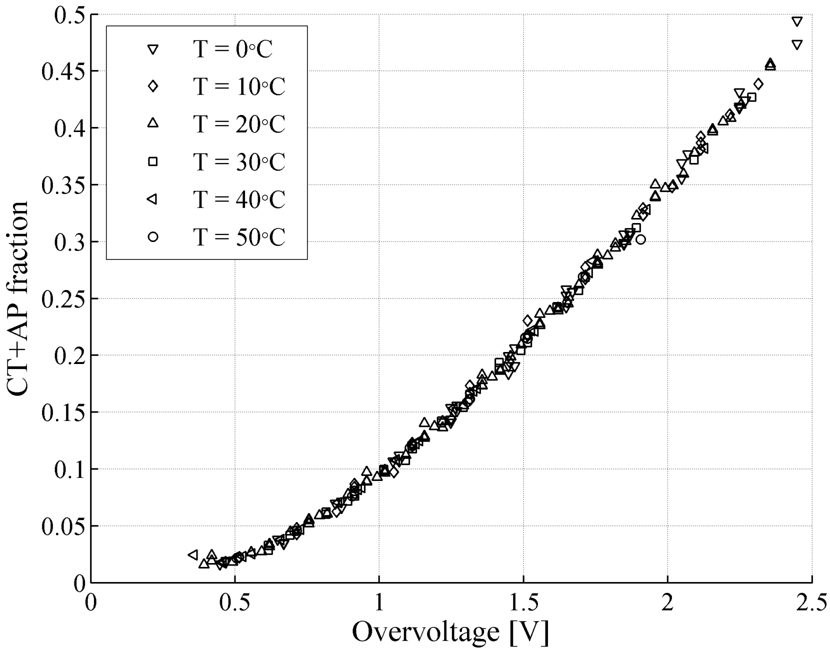

Figure 6.18: The CT+AP fraction as a function of ΔV and temperature for one MPPC: TA8744

Finally, the fraction of CT+AP should be eventually represented as:

$$\text{CT+AP} = A \cdot G \cdot \text{PDE} \ , \tag{6.9}$$

where A is a factor characterizing the fraction of CT+AP (determined probably separately for each MPPC).

To be precise, equation (6.9) is true only for small values of CT+AP – the reason is hidden in the specific definition of this parameter, because it is not talking about *average* number of secondary avalanches generated, but about the likelihood of generating *at least one* avalanchee. Therefore, the equation (6.9) can not be longer justified, if there is a significant fraction of events where at least two secondary avalanches are generated. Nevertheless, assuming that the number of secondary avalanches has a Poisson distribution, a corrected model can be derived, which is consistent with the given definition of CT+AP:

$$\text{CT+AP} = 1 - e^{-A \cdot G \cdot \text{PDE}} \ . \tag{6.10}$$

Figure 6.19 shows an attempt to verify the described dependence. As it's shown, the dependence of CT+AP on the product $G \cdot$ PDE is almost linear (most probably, the systematic errors associated with relatively complex calculations leading to calculate

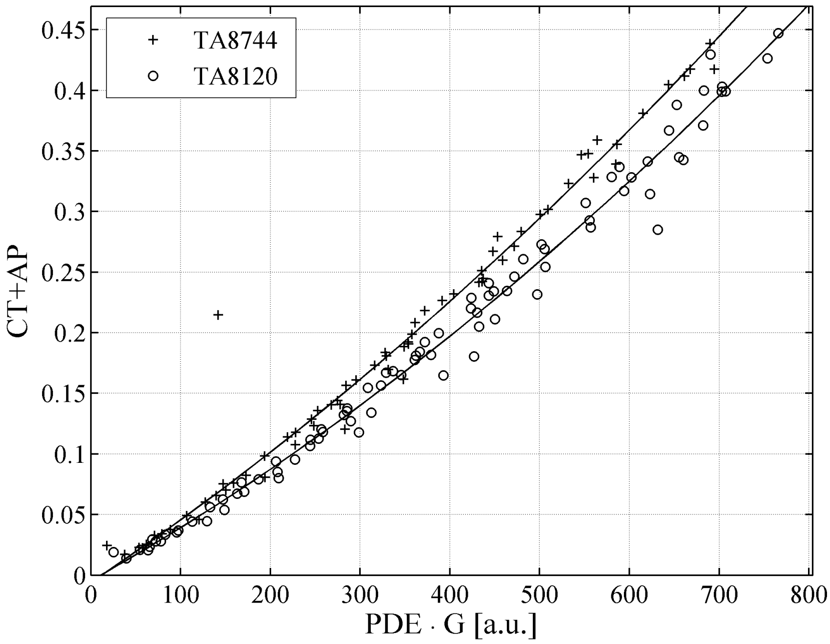

Figure 6.19: Dependence of the CT+AP on the product of PDE for two MPPCs. Data was acquired for 11 temperatures from 0 up to 50°C

the value of PDE are one of the reasons for slight non-linearity[10], another one is the aforementioned issue of the definition of CT+AP). The plot shows the data for two MPPCs to show existing production dispersion.

Since only the series of detailed measurementsthe is suitable for calculations of CT+AP and PDE, and this series consists of only seven MPPCs, it was not possible to plot a distribution of CT+AP among specimens, as it was done for the dark rate.

Photon detection efficiency

Although the results of determining the photon detection efficiency (PDE) have been used already in previous sections, they are presented at the end due to the hierarchy of the calculations (to calculate PDE, one needs to calculate the gain, dark rate and CT+AP first, as it was described in section 5.7).

Figure 6.20 shows the dependence between PDE and ΔV at six different temperatures for a single MPPC. A quite large dispersion at higher voltages is observed, but the shape of the function is consistent with earlier assumptions and also with data reported by other institutes.

[10] At the same time, high data dispersion at larger values of CT+AP indicate an increase in random errors. They are also primarily related to the calculation of PDE.

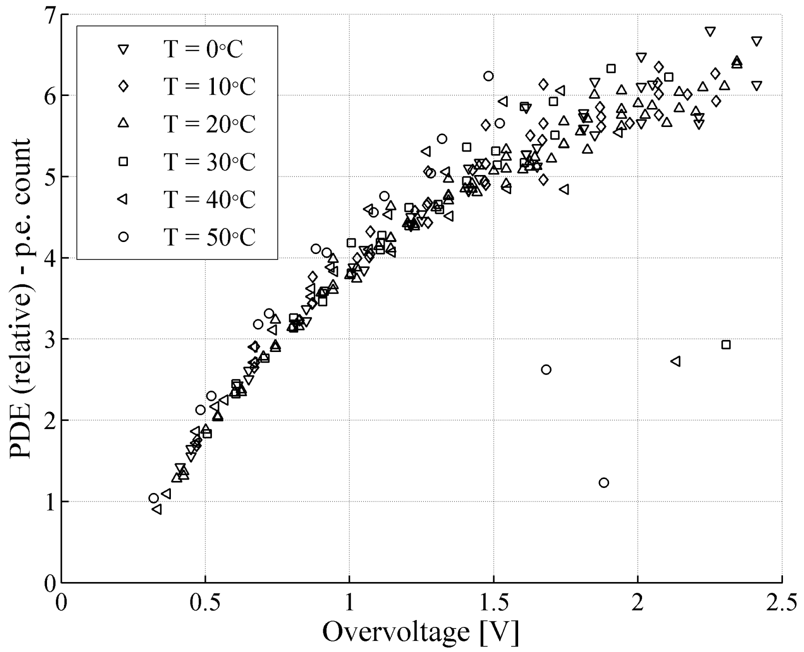

Figure 6.20: Dependence of photon detection efficiency (PDE) on ΔV and temperature for one MPPC: TA8160

– For low values of ΔV (not exceeding 0.8 V), the dependence of PDE(ΔV) is almost linear.

– For higher voltages, the curve gradually bends, up to saturation.

The presented curve can be fairly well approximated with a quadratic function, but one has to remember the limitations of such an approximation for large valuesof ΔV (large enough to go beyond the normal working conditions of the MPPC), where analytical function's value falls, which has no reflection in reality. The data can also be approximated with acceptable accuracy by a function of $1-e^{-x}$, which asymptotically tends to a constant value. It should be borne in mind that both of the functions have no physical basis, but were chosen arbitrarily.

Unfortunately, the collected data does not allow to plot the distribution of PDE for a large quantity of MPPCs.

Useful range of operating conditions

The measured characteristics of MPPC make it possible to determine the conditions under which the device should work with best performance. When searching for such optimal conditions, the following factors should be taken into account:

– Maintaining a moderate dark rate, or rather moderate value of DR/PDE. At a constant DR/PDE ratio, these conditions are better where higher PDE is achieved. In this case, the point of interrest is not the actual dark generation rate, but the total rate – including the effects of CT+AP. Moreover, this value should be given for a particular discriminator threshold level, which will be set basing on the pulse amplitude in the target application. When analyzing the dark rate at higher thresholds, one should also take into account the pulse shaping.

– Maintaining low values of CT+AP. A high fraction of CT+AP will result in significant pulse amplitude spread, and thus, a significant decrease in the energy resolution of the entire scintillating detector equipped with the MPPC, especially when working with very weak pulses of light (few photons).

– Achieving possibly high electron gain. High gain allows one to reduce the requirements regarding the noise of the preamplifier coneccted to the MPPC.

The MPPC working conditions are determined by two parameters: the bias voltage (V_{op}) and the temperature. The temperature should be as low as possible, because the lower the temperature, the lower is the dark rate. In practice, the MPPC can easily operate at a room temperature (20-25°C). Cooling down the structure by a few degrees can significantly reduce the dark noise. On the other hand, raising the temperature to above 45°C will make the MPPC virtually useless for most purposes.

Selection of an appropriate bias voltage requires a deeper analysis. Figure 6.21 shows the dependence of various parameters on the MPPC overvoltage (ΔV) at a temperature of 20°C. As one can see, from the point of view of the MPPC noise (PDE/DR), operation at rather low overvoltage is reasonable. This is important especially at higher discriminator thresholds, which are characterized by a strong dependence of the dark rate on the overvoltage. On the other hand, limiting the bias voltage leads to a decrease of electron gain, which puts high requirements on the noise performance of the preamplifier and good shielding from interference. In practice, it may be even more important that working with low ΔV leads to PDE reduction – when working with small pulses, it will cause a deterioration of counting statistics, which will affect the overall SNR and energy resolution of the scintillating detector.

As a result, the bias voltage should be selected so as to find a compromise between a number of phenomena, and the optimum value will depend on the average number of photons, and the pre-amplifier noise. The operation at low light levels (typical for MPPC) requires the ΔV to be around 1.3 - 1.5V (fig. 6.22), while working with larger number of photons may be a reason to reduce this voltage. Eventual increasing of ΔV

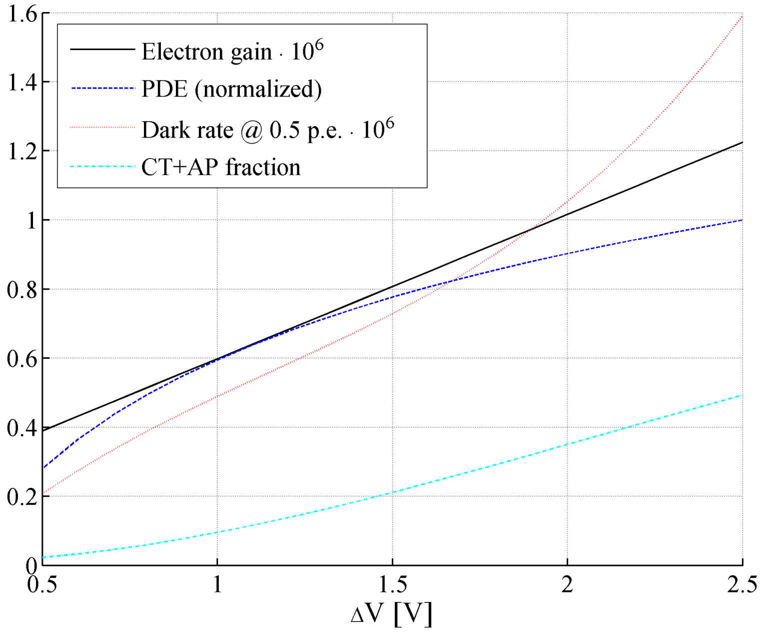

Figure 6.21: Approximate dependence of basic parameters of the MPPC on ΔV

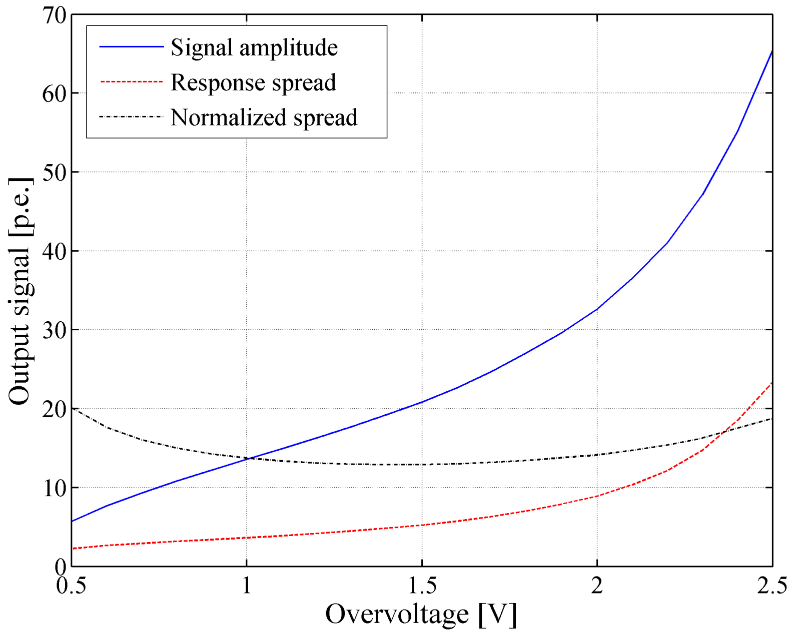

Figure 6.22: MPPC response to pulses with an amplitude of 50 photons (blue line), the value of standard deviation of the response, taking into account the dark pulses, counting statistics and the effects of CT+AP (red line) and the standard deviation, normalized to the average amplitude of the response to one photon for 50-photon pulse (black line) as a function of ΔV – expressed in p.e. This line can be regarded as the relative noise of the MPPC. The integration window length is set to 500 ns. The analysis does not take into account the preamplifier noise

may be desirable for small signals due to the preamplifier noise. Figure 6.22 shows an attempt to find an optimum, defined as the place where the relative amplitude fluctuations are smallest (excluding preamplifier noise). The curves are plotted basing on fitted measurement data; small dispersions observed in the plot are a result of using Monte Carlo methods to calculate the effects of a CT+AP. A similar analysis, but done by another research centre, with a bit more complicated assumptions and based entirely on data obtained by computer simulation, is presented in the work [25].

The value of V_{op}, given by Hamamatsu, is higher than the V_{br} by 1.3 V ($\Delta V = 1.3V$) for all tested MPPCs. In general, it seems to be a quite reasonable value (this is more or less the middle of the area of the proper MPPC operation), but it does not give any special features – which is why it should be regarded more as a 'initial value' for further improvements, rather than as universal optimum. As shown in figure 6.22, the dependence of the relative noise on the bias voltage of the MPPC is not very strong.

The useful values of ΔV for operation with weak light pulses (few photons) are comprised in the range of 0.5-2.5V. At lower voltages, the electron gain becomes so low that the SNR of the detector will be determined by the preamplifier noise (by the way, it should be noted that the analysis of data from various institutes shows that the pre-amplifier presented in chapter 4 and used for our MPPC tests, had very good parameters). When the voltage is too high, the fraction of CT+AP begins to affect dramatically all the characteristics, and to increase the dispersion of the pulse amplitude.

6.3 The quality of performed measurements

The range of utility of the results

The designed device allowed for a fairly comprehensive examination of MPPC photodiodes, allowing measurements of such parameters as electron gain, relative photon detection efficiency, dark rate (measured at any given threshold, but also the actual rate of thermal generation), the fraction of CT+AP – all in a wide temperature range and with practically any reasonable bias voltage. An ability to examine 1200 photodiodes gave an opportunity for a reliable statistical analysis of at least some of these parameters, as well as to estimate the the production dispersions.

Unfortunately, it was not possible to perform a thorough analysis of the dark rate, PDE and CT+AP phenomena for a large number of MPPCs (in particular, we could not determine production dispersions of some of these these parameters). It is not without significance that the data acquisition of the first measurement series and their detailed analysis were two activities separated in time. In the process of data analysis, it became clear what kind of measurements should be made to complete a set of results. Unfortunately, at that moment most of the photodiodes were already installed at the target device (SMRD sub-detector of T2K) and more detailed measurements could be carried out only on a small number of a few MPPCs.

The testing device was not able to perform some more detailed measurements, such as the separation of crosstalk and the afterpulse phenomena. It should be noted, that the designers were not going to provide such a functionality. The study of the crosstalk requires a fairly complicated optical setup, which greatly complicates an automated device, reducing its reliability. The analysis of afterpulses requires an analysis of signal timing with a resolution exceeding the performance of the 200-MHz ADC converter used.

The apparatus did not provide tests of the MPPC properties under forward polarization, which would allow for a direct measurement of the series resistance. Similarly, it was not possible to directly measure the terminal capacitance. Such studies require a separate sub-system to be installed into the device. It is possible that it will be developed in the future. This is allowed by the open architecture of the electronics.

The accuracy of the measurements

In general, the results obtained by the device can be considered very accurate, if compared with today's knowledge. The main factor determining the measurement accuracy is the amplitude resolution of the equipment, which conditions obtaining a good separation between the peaks in the pulse amplitude histograms. This allows one to determine the position of the peaks with high accuracy, which directly reflects in the accuracy of gain measurement. This, in turn, affects the determination of V_{br}, and the setting of the discriminator level in the dark rate measurement. Any error is transferred to next steps of calculations – like these for CT+AP and PDE.

The PDE value has the lowest accuracy among all the parameters (especially for relatively large values of ΔV). It is associated with quite complicated and poorly conditioned method of its determination. Therefore, some institutes use other methods for measuring the PDE, utilizing current measurement under a constant light illumination, after previous estimation of electron gain and saturation effects. It must be remembered that despite of quite considerable errors, a large sample of the data collected by us, allows at least rough definition of the nature the PDE(ΔV) dependence.

We could not avoid some problems during the measurements, that caused some deterioration in the quality of the data. The first problem was a sudden change in dark

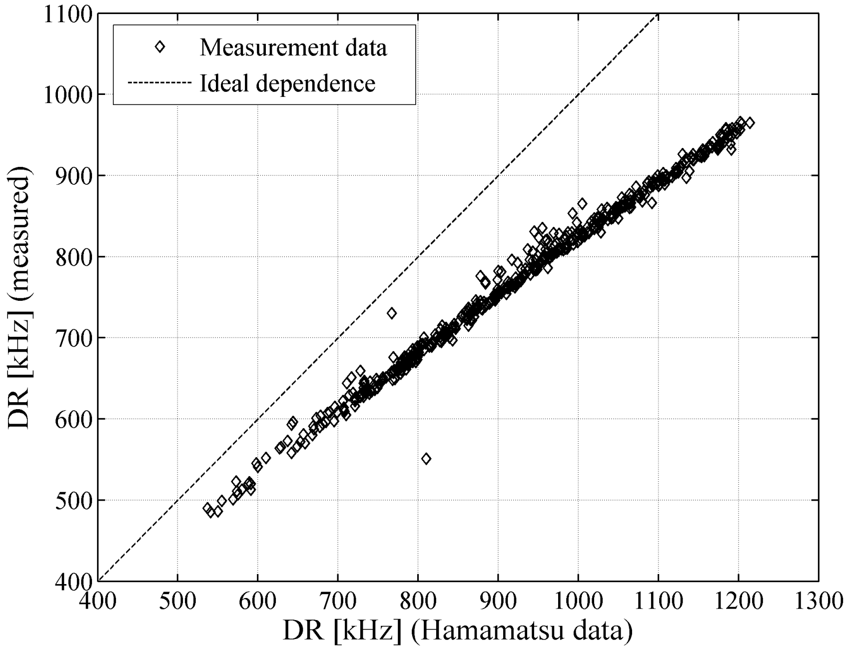

Figure 6.23: Comparison of the measured values of dark rate (0.5 p.e.) with the data provided by the manufacturer. The systematic difference between the data from both sources is mainly due to the different dead times of the discriminator

rate measurement results, probably due to unmeant equipment re-calibration, which was already mentioned. The second case concerned one of the temperature sensors, which gave uncertain readout due to a broken cable. This resulted in some smalll temperature variations, which, fortunately, had not a great influence on the overall measurement accuracy.

In retrospect, it's rather obvious that the data from the slow-control system should be stored together with the measurement data. Perhaps this would further increase the accuracy of some measurements. After all, it should be noted that the slow-control system was operating very well and the actual values of voltage and temperature were always very close to their setpoints.

The results of the measurements were continuously compared (whenever it was possible) with the data provided by the manufacturer. While the purpose of the study was to obtain accurate and comprehensive data independently from Hamamatsu, and to detect possible errors in the specifications provided, a quick comparison of the results with the manufacturer's documentation allowed to avoid accidental mistakes. An example of such a comparison, made during the first series of measurements, is shown in figure 6.23.

Chapter 7

Summary

The project related to the studies of MPPC properties took about three years. The results, obtained during the measurement process, undoubtedly helped to better understand the operation of tested elements. The process of data analysis has contributed to better understanding of the mechanisms that have been unclear, unexplored, or even unnoticed. It was possible to determine the analytical form of the various relationships, and in some cases (such as dark rate dependence on temperature) to find their physical explanation. With a small spread of the data it was possible to analyze the characteristics of non-linearity in the gain-voltage characteristics of the MPPC, which has so far been defined more qualitatively than quantitatively.

The results of the measurements enable us to determine the working conditions of the MPPC and optimize them for specific applications. A large number of measured elements allowed to find the production dispersion of some parameters and their typical values.

The author may include as his personal achievements in particular:

– a concept of a single-channel measuring device with a specimen feeder, allowing to maintain a high repeatability and precision of the measurements while providing adequate throughput and relative simplicity;

– good quality of the results delivered by a carefully selected methods of data processing;

– development and verification of the physical model of dark generation, improved electrical model of the MPPC including parasitic capacitances, and the determination of the parameters of the quadratic electron gain dependence on the supply voltage.

Meanwhile, the MAPDs begin to be more widely used in science. Currently, the Author participates in the construction of the electromagnetic calorimeter ECAL0 for the COMPASS experiment at CERN. The MAPD photodiodes without quenching resistor with a very high density of pixels will be used there. So far, most of the calorimeters were built based on photomultipliers, which were sometimes replaced with proportional-mode avalance photodiodes.

Increasingly, there are new attempts to use MAPD in industrial and commercial applications. The idea of using the new photodiodes for PET is one of most interesting. It seems that the MAPDs have a great chance to succeed in this application.

A fast-growing market offer, the regular publication of new solutions by the producers and intensive promotion seem to confirm the wide range of potential applications of the described photodetectors. It seems that the MAPDs are able to find application in the majority of devices, which measure weak light, often replacing photomultiplier tubes.

On the basis of the experience with the MAPD, one could try to answer the question: Is the new element able to win the competition with the photomultiplier?

Indeed, it seems that it is able to replace it in many cases. Its parameters such as the electron gain or the photon detection efficiency, stable performance, proven reliability, no high demands on the operating environment or – finally – ease of application, can easily convince the designers to introduce them to the newly built installations. However, some flaws of semiconductor devices, such as high dark generation, cause that photomultipliers will continue to be indispensable in some cases.

Certainly, the MAPD can be used in these applications where the vacuum technology of PMTs is a drawback, for example because of the price. The models with a high pixel density can be used in these solutions, where previously ordinary PiN or avalanche photodiodes and sensitive preamplifiers were used.

A novel PMT made using MEMS technology can be a potential competitor for the MAPD, although one should wait with this opinion until the wide market introduction of these elements.

Appendix A

List of abbreviations and symbols

ΔV	Overvoltage, the difference between working voltage and breakdown voltage for Geiger-mode photodiodes.
ε_0	Vacuum electrical permitivity.
ε_r	Relative electrical permitivity (of the semiconductor)
λ	Poisson distribution's expected value
τ_r	Recovery Time
ADC	Analog-to-Digital Converter
AP	Afterpulses
APD	Avalanche Photodiode
BLR	Baseline Restorer
CAMAC	Computer Aided Measurements and Control, a standard for a digital bus and modular electronic devices
CMRR	Common Mode Rejection Ratio
C_j	Junction capacitance
C_{pix}	Pixel capacitance
CT	Cross-Talk
CT+AP	The total fraction of Cross-Talk and Afterpulses
DR	Dark Rate
DAC	Digital-to-Analog Converter
ENC	Equivalent Noise Charge
F	Excess Noise Factor
FF	Fill Factor
FIR	Finite Impulse Response (filter)
FPGA	Field-Programmable Gate Array
FWHM	Full Width at Half Maximum

G	Electron Gain
GAPD	Geiger-Mode Avalanche Photodiode
I^{2}C	Inter-Integrated Circuit,
	a type of a serial bus
LCD	Liquid-Crystal Display
LED	Light-emitting Diode
LVDS	Low-Voltage Differential Signaling
M	Multiplication Ratio
MAPD	Multi-Pixel Avalanche Photodiode
MPPC	Multi-Pixel Photon Counter
MRS-APD	Metal-Resistor-Semiconductor Avalanche Photodiode
N_a	Acceptor concentration.
N_d	Donor concentration
n_i	Intrinsic concentration
P_{av}	Avalanche generation probability
p.e.	Photoelectrons
PDE	Photon Detection Efficiency
PiN	A diode with intrinsic layer
QE	Quantum Efficiency
R_{pix}	Quenching resistance.
SIPM	Silicon Photomultiplier
$SPAD$	Single Photon Avalanche Diode
VME	earlier VERSAmodule Eurocard bus,
	a standard for digital bus and electronic equipment
T	Temperature
TTL	Transistor-Transistor Logic
TCP/IP	Transmission Control Protocol/Internet Protocol
V_{br}	Breakdown voltage
V_{br}^*	Breakdown voltage calculated basing on dark rate characteristics
V_{op}	Operating voltage
V_d	Diffusion voltage
V_r	Reverse voltage
W_d	Depleted layer depth
WLS	Wavelength Shifter

Bibliography

[1] AdvanSiD. *ASD-SiPM3S-M*, 3 edition, Jan 2012.

[2] AdvanSid. *ASD-SiPM4S-P-4x4T*, 3 edition, Jan 2012.

[3] A. Akindinov et al. Long-term operation of a multi-channel cosmic muon system based on scintillation counters with mrs apd light readout. *Nuclear Instruments and Methods in Physics Research Section A*, 610(1):431–435, Oct 2009.

[4] Amplification Technologies. *DAPD10C Series, Discrete Amplification Photon Detector*, Jan 2008.

[5] Amplification Technologies. *NIRDAPD TEC Series, Discrete Amplification Photon Detector*, Oct 2009.

[6] Analog Devices. *AD8000, 1.5 GHz Ultrahigh Speed Op Amp*. Rev. A: Mar 2010.

[7] N. Anfimov, I. Chirikov-Zorin, Z Krumshteyn, R. Leitner, and A. Olchevski. Test of mocropixel avalanche photodiodes. In *10th Pisa Meeting on Advanced Detectors «Frontier Detectors for Frontier Physic»*, La Biadola, Isola d'Elba, Italy, May 2006.

[8] F. Corsi et al. Modelling a silicon photomultiplier (SiPM) as a signal source for optimum front-end design. *Nuclear Instruments and Methods in Physics Research Section A*, 572(1):416–418, Mar 2007.

[9] A. Czitrowsky et al. Measurements od quantum efficiency using entangled photons. *Laser Physics*, 10(1):86–89, 2000.

[10] N. Dinu, C. Bazin, C. Chaumat, A. Cheikali, A. Para, V. Puill, C. Sylvia, and J. F. Vagnucci. Temperature and bias voltage dependence of the MPPC detectors. In *2010 IEEE Nuclear Science Symposium, Medical Imaging Conference and 17th Room Temperature Semiconductor Detector Workshop, Knoxville*, 2010.

[11] M. Dziewiecki, R. Kurjata, J. Marzec, R. Sulej, K. Zaremba, and M. Ziembicki. A system for automated measurement of parameters of large quantities of MPPC detectors. In *International Workshop on New Photon Detectors (PD09)*. Shinshu University, Matsumoto, Japan, Jun 2009.

[12] B. Efron and R.J. Tibshirani. *An Introduction to the Bootstrap*. CRC Press, 1994.

[13] V. Golovin and V. Saveliev. Novel type of avalanche photodetector with Geiger mode operation. *Nuclear Instruments and Methods in Physics Research Section A*, 518(1–2):560–564, Feb 2004.

[14] Hamamatsu Photonics. *Multianode Photomultiplier Tube Assembly H8711, H8711-10*, Apr 2003.

[15] Hamamatsu Photonics K.K., Solid State Division. *MPPC. Multi-Pixel Photon Counter. Technical Information*, Sep 2010.

[16] J.S. Kapustinsky, R.M. De Vries, N.J. Di Giacomo, W.E. Sondheim, J.W. Sunier, and H. Coombes. A fast light pulser for scintillation detectors. *Nuclear Instruments and Methods in Physics Research Section A*, 241(2-3):612–613, Dec 1985.

[17] J. Krupka, J. Breeze, A. Centeno, N. Alford, T. Claussen, and L. Jensen. Measurements of permittivity, dielectric loss tangent, and resistivity of float-zone silicon at microwave frequencies. *IEEE Transactions on Microwave Theory and Techniques*, 54(11):3995–4001, Nov 2006.

[18] R.J. McIntyre. Multiplication noise in uniform avalanche diodes. *IEEE Trans. Electron Devices*, ED-13(1), Jan 1966.

[19] O. Mineev et al. Scintillator counters with multi-pixel avalanche photodiode readout for the ND280 detector of the T2K experiment. *Nuclear Instruments and Methods in Physics Research A*, 577(3):540–551, Jul 2007.

[20] PerkinElmer, Inc. *Avalanche Photodiodes: A User's Guide, 1998-2003.*

[21] F. Retierre et al. Characterization of multi pixel photon counters for T2K near detector. *Nuclear Instruments and Methods in Physics Research Section A*, 610(1):378–380, Oct 2009.

[22] A. Ronzhin et al. Testing a silicon photomultiplier time-of-flight (TOF) system in Fermilab test beam facility. In *Nuclear Science Symposium Conference Record, NSS '08*, pages 2392–2394. IEEE, 2008.

[23] SensL. *ArraySL-4: Scalable Silicon Photomultiplier Array*, 1.3 edition, Sep 2011.

[24] SensL. *MicroSL: Silicon Photomultiplier Detectors*, 1.3 edition, Sep 2011.

[25] A. Vacheret, M. Dziewiecki, J. Marzec, R. Kurjata, K. Zaremba, M. Ziembicki, et al. Characterization and simulation of the response of multi pixel photon counters to low light levels. *Nuclear Instruments and Methods in Physics Research Section A*, 656(1):69–83, Nov 2011.

[26] A. Vacheret, S. Greenwood, M. Noy, M. Raymond, and A. Weber. The front end readout system for the T2K-ND280. In *Nuclear Science Symposium Conference Record, NSS '07*, volume 3, pages 1984–1991. IEEE, 2007.

[27] Voxtel, Inc. *YAKIMA Silicon Photomultiplier (SiPM) Products*, Jun 2010.

[28] L. Weber and E. Gmelin. Transport properties of silicon. *Applied Physics A*, 53(2):136–140, 1991.

[29] K. Yamamoto, K. Yamamura, K. Sato, S. Kamakura, T. Ota, and H. Suzuki. Newly developed semiconductor detectors by Hamamatsu. In *International workshop on new photon-detectors PD07*. Kobe, Jun 2007.

[30] M. Yokoyama et al. Mass production test of Hamamatsu MPPC for T2K neutrino oscillation experiment. *Nuclear Instruments and Methods in Physics Research Section A*, 610(1):362–365, Oct 2009.

[31] M. Yokoyama et al. Performance of multi-pixel photon counters for the T2K near detectors. *Nuclear Instruments and Methods in Physics Research Section A*, 622(3):567–573, Oct 2010.

[32] M. Ziembicki, J. Marzec, and M. Dziewiecki. Monte Carlo study of the time resolution of scintillating fibre detectors. *Measurement Science and Technology*, 18(8):2477–2485, Aug 2007.

[33] M. Ziembicki, A. Nawrot, K Klimaszewski, P. Żabowski-Zychowicz, M. Dziewiecki, and R. Kurjata. Construction and performance of scintillating fiber detectors. In *2008 IEEE Nuclear Science Symposium Conference Record*, pages 1191–1194, 2008.